

THE MORPHOLOGY AND ENERGETICS OF DISCRETE OPTICAL
EVENTS IN COMPACT EXTRAGALACTIC OBJECTS

BY

JOSEPH THOMAS POLLOCK

A DISSERTATION PRESENTED TO THE GRADUATE COUNCIL OF
THE UNIVERSITY OF FLORIDA
IN PARTIAL FULFILLMENT OF THE REQUIREMENTS FOR THE
DEGREE OF DOCTOR OF PHILOSOPHY

UNIVERSITY OF FLORIDA

1982

ACKNOWLEDGMENTS

With this dissertation a quarter of a century of my education ends. Throughout this time I have received the constant encouragement and support of my parents, Joseph and Cecelia Pollock. They instilled the common sense, inner strength and sense of humor necessary to complete this endeavor, and it is to these two very special people that this work is lovingly dedicated.

Dr. Peter D. Usher and Dr. Alex G. Smith, my master's and doctoral advisors, together have converted a fledgling graduate student into a professional astronomer. I can only hope that my research and teaching abilities, and general professionalism can someday approach the examples of these two men. To each of them goes my deep gratitude. I would also like to thank the other members of my committee, Dr. T. D. Carr, Dr. J. P. Oliver, Dr. H. C. Smith and Dr. P. Kumar.

It is a pleasure to recognize three other fine professionals who have opened doors of opportunity. Mr. Stanley Walker allowed me to obtain advanced mathematical training in high school. Dr. Satoshi Matsushima gave a shakey undergraduate the chance to prove himself in graduate school. Dr. William Liller provided the opportunity for me to do extensive research and to publish the same.

All of my fellow graduate students have provided invaluable support, both scientific and spiritual. My special thanks go to Betty Whitmire, Greg Fitzgibbons, my shadow Andy Pica, Dan Caton and Jim Webb.

Special thanks go as well to Irma Smith, my typist, whose ability and knowledge made creation of the final copy so painless.

My thanks go as well to all the other people who, from day 1, have helped to smooth out the rough spots.

For as long as I can remember my Grandmother asked me, "Are you finished school yet?" This past Christmas day she passed away at the age of 96. I hope she knows that I finally made it.

TABLE OF CONTENTS

ACKNOWLEDGMENTS.	ii
LIST OF TABLES	vi
LIST OF FIGURES.	vii
ABSTRACT	viii
Chapter	
I. INTRODUCTION	1
Historical Background.	1
Group Subdivisions	3
Overall Problems Relating to Compact Sources	5
Objectives of This Study	6
II. OPTICAL VARIATIONS OF COMPACT OBJECTS.	8
Discovery of Optical Variability	8
General Variability Characteristics.	9
Data Acquisition and Reduction Techniques.	11
Sources of Compact Object Variability Data	17
III. THE VARIABILITY PROBLEM.	21
Apparent Magnitude	22
Absolute Magnitude or Emitted Flux	23
Rest Frame-Standard Wavelength Flux.	24
IV. DATA HOMOGENIZING AND TRANSFORMATION	25
Photometric Systems.	25
Standard Rest Frame System	27
V. EVENT DETERMINATION AND ANALYSIS	30
Event Definition	30
Identification of Events	31
Event Objects.	36
Event Parameter Calculations	39
Extreme Luminosity Changes	45
Normalized Event Luminosity Curves	45
Event Morphology	47
Individual Event Morphologies.	49

Individual Event Comments.	53
Variability and Emitting Region Sizes.	56
Bolometric Luminosities.	58
VI. COMPARISONS WITH THEORETICAL MODELS.	68
General Energy and Emission Constraints.	69
Black Hole Models.	75
Supermassive Rotating Magnetoplasmic Body.	91
Multiple Supernovae.	92
Final Comments and Suggestions for Future Work . .	92
LIST OF REFERENCES	95
APPENDICES	98
A. LIST OF VARIABLES AND SYMBOLS.	99
B. REFERENCES TO OPTICAL VARIABILITY DATA	102
C. NORMALIZED EVENT LUMINOSITY CURVES	110
BIOGRAPHICAL SKETCH.	177

LIST OF TABLES

1.	EVENT MAGNITUDE CHANGES.	21
2.	PG MAGNITUDE CORRECTIONS	26
3.	EVENT OBJECT PARAMETERS.	37
4.	EVENT PARAMETERS I	40
5.	EVENT PARAMETERS II.	42
6.	FRACTIONAL FLUX DURATIONS.	50
7.	FRACTIONAL LUMINOSITY FACTOR	57
8.	EMITTING REGION SIZES AND VARIABILITY TIMESCALES	59
9.	EVENT LUMINOSITIES AND ENERGIES.	64
10.	EVENT ENERGY DENSITIES AND MAGNETIC FIELDS	70
11.	EVENT PARAMETERS III	73
12.	MASS ACCRETION RATES	77
13.	EVENT ENERGIES AND CONVERTED MASSES.	78
14.	UPPER AND LOWER MASS LIMITS.	84
15.	DISK PULSATION PERIODS	86
16.	MAGNETIC FLARE MODEL PARAMETERS.	89

LIST OF FIGURES

1.	Sample light curves containing long term trends.	32
2.	Sample light curves containing discrete events	33
3.	Sample light curve containing intermediate events.	34
4.	Normalized event luminosity curve for a type I supernova . . .	48
5.	Log of the variability timescale in seconds versus the log of the bolometric luminosity in ergs/sec	81

Abstract of Dissertation Presented to the Graduate Council
of the University of Florida in Partial Fulfillment of the
Requirements for the Degree of Doctor of Philosophy

THE MORPHOLOGY AND ENERGETICS OF DISCRETE OPTICAL
EVENTS IN COMPACT EXTRAGALACTIC OBJECTS

By

Joseph Thomas Pollock

May 1982

Chairman: Alex G. Smith
Major Department: Astronomy

All available optical variability data for compact extragalactic objects were assembled. For objects showing evidence for one or more discrete events, this magnitude and data information was digitized, composite light curves generated and discrete events identified. All event data were converted to rest frame 2500 Å monochromatic luminosities. The base luminosity was determined for and subtracted from each set of event data, and normalized event luminosity curves were generated. The morphology of these events was examined, both for single events and for groups of events.

Determinations were made of event parameters such as the rest frame durations, 2500 Å peak and base luminosities, event to base energy ratios, total event energies and shortest significant variability timescales. From these and object parameters, values were obtained for lower limits to the peak bolometric luminosities and event energies, as well as the maximum size of the emitting region and resulting limits on the energy densities.

Under the assumptions of various models for these types of objects (mostly involving mass accretion onto a central black hole), further parameters such as mass accretion rates, total accreted masses, upper and lower limits on the mass of the central object and magnetic field strength limits were determined.

In only a few cases were these objects found to be emitting at a rate greater than their Eddington luminosities. A possible correlation between higher luminosities and shorter variability timescales was found, indicative of beamed radiation. Not all events could be explained in terms of non-radial pulsations of accretion disks. A model employing quiescent luminosity from mass accretion and event luminosity from magnetic flares on the accretion disk appears promising in terms of both energetics and emitting region sizes. The masses converted during the events were found to lie within the range of typical stellar masses.

CHAPTER I INTRODUCTION

Historical Background

N-galaxies

The objects known as N-galaxies (for nuclear) are so classified because their optical appearance is that of a relatively faint galaxy with an extremely bright, compact nucleus. The classification is a morphological one and is thus dependent on the distance to the given object.

A group of objects, later to be designated a subset of the class of N-galaxies, was examined by C. Seyfert in his doctoral dissertation in 1945. He investigated a small set of spiral galaxies which exhibited two properties not seen in most other "normal" spirals. This set of objects, now designated as Seyfert galaxies, showed extremely bright, compact nuclei (thus making them N-galaxies) and their spectra displayed strong, broad emission lines. Later studies have shown some of these objects to be strong radio emitters and X-ray sources, and to be variable in their radio, infrared and optical emission. These additional properties are more recent discoveries that resulted, to some extent at least, from the discovery and study of a second class of compact extragalactic objects. These are the quasi-stellar objects or "quasars" as they are now commonly referred to. It should be noted that not all N-galaxies exhibit the Seyfert characteristic of strong emission lines, a point which is often confused.

Quasars

The discovery of quasars was a direct result of the increase in the accuracy of positional measurements for radio sources in the late 1950's. T. Matthews and A. Sandage in 1963 found that a 16th magnitude "star" coincided with the position of the Cambridge radio source 3C 48. Optical spectra of this "radio star" contained unidentifiable, broad emission lines unlike those found in the spectra of normal emission line stars. A stellar object with characteristics similar to 3C 48 was then found at the position of 3C 273. Finally Schmidt (1963) recognized the spectral lines of 3C 273 to be the Balmer series of hydrogen, but highly redshifted from their normal rest wavelength. This was tremendously significant since redshifts of this nature were seen only in extragalactic objects whose distance was then determinable using Hubble's law. Using the distance derived in this way, the bolometric luminosity of 3C 273 could be calculated from a knowledge of the flux received from the object at all observable wavelengths (in principle). The result was about 3×10^{47} ergs per second (this notation for powers of ten will be maintained from this point on), which is about 6000 times that emitted by our own galaxy and about 300 times that of NGC 1275, one of the brightest known Seyfert galaxies. However, 3C 273 was of a size such that it could not be resolved by optical telescopes.

There is a caveat which must be placed here, however, concerning the determination of the distance to 3C 273 and all other quasars. It has been tacitly assumed that the origin of the redshifts of these objects is cosmological--that is, the redshift is a result of the object's taking part in the general expansion of the universe. If these

redshifts originate from another mechanism, such as gravitational redshift or local acceleration, then distances obtained through the use of Hubble's law are meaningless and the calculated luminosities will be wrong. This, of course, grossly affects the nature of such problems as the method of energy generation. Debate over quasar redshift origins has raged for almost twenty years. The presently prevailing opinion is that the redshifts are indeed cosmological; however smaller groups of vocal dissenters continue to feel that their evidence points to a non-cosmological origin. It will be assumed from here on in this work that the redshifts of these objects are valid indicators of the distance to them.

Group Subdivisions

As is always the case when a class of objects is scrutinized closely and is expanded in total membership, subdivisions based on differing observed properties are created. Major subdivisions of Seyfert galaxies and quasars are briefly described below.

Seyfert Galaxies

Seyfert galaxies are divided into types I and II depending on the width of the forbidden emission lines in their spectra. Type I exhibit narrow forbidden lines whereas those seen in type II are broad, often having widths of several thousand kilometers per second.

Quasars

There is a variety of criteria which are employed to divide up the general population of quasars as indicated below.

- (a) Optical spectral features
- (b) Presence or absence of strong radio emission
- (c) Centimeter "excess" radio sources

- (d) Nature of optical variability
- (e) Method of discovery
- (f) X-ray emission

The above list is by no means exhaustive. The three earliest subdivisions which developed were "classical" quasars, "radio-quiet" quasars and BL Lacertae objects. These classes can be compared and contrasted in the following ways.

3C 273 is a prototype of the classical quasars. It is starlike in its optical appearance (excepting a faint jet of material apparently emanating from the central region), has a highly redshifted emission line spectrum, has a partially polarized non-thermal optical continuum showing both ultraviolet and infrared excesses and is a strong radio emitter.

Not all quasars, however, emit a detectable radio flux. Those which do not are the radio-quiet quasars which are usually discovered by searching for objects with ultraviolet excesses and then obtaining their spectra in order to confirm their nature. Many of these blue stellar objects (BSO's) were catalogued, well before the identification of 3C 273, by means of multi-color surveys carried out at observatories such as Tonantzintla and Mount Palomar in programs to search for very blue stars. However, spectra were never obtained for them and their actual nature remained unknown at that time. A second search technique now extensively employed involves the examination of objective prism or grating plates to locate and classify these objects in a single step. Such surveys are beginning to indicate that a major fraction of all quasars may be of the radio-quiet variety.

The third class is comprised of the BL Lacertae objects. The prototype of this category, BL Lacertae, was originally classified as a variable star but was later found to coincide with a strong radio source. A major difference between these objects and the classical quasars is that the BL Lacs have very weak emission lines or totally continuous optical spectra. In addition they are usually neutral in color, not having strong ultraviolet excesses. These properties limit greatly our ability to identify this type of compact source and we must rely, in general, on a positional coincidence with a radio source to locate them. Some of the spectra, as mentioned earlier, are devoid of any emission or absorption features. This makes it impossible to determine their distance from Hubble's law and thus one cannot calculate directly their luminosities. Because BL Lacertae objects are usually extremely violent optical variables, their light curves are very conducive to the study of the phenomenon of variability. Unfortunately, for some of these objects the physical parameters that one would like to derive from such a study cannot be determined since the distance to the object remains unknown.

Overall Problems Relating to Compact Sources

The ultimate goal of the study of compact extragalactic objects is to devise a model that satisfactorily predicts the observed characteristics. One would hope that at some point in the future these models would be as successful as present day models for stellar atmospheres and interiors. It is possible that these objects are so physically complex and varied, however, that no such unified theory could ever be devised. The potential exists as well, as it did with the source of

stellar energy at the turn of this century, that the physical principles necessary to the solution of the problem have not yet been discovered.

A few of the major questions to be answered are given below. Some of these seem to have fairly satisfactory explanations while others are little understood.

- (a) What is the "engine" which can provide the vast quantities of energy which are emitted?
- (b) What causes the luminosities to change by a factor of two in a day or one hundred in a month in some of the most violent objects?
- (c) Are normal galaxies, Seyfert galaxies and quasars linked by morphology alone, or do they represent different phases within a single object's evolution?
- (d) What are the physical conditions which give rise to the emission and absorption line systems?
- (e) What is the mechanism which is responsible for the polarized, non-thermal continuum?
- (f) What causes the apparent super-relativistic velocities seen in some radio interferometric observations?

There are many more detailed problems as well.

Objectives of This Study

Since 1963, a tremendous amount of data on the optical variability of these objects has been gathered. In few instances, however, have the data been thoroughly analyzed in terms of the physical parameters they imply for the emitting objects. Even less has been done to intercompare the results so obtained among a large sample of these objects.

In order to make a comprehensive study of this sort it is necessary to proceed in a fashion similar to the one which follows. First, locate and gather together all of the available optical variability data references. This is a somewhat large and unexciting chore, which may explain

why it has not been done before, at least as thoroughly as is necessary. Then the data must be organized so that all observations of an individual object can be gathered together and examined. Next, all of the data to be used in the analysis need to be put into machine readable form, which consists of typing thousands of pieces of data by hand. These data must then be converted to a standard system and finally, using other known object parameters, these standardized data are converted to physical quantities in the rest frame of the object. Once this stage has been reached it is possible to analyze the information and intercompare results within the group of objects under study.

The focus of this study is what can be described as discrete optical events (commonly referred to as flares or outbursts). It is during these periods of intense activity that the most extreme physical conditions occur. These extreme physical conditions place the severest constraints on the "physics of what is going on," including the energy generation mechanism, emission and transfer of radiation processes and actual macroscopic structural changes. In addition, these events allow a determination of the actual size of the region where the emission is taking place. It is the intention of this study to obtain realistic and self-consistent values for those extreme physical conditions in as large a sample of objects as is possible. Then these parameters will be compared with the predictions of present theories in hopes of narrowing down the possible processes which are occurring in these enigmatic objects.

CHAPTER II OPTICAL VARIATIONS OF COMPACT OBJECTS

Discovery of Optical Variability

The earliest known information on the optical brightness of compact objects was recorded in the late 1880's as photographic astronomy developed and sky mapping and photographic patrol programs, such as those of the Harvard College Observatory, were initiated. These observations were, of course, serendipitous. Several variable "stars," which in recent times were found to be quasars, were observed and cataloged in the early part of this century. Among these were AP Librae, W and X Comae and BL Lacertae.

The first variability observations of an identified compact source were made by Matthews and Sandage (1963) for the source 3C 48. Although the total range in magnitude was relatively small ($B=16.44$ to 16.68), it pointed the way to more intensive studies of the optical behavior of these objects. Matthews and Sandage also reported significant variations on a timescale of 15 minutes. Such "short-timescale" variability will be examined in more detail later. Smith and Hoffleit (1963) soon published the first historical light curve for a QSO (3C 273) derived from the Harvard photographic archives. In about 80 years of coverage 3C 273 varied irregularly between $B=11.8$ and $B=13.2$, about one and one-half magnitudes. Also, it was seen to change a magnitude or more in just a few months. At this point various groups initiated optical monitoring of the few objects of this type known at that time. In addition, more historical light curves were being derived and the data accumulated very rapidly.

General Variability Characteristics

What these early studies indicated, and what studies since then have confirmed, is that there is no known compact extragalactic object whose variations have any strict periodicity. Several cases of short term quasi-periodicity have been reported (most notably in 3C 345 by Kinman et al., 1968). This case led Morrison (1969) to propose a model of these sources as giant pulsars. Sadly, future cycles of this periodicity failed to appear, leaving the interpretation of the earlier observations in doubt.

If one examines historical light curves of these objects extending for 30 or more years, one sees little to suggest any regular behavior. Some 60 light curves of this type have been published (see the References to Optical Variability Data Appendix) and the end result is that the only regular feature of the light curves is their irregularity. One important point has emerged, however. The number of non-variable objects (having this type of coverage) is small.

Shorter term contemporary monitoring studies (5-15 years) such as those in progress at Herstmonceux, the University of Florida and the Trudy Observatory of Leningrad do indicate some differentiation in variability behavior over this sort of period. An initial classification of the objects, based on their variability, was made by Penston and Cannon (1970). Objects which displayed changes of a magnitude or more on a timescale of days or weeks were designated as OVV's (Optically Violent Variables), whereas objects not yet found to vary in this way were called non-OVV's. If one has a sufficient number of datum points and a long enough time baseline, other general light curve subclasses can be defined.

Subclass I includes objects whose behavior is dominated by rapid flickering without underlying long term trends. Objects of Subclass II, conversely, show long term changes in their mean level which are much larger than any short term flickering. In Subclass III the short and long term effects are of comparable amplitudes. Finally, Subclass IV is episodic, displaying long intervals of quiescence interrupted by short periods of activity. As Pollock et al. (1979) point out, however, some (or perhaps all) of these objects may alter their variability characteristics from epoch to epoch (see, e.g., OJ 287, Pollock, 1975). Thus it is preferable to consider these classifications as representative of recent behavior, rather than as necessarily indicating some intrinsic differences between the sources. It seems quite likely that the overall variability classes are related to the macroscopic structure of the objects in some way. The OVV, non-OVV classification is subject to temporal variations as well, as shown by the historical light curves of 1156+295 and 3C 454.3.

Large variations, on the order of one magnitude, are well documented for timescales as short as a day. Significant variations (that is variations which are well above the experimental errors involved and which are confirmed by two or more observers) are nearly as well documented for periods of a few hours. Changes of this type, not surprisingly, are usually detected during violent outbursts of objects and often are a segment in a larger, longer variation in flux.

Attempts to detect significant variations on timescales of a half-hour or less have met with mixed success and great controversy. In at least two cases, detection by one observer of rapid variations well

above the formal error of the observations was not confirmed by a second, simultaneous but independent set of observations. Detection of small changes (less than 0.10 magnitude) in short time periods is not a simple procedure, especially when the variations are irregular in nature. Capabilities and limitations of various observational methods are detailed in the next section. It seems at present that caution will reign concerning very short timescale variability measurements, and that it will take two or more simultaneous and independent observations of the same variation to instill confidence concerning their reality.

Data Acquisition and Reduction Techniques

The two major observational techniques employed to obtain magnitudes for compact extragalactic objects are direct photography and photoelectric photometry. Each is discussed in more detail below concerning its applications, characteristics and accuracy.

Photographic Photometry

A majority of the compact source magnitudes used in this study were derived by means of photography, utilizing either existing plates taken for some other purpose or plates taken specifically of an object or objects of interest.

In the case of already existing exposures, such as those in the Harvard Archives, one must deal with plate materials which vary greatly in terms of types of emulsions and filters used, plate limiting magnitudes, types of recording instruments and off-centering of the field of interest, along with general plate quality (which deteriorates with time). Fortunately, most of the exposures taken employed a plate-filter-instrument

combination which yielded a photometric system reasonably close to the standard Johnson B-magnitudes. Indeed, a majority of the blue spectral region plates taken since 1960 used an -0 spectroscopic emulsion and a Schott GG13 filter, which is the standard photographic Johnson B combination. The two main limiting factors in the use of archival data to study the variability of compact sources are the plate limits and the temporal coverage. Few plates will have limiting B-magnitudes of fainter than 16 or so, and a majority of the quasars are fainter than this on the average. For 3C 273 ($B_v 13.0$) Smith and Hoffleit (1963) found over one thousand Harvard archival images, whereas for 1538+14 ($B_v 17.0$) Pollock (1975) found only 18 images. The number of plates containing a given field will vary as well, especially for the non-patrol plate series.

How well an object is covered in time is another factor. For 2254+07 (Pollock, 1975) 86 images were found, but 65 of these were from the period 1938-1940. This gave excellent coverage for that period but a poor determination of the long term light curve characteristics.

The second source of brightness determinations is from monitoring programs such as that conducted at the University of Florida. Here controls are exerted so as to produce standard system plates having adequate plate limits for quasar study. In addition, the temporal coverage can be defined as well.

Once an exposure has been obtained, how is an actual magnitude for the object extracted from it? The two standard approaches are iris photometry and visual estimation (the Argelander method) by comparison with a nearby set of standard stars.

Iris photometry involves the determination of the relationship between object apparent magnitude and image size and density for each individual plate. This relation, the so called calibration curve, can be determined only if there exists a series of stars of known apparent magnitude in the vicinity of the object on the plate. By measuring the object in the same manner as the stars used to determine the calibration curve, the object's magnitude can then be determined by means of that calibration curve. In general, for an object of typical quasar magnitude (14 to 20), the estimated error in the magnitude determination ranges from about 0.05 to 0.15 magnitude as indicated by the rms scatter of the comparison stars about the adopted calibration curve. In the Florida program the time necessary to measure the object and from 10 to 20 comparison stars, plus that required to computer-fit a least squares calibration curve, is about 15 minutes. To reduce 1000 plates of 3C 273 by this method would thus have required about 10 man-days.

The quicker, but somewhat less accurate, method of visual interpolation may instead be employed, if the object's comparison sequence meets certain criteria. Both the object and the sequence should be simultaneously viewable with a magnifier. The magnitude limits of the sequence should encompass the variability range of the object and the magnitude interval between successive comparison stars should be no more than 0.5 magnitude. Then the trained eye can estimate the object's magnitude to within about ± 0.10 of the value determined off the same plate by iris photometry (Pollock, 1975). This implies a total estimated error of about ± 0.20 magnitude from the "true" value. An estimate of this type takes about thirty seconds, a factor of 30 less than that of iris photometry.

Uniformity of the data, as pointed out earlier, is of great importance to this study. The zero-point errors inherent in either of these techniques depend upon the accuracy of the comparison sequence. Ideally one wishes to have photoelectrically determined magnitudes for the comparison stars to be used. If carefully done, there should be no significant zero-point error and less than 0.05 magnitude of random error in each star's magnitude. Many objects, however, do not yet have such sequences available.

Some sort of photographic transfer is the next choice. This usually involves taking four equal length exposures on the same plate, two of which are the object field and two are of a nearby field which contains a sequence of photoelectrically calibrated stars. Four exposures are necessary to eliminate the errors due to changes in plate sensitivity, the extinction coefficient, seeing and focus (Stock and Williams, 1962). The calibration curves derived for the standard fields are then used to determine magnitudes of the selected comparison stars in the object field. This technique requires relatively constant sky transparency and guiding, equal exposure times and constant and uniform emulsion sensitivity. If all these conditions are met, zero point errors should be small (less than 0.10 magnitude), while random errors in the initial magnitudes will be typical of iris photometry.

A third, rough calibration technique has been, rather unfortunately, extensively used by some workers in recent archival studies. The "diameter of the stars on the POSS" (Palomar Observatory Sky Survey) technique involves measuring the diameter of the comparison star images on the POSS print and then applying a general relationship between magnitude and

image diameter which is assumed to hold for all of the Sky Survey fields. The relation most often quoted is that given by Liller and Liller (1975). Differences in transparency, seeing and plate sensitivity cause individual plates to deviate from this relation. This plate-to-plate variation was estimated by Liller and Liller to be ± 0.4 magnitudes. If one examines the results of the extensive study of the POSS by Dorschner and Gurtler (1963) the situation does not appear so good. They list, for 33 blue prints, the deviation of the individual calibration curves (Δm). For ten of the prints the magnitude of Δm exceeds 0.40, with four of these greater than 0.85. The total range of deviations from the mean is from 0.69 to -1.52 magnitudes. This gives a zero-point difference of 2.2 magnitudes between the two "extreme" prints. A great potential exists for unacceptable zero-point errors when using this technique. Data reduced employing sequences of this type have been used in this study only if it was possible to determine that no significant zero-point error existed.

Nuclear brightnesses of compact objects which exhibit a significant non-stellar component are difficult to measure accurately photographically. For iris photometry to yield valid, consistent results for these objects exposure times must be adjusted (empirically) so as to record on the plate only the stellar component. This becomes more and more difficult to accomplish as the nebular component becomes comparable in surface brightness to the nuclear component. Archival plates rarely meet this criterion and magnitude estimates made from them of non-stellar objects must be treated with caution. In the worst cases the nebular contribution

can cause the measured brightness to be too bright by a magnitude or more. Even the use of a fixed iris diameter (in terms of the angular size on the sky) does not eliminate the problem because of the non-linear response of photographic emulsions. Each case of a non-stellar object must be considered separately.

In summary, using photographic techniques it is possible to obtain compact object brightnesses to ± 0.10 magnitude with time resolution of a minute or so. The time resolution obtainable is a function of the aperture and focal ratio of the instrument and the time necessary to insert a new plate. Photography's main advantage is that it allows relatively small instruments to record faint objects, the only limiting factors being the night sky brightness and patience. In addition, one can observe through skies of poorer photometric quality than one requires for photoelectric measurements, allowing more continuous monitoring.

Photoelectric Photometry

All photoelectric (p.e.) work on compact objects has been carried out in the last 20 years. Its advantages are high accuracy (0.01 to 0.05 magnitude), high time resolution (as short as 1 second for compact sources) and automatic digitization and reduction of the resulting data. Its major disadvantage is that for objects fainter than about $B=15$, that is 95% of all known quasars, a telescope of 30 inches or more aperture is needed. There are few telescopes this size which can have large portions of their time devoted to a single observing project. Consequently, most p.e. photometry programs for compact objects are of short duration and/or the interval between observing sessions is very long. In addition, highly photometric sky conditions are required.

It is with photoelectric photometry that the best hope for the detection of very short timescale variability lies. More specifically, it lies with the two-star photometer. When using a single-channel photometer it is necessary to move back and forth between the object under study and the comparison star. In addition, frequent sky measurements must be made. The two-star design utilizes two separate channels, one which constantly monitors the object while the other observes the comparison star. This gives a 100% duty cycle and the results are not affected by small changes in transparency. To date only a few attempts have been made to examine an active compact object with this type of instrument. If such an instrument could be devoted exclusively to the study of short timescale variability, many of the questions about it would be quickly answered.

Studies of the radial light distribution of non-stellar objects are more easily accomplished photoelectrically. If the proper observations are made, precise corrections for the non-stellar contributions can be determined, as we shall see in the case of NGC 4151.

Sources of Compact Object Variability Data

Location of Data

Aside from the data obtained from the Florida quasar monitoring programs, all data used in this study were obtained from the general astronomical literature. This includes all astronomical journals as well as available circulars and observatory reports and publications. One is fortunate in that these objects have been studied only since about 1963. For the period from 1969 through the present the Astronomy

and Astrophysics Abstracts provide references to and descriptions of articles published in the general astronomical literature. From this it was possible to assemble all references or potential references to optical measurements of compact extragalactic objects. A significant number of these references were not listed in either the "Revised Catalog of Quasi-stellar Objects" of Hewitt and Burbidge (1980) or the "Optical Catalog of Radio Galaxies" of Burbidge (1979). For the period from 1963 through 1968, it was necessary to examine each journal individually. Many observatory reports and publications from this period were not available to the author, so it is possible that some data from these sources were missed.

Once all of the potentially useful references were found and sorted by journal it was then necessary to examine each article individually. If it contained no useful information it was discarded. Otherwise the reference was assigned an identification number and notes were made of which objects were reported on and the nature of the observations. Objects were recorded initially by their co-ordinate designation to avoid the confusion associated with multiple names for the same object arising from various radio source catalogs. An identification number was assigned to each object as well. All references were then photocopied.

This resulted in about 180 references containing potentially useful data on 260 different objects. This information was then arranged so that on a 4x6 card were the cross reference numbers to all papers presenting data on a given object. At this point it became possible to determine rapidly if a given object had sufficient information to warrant further study.

The data in these studies ranged in scope from a single (but occasionally critical) point to hundreds of points spread over as much as 80 years. The formats of data presentation varied greatly. In terms of this study, the ideal format would have been a combination of both tabular and graphical data. The graphs would be of sufficient scale that significant, continuous (multi-point) events were recognizable. The tables would present the magnitude, rms error and Julian Date (to thousandths of a day) for each observation. In addition, if photoelectric photometry was employed, an indication of the diaphragm size which was used would be given.

Deviations from the above format were handled in various ways. Times of observations were often given as decimal U.T. (Universal Time) Date or U.T. Date and time. These were converted to Julian Date using auxiliary computer programs after the data had been initially digitized. Occasionally the date (J.D. or otherwise) was quoted only to the nearest day. In this case a "probable time of exposure" was calculated on the basis of the location of the observatory. The given date was then corrected by this amount and, when digitized, these points were annotated as to their nature.

When no individual errors were quoted for the measurements, the "typical error" given by the author of the paper was used for each of the datum points. If no typical error was given, errors were assigned on the basis of observational and reduction techniques. Errors of 0.05, 0.15 and 0.20 were adopted as standards for photoelectric and iris photometry and visual interpolation respectively.

Data reproduced only in graphical form presented other difficulties. In a few cases it was possible to obtain the tabular data used to create

the original plots. When this was not possible one was faced with the task of reading the data directly off the graph. Test measurements were made using the University of Florida binocular microscope XY-measuring engine on published light curves from the Florida program. An accuracy of ± 0.01 magnitude and ± 2.0 days was attainable for these plots whose scales were about three magnitudes per inch and 800 days per inch. Considering the time necessary to determine the co-ordinates of a given point and the relative inaccuracy of the date determination, only a few key points and events were digitized in this way.

In order to perform various transformations and analyses on the light curves it was necessary to have the data in machine readable form. All data from the Florida monitoring program were available in this form; however, all other data had to be hand entered. To facilitate this process it was decided to encode only data for objects which, upon initial examination of all pertinent references, showed definite or possible discrete events. Nonetheless, over 10,000 individual points (representing 40,000 pieces of data) were entered.

CHAPTER III THE VARIABILITY PROBLEM

In present usage a celestial object is termed optically variable if one is able to detect a statistically significant change in its apparent magnitude. This standard definition and conception of variability can severely mask and distort certain physical characteristics of an object or group of objects, and it disguises some observational selection effects.

The typical 2500 \AA monochromatic absolute magnitudes M for compact objects run from about -21 to -30. Consider an event, an added source of energy, to have (unto itself) a peak absolute magnitude of -24. Suppose now that identical events occur within objects whose quiescent or background absolute magnitudes range from -21 to -30. The resulting maximum magnitude change ΔM for each object is given in Table 1. The

TABLE 1
EVENT MAGNITUDE CHANGES

M	ΔM
-21	3.07
-22	2.16
-23	1.36
-24	0.75
-25	0.36
-26	0.16
-27	0.07
-28	0.03
-29	0.01
-30	0.00

observed results of the event in the various objects are quite different. In the -21 object a major outburst would be reported, a violent event, and in the -25 object a minor brightening would occur. Photographic and photoelectric techniques could not reliably detect the event for objects brighter than -26 and -28, respectively.

The question then becomes, are the objects "variable?" In terms of an absolute change in luminosity, yes, but in terms of an observable change in magnitude, employing present techniques, no. There are physically meaningful interpretations of each of these results.

By examination of Table 1 it can be seen that, if event energies were not proportional to the luminosity of the object involved, there would be fewer events detectable in the brighter objects and the morphology of those events would be different as well. In addition, because intrinsically fainter objects are more difficult to detect and study, one might conclude, perhaps erroneously, that high-redshift objects were less "variable" than their low-redshift counterparts. Analyses of the variability phenomenon which deal strictly with changes in apparent magnitude necessarily have these problems inherent in them.

For extragalactic objects variability data can be examined in various forms. What assumptions and additional object parameters are required and what can be learned physically from each of these forms are examined below.

Apparent Magnitude

An apparent magnitude light curve derived directly from observations involves no assumptions other than reliable technique and equipment. It is sometimes done for multiple received wavelengths. The

term "received wavelength" is important here because of the large range of Doppler shifts occurring in these types of objects.

For an individual object one can determine whether or not the object varies in magnitude and the morphology of those variations (shapes, periodicities, etc.). Colors (spectral indices), variation in color, and the timescale of variations can also be determined. The only absolute physical parameter which can be obtained is an estimate of the upper limit to the size of the emitting region during an outburst. This is derived using light travel time arguments. For a group of objects qualitative similarities in light curve morphology and color can be obtained. The problem with intercomparing objects in this situation is that the information obtained in a given bandpass (say the B at 4400\AA) represents different emitted frequencies in the rest frames of the objects. For objects having $z=0.05$ and $z=2.50$, the 4400\AA received radiation corresponds to 4190\AA and 1257\AA emitted radiation, respectively. In addition, the rest time frames are different. A 10-day observed event actually spanned $10/(1+z)$ days at the objects, that is 9.5 and 2.9 days, respectively.

Absolute Magnitude or Emitted Flux

Knowledge of the absolute magnitude or the emitted flux implies a knowledge of the distance and, for these objects, that means a redshift determination and the use of Hubble's law.

Often a value of the absolute B-magnitude is quoted, calculated from the apparent B-magnitude, the distance and the inverse square law. This does not represent, however, the flux emitted by the object at

4400Å, unless the optical spectral distribution is flat or $z=0$. What properly should be derived is the emitted flux at whatever wavelength 4400Å represents in the rest frame of the object. When one examines a group of objects with differing redshifts, the rest frame flux curves derived will be for different emitted wavelengths.

Rest Frame-Standard Wavelength Flux

If the redshift and the spectral energy distribution of an object are available, one can in principle determine the flux at any wavelength within the known range from the flux at one wavelength. It is also possible to extrapolate the spectral distribution to regions not directly measured, but such a process requires great care. Thus for two objects with observed B light curves, differing redshifts and known spectral indices, it is possible to transform their apparent magnitudes at 4400Å into emitted fluxes at, say 2500Å. This then allows a direct comparison of the physical behavior of the objects at that wavelength. One can create a "standard rest wavelength" to which all light curves will be transformed. In the process of this standardization the time axes of these light curves will be compressed by a factor of $1+z$. If one wishes to determine the total amount of energy being emitted in all directions by the object it is necessary to assume some angular dependence of the emitted radiation. The usual approach is to assume isotropic emission. If, in fact, the radiation is generated by a beaming process of some sort, the above assumption could lead to an overestimation of the luminosity of the object. Ramifications of various assumptions will be discussed in later sections.

CHAPTER IV DATA HOMOGENIZING AND TRANSFORMATION

Photometric Systems

Nearly all of the raw data which was employed in this study was in one of the following forms.

- (a) Johnson U,B and/or V-magnitudes
- (b) International Photographic (P) magnitudes
- (c) Millijansky flux at (or about) 4400Å

Over 75% of the data was in the form of B-magnitudes, with only a small quantity as U-magnitudes and millijansky fluxes. The remaining data were about equally divided between V and P-magnitudes.

For a given object, in order to be able to combine data from all available sources it was necessary to put the data on the same photometric system. Because a majority of the data was already in the form of B-magnitudes, the Johnson B system was chosen as the standard. If U or V-magnitudes and U-B and B-V color indices were given for each point, the determination of the B-magnitudes was straightforward. If individual color indices were not given, then color indices obtained for that object from other observations were used. Use of this single value for the color index assumes that no temporal color changes occur. Color changes of a few tenths of a magnitude have been seen in some objects. Fortunately, few conversions utilizing "typical" color indices were necessary. For all objects where U and V-magnitudes were quoted, color indices were available in one of the above forms.

Millijansky 4400Å-received fluxes were converted to B-magnitudes using the standard flux-magnitude conversion formulae of Johnson (1966).

Conversion to magnitude form was necessary in order to perform other corrections discussed in the next section.

The P-magnitude system has a bandpass which encompasses the entire Johnson B and U ranges. Thus the value B-P, needed to convert to the B system, is a function of the color of the object. This was demonstrated by Arp (1961) for main sequence stars and by Lu (1972) for QSO's. The correction for QSO's averages about 0.35 magnitude but ranges between 0.20 to 0.50 for objects whose U-B values range from -1.25 to 0.00. If one or more nearly simultaneous observations in the B and P were available, the average value of B-P obtained from them was used to convert the P-magnitudes to the B system. Otherwise empirical corrections as listed in Table 2 were made.

TABLE 2
PG MAGNITUDE CORRECTIONS

U-B	B-P
0.00	0.20
0.00 to -0.50	0.30
-0.50 to -1.00	0.40
-1.00	0.50
Unknown	0.35

Once all the observations of a single object were on the B system a composite data set and light curve could be generated and the search for discrete events undertaken. However, before data examination and manipulation were actually begun a final intercomparison of the data from different sources was made. After digitization the data were sorted by Julian Date. If two or more points on the same date from

different sources were found, these were carefully examined for indications of zero point differences, even if the data were taken in the "same" photometric system. Once this was done the data were pronounced fit for analysis and transformation.

Standard Rest Frame System

As mentioned earlier, in order to intercompare these objects it is necessary to convert the available data back to the rest frame of the objects. In addition, one wishes to choose a single standard rest wavelength. The approach taken is essentially that of Schmidt (1968) and Richstone and Schmidt (1980), and is discussed below.

The standard rest wavelength was chosen as 2500\AA because of the relative lack of strong emission lines in this region of the typical QSO spectrum, and because this wavelength range is redshifted into one of the Johnson bandpasses for a significant percentage of the known range of z 's for these objects. To obtain the monochromatic luminosity at 2500\AA in the rest frame of an object, the following procedure is employed. The case examined below is for conversion from B-magnitudes, but the method is basically the same for U and V-magnitudes.

First, it is necessary to correct for galactic extinction in one of two ways. Multicolor photometry of standard stars in the same direction as the object of interest can be obtained and the absorption coefficient in that direction can be specifically determined. Instead, if one is working away from the galactic plane, one can employ a standard extinction law where the absorption coefficient is a function of the object's galactic latitude. This is satisfactory for most extragalactic objects and the extinction law given by Tapia et al. (1976) has been used in this study.

The spectral index α (for power law spectra $f(\nu) = \nu^{-\alpha}$) must be calculated in most cases from the U, B and V-magnitudes for the object. Since α defines the slope of the non-thermal continuum in the optical region, it is not dependent on the nature of the emission lines. However, the broadband UBV magnitudes contain not only continuum radiation but any line radiation which happens to lie in their respective bandpasses as well. Thus, before these magnitudes can be used to determine α they must first be corrected for the presence of emission line radiation. Which lines contribute to the various bandpasses depends upon the redshift of the object. The amount of the contribution depends on the equivalent width of the line. Thus, in the calculations of α done here, if the equivalent width of a line for a given object is known (and is significant) it is corrected for.

Whenever possible the values of U-B, B-V and z from Hewitt and Burbidge are used. For some objects not given in this catalog, parameter values are obtained elsewhere. A summary of the adopted parameters is given in Table 3 in the next chapter.

At this point the B bandpass received flux is determined from the formula of Johnson (1966) as

$$f_{44} = 4.44 \times 10^{(15.0 - B_c)/2.5}$$

where B_c is the B-magnitude corrected for galactic extinction and the presence of emission lines. Now, using the value of α previously calculated, the 2500 \AA flux received can be expressed as

$$f_{25} = [2500(1+z)/4409]^\alpha f_{44}$$

where f_{25} has units of ergs/sec cm^2 Hz. Assuming isotropic emission of radiation and an empty ($q_0=0$) Friedman universe, the 2500\AA monochromatic luminosity is given by

$$L_{25} = 4\pi[H_0 c(z + \frac{1}{2}z^2)]^2 f_{25}$$

where L_{25} has units of ergs/sec Hz.

For this study the values chosen for Hubble's constant H_0 and the cosmological constant q_0 were 75 km/sec Mpc (lying in the middle of the currently accepted range of values) and 0 respectively.

CHAPTER V EVENT DETERMINATION AND ANALYSIS

Event Definition

It is the objective of this study to examine the discrete events in the light curves of compact extragalactic objects. Thus it is necessary to define what such an event is and how they are picked out of the actual light curves.

In the broadest sense an event occurs whenever there is an observationally significant difference between two temporally adjacent flux measurements. Identification of such an "event" involves no subjectivity (other than the choice of the significance level), but also does not yield more than the rate of change of flux with time, an important quantity but far from a complete description of the behavior of the object.

The problem can be approached in a manner similar to the recognition and analysis of emission features in the spectra of astronomical objects. In most astronomical spectra any emission lines are superimposed upon a continuum. To be recognized as discrete emission features they must be of sufficient intensity to cause a discontinuity in the continuum. In order to determine the actual amount of flux present in the emission line, the continuum level must be subtracted. In addition, these spectral lines may be rendered more difficult to detect if they are broadened by any of a number of mechanisms. Also, the continuum may not be smooth and monotonic (consider, for example, the Balmer discontinuity).

Looking for and analyzing events in compact object light curves follows essentially the same path. Two useful features are often found in spectral analysis and rarely in light curve analysis. First, for light curves, the data sampling rate is generally non-uniform, often showing large gaps. Secondly, one does not have an a priori knowledge of where the features are expected to occur.

The flux variations that occur in these objects are of two major types, which at some point blend into one another. Most objects show long term trends (duration >2 years), some examples of which are shown in Figure 1. These, and the other light curves discussed in this section, are reproduced from Pollock et al. (1979). Then there are discrete events such as those seen in the light curves of 0235+164, 2345-16 and 3C 446 shown in Figure 2. In these cases the object goes through a relatively rapid, monotonic increase in brightness followed by a return to the base level that existed before the event.

Figure 3 shows the recent behavior of OJ 287, 3C 345 and 0420-01. For each of these there appear events which have the characteristics of both types of variations discussed above. Are these events or continuum level changes, and at this point are the two in any way distinguishable? In this study they have been analyzed in the same manner as the shorter-term outbursts. Similarities and differences in the calculated event parameters can therefore be examined.

Identification of Events

Using our present definition, the smallest number of points required to define an event (to be able to specify its duration, peak and total energy) is three. Obviously this would be a most unsatisfactory situation.

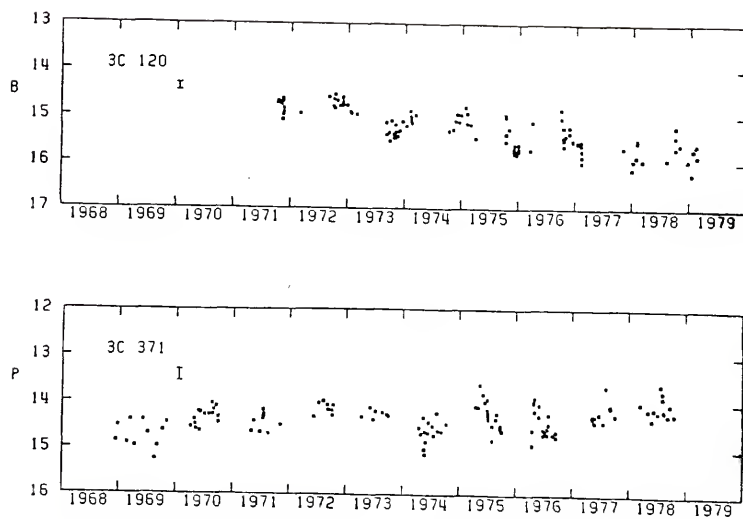


Figure 1. Sample light curves containing long term trends.

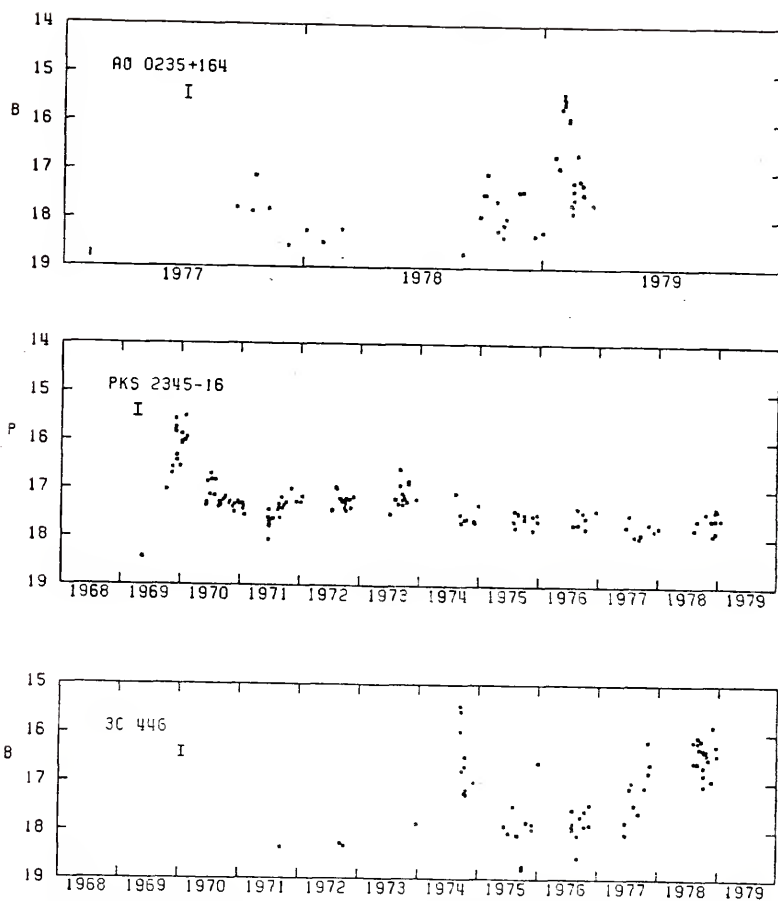


Figure 2. Sample light curves containing discrete events.

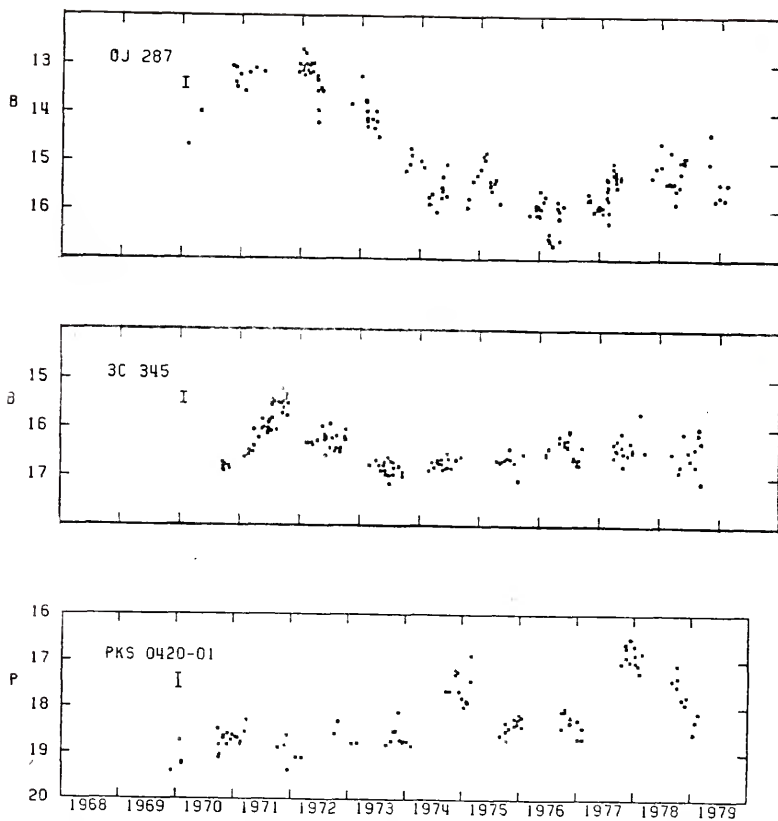


Figure 3. Sample light curve containing intermediate events.

It would be of no use unless the magnitude change was quite large, so as to cast no doubt on the single peak point's validity, and of very short duration so that a reasonably high average sampling rate still existed. Here the average sampling rate is simply the total number of event measurements divided by the duration of the event in days. No cases of three-point events were examined in this study. The single four-point and two five-point events in this study had durations of 1.6, 2.3 and 11 days and magnitude changes of 2.0, 1.8 and 1.6, respectively.

The actual procedure used for picking out events was as follows. Magnitude data from all available sources were digitized and sorted by Julian Date as described earlier. A data file and table of this information was then produced. A line printer plot of magnitude versus Julian Date was created with a resolution of <0.04 magnitudes/line and <7 days/line. Visual examination of the plot and table were then used to identify events and to establish the base level of the object at the time of each event. A subset of the original object data set was created containing only those points within the defined event. The lower of the two event endpoints was defined as the base level for that event. The event magnitudes and the corresponding object parameters (redshift, spectral index, right ascension, declination and emission line strengths) were supplied to a program which produced a data set having for each point

- (a) Julian Date
- (b) Object Event Date
- (c) Log of received flux at 2500\AA
- (d) Log of the luminosity at 2500\AA
- (e) Logs of the errors in the 2500\AA luminosity

The Object Event Date gives, for each point, the number of rest frame days which have elapsed since the start of the event. The errors in the 2500Å luminosity are the uncertainties resulting from the observational errors for a given point. The upward and downward errors are not equal because of the nature of the magnitude system and will be used in later analyses to determine the significance of luminosity changes.

Event Objects

Twenty-four compact object composite light curves contained useful events. Table 3 lists these objects in right ascension order and contains various important object parameters. Column 1 gives the co-ordinate designation, 2 the most common name (if different from 1). Objects from this point on will be referred to by their common names. Column 3 gives the adopted U-B and B-V colors, 4 the calculated spectral index, 5 the correction for galactic absorption, 6 the redshift and 7 the classification of the object. Emission line corrections were necessary for only two objects, 3C 345 and 3C 446, and were 0.14 and 0.04 magnitude respectively. That there were so few corrections of this type is not surprising. A majority of these objects are OVV's, which, as a class, are usually weak-line or BL Lacertae objects.

The general characteristics of all but six of these objects have been discussed by either Pollock et al. (1979) or Pica et al. (1980). A short characterization of the remaining six objects is given below before beginning the general discussion of the events themselves.

0039+40.--Zwicky et al. (1969) note that this Seyfert galaxy shows a variable nucleus superimposed on a faint halo. They comment that the absolute energy distribution bears a "striking resemblance" to 3C 120,

TABLE 3
EVENT OBJECT PARAMETERS

Co-ordinate Designation	Common Name	Adopted		Spec. Index	Gal. Abs.	z	T
		U-B	B-V				
0039+40	--	--	--	0.84a	0.42	0.103	S
0219+42	3C 66A	-0.58	0.33	1.30	0.64	0.444	B
0235+164	--	0.14	0.96	3.89	0.12	0.852	B
0420-01	--	--	--	0.70b	0.20	0.915	Q
0440-00	NRAD 190	-1.05	0.37	1.00	0.28	0.850	Q
0521-36	--	-0.30	0.67	2.27	0.21	0.055	N
0735+17	--	-0.58	0.47	0.97	0.58	0.424	B
0851+20	OJ 287	-0.64	0.39	0.98	0.17	0.306	B
0906+01	--	--	--	0.70b	0.24	1.018	Q
1156+295	--	-0.56	0.44	1.38	0.00	0.728	B
1209+39	NGC 4151	--	--	0.05c	0.00	0.003	S
1253-05	3C 279	-0.56	0.26	1.55	0.00	0.538	Q
1308+326	--	-0.59	0.40	1.23	0.00	0.996	B
1510-08	--	-0.74	0.17	0.90	0.11	0.361	Q
1545+21	3C 323.1	-0.85	0.11	0.26	0.01	0.264	N
1633+38	4C 38.41	--	--	0.70b	0.09	1.814	Q
1638+39	NRAD 512	--	--	0.70b	0.10	1.6d	Q
1641+39	3C 345	-0.50	0.29	1.11	0.10	0.595	Q
1730-13	NRAD 530	--	--	0.70b	1.10	0.9e	Q
1807+69	3C 371	-0.25	0.83	2.68	0.27	0.050	N
2200+42	BL LAC	-0.10	0.97	1.90	1.15	0.069	B
2223-05	3C 446	-0.90	0.44	1.77	0.01	1.404	Q
2251+15	3C 454.3	-0.66	0.47	1.49	0.14	0.859	Q
2345-16	--	--	--	0.70b	0.00	0.600	Q

Notes to Table 3:

- From published spectrum of Zwicky et al. (1969)
- Adopted "typical" value
- Deconvolved nuclear spectrum of Penston et al. (1971)
- Private communication, B. Lynds
- Tentative, private communication, A. Marscher
- Final column abbreviations:
 - N, N-galaxy
 - B, BL Lacertae Object
 - S, Seyfert galaxy
 - Q, QSO

with the absolute flux at a rest wavelength of 5000\AA differing by only about 20%. Unlike 3C 120, 0039+40 is radio quiet, with $S(408\text{ MHz}) < 0.012$ flux units. Optical monitoring at Assiago has shown 0039+40 to vary erratically between $B=16-18$.

0521-36.--Eggen (1970) summarizes the data available for 0521-36. It is an N-galaxy and a strong radio source (19.0 flux units at 1410 MHz). The object's color becomes redder as it decreases in brightness, similarly to 3C 371 and 3C 390.3. Shen et al. (1972) found, from the Harvard Archives, short-term variability superimposed on a long-term component, the later variation spanning on the order of a decade.

1156+295.--This object was not widely known until the detection of a major outburst in 1981. It is a BL Lac object whose historical light curve (Pollock, 1982) showed the object to be very quiescent until recently.

NGC 4151.--This prototype Seyfert galaxy is extremely well known. Cannon et al. (1971) summarize references to its optical variability. Photometry of the object is complicated by a bright, extended galaxy component, which, through a $10''$ aperture, is brighter than the central point source from the V to K bands (Penston et al., 1971). They have used a series of photoelectric observations through various diameter apertures to deconvolve the galaxy and nuclear component spectra. The spectral index used in this work for NGC 4151 was determined from their nuclear component spectrum.

In addition Penston et al. (1971) determined the galaxy flux contribution through a given aperture to be

$$f(D'') = f(10'') (D/10)^\alpha$$

where they found $\alpha = 0.6 \pm 0.05$. For the B-bandpass we thus obtain

$$f(10'') = 1.45 \times 10^{-2} \text{ Janskys}$$

which in combination with their earlier expression gives

$$f_B(D'') = 1.45 \times 10^{-2} D^{0.6} (.1)^{0.6}$$

$$f_B(D'') = 3.64 D^{0.6} \text{ millijanskys}$$

Since, in this work, we are interested in only the compact central source, the following special reduction procedures were employed for NGC 4151. Photoelectric observations, which reported the aperture size which was used, were first converted to B-magnitudes, if necessary. These were then converted to received fluxes, corrected for the galaxy contribution and then converted back to B-magnitudes to be treated in the standard fashion.

1545+21.--This source, also known as 3C 323.1, was identified by Wyndham (1966) as a slightly diffuse object with a very blue nucleus. Schmidt (1968) determined its redshift and Lu (1972) carried out the variability observations used in this work. The Harvard historical light curve of Angione (1973) showed variations between B=15 and 17.

4C 38.41.--Other than its identification as an optical counterpart of a radio source and its redshift determination little has been published concerning this quasar.

Event Parameter Calculations

Various parameters describing each event have been determined and are summarized in Tables 4 and 5. Given below are descriptions of the contents and format of Tables 4 and 5 and, when necessary, an explanation of the procedure used to obtain a given parameter.

TABLE 4
EVENT PARAMETERS I

Event		Julian Date		Duration days	S _e pts/d	B-Magnitude	
		Start	End			Peak	Base
0039+40	A	41513.465	41927.597	375.460	0.04	16.90	17.80
3C 66A	A	42667.847	42834.440	115.369	0.10	15.10	16.00
0235+164	A	42688.7	42780.7	49.7	0.26	15.25	18.04
	B	43751.853	44136.843	175.497	0.19	15.44	19.39
	C	44136.843	44305.547	91.093	0.18	17.16	19.39
	D	44487.779	44629.580	76.566	0.22	17.04	19.54
0420-01	A	42089.544	42700.932	319.263	0.05	17.24	19.19
	B	43183.612	43892.603	370.230	0.06	16.86	19.03
	C	43892.603	44487.801	310.808	0.05	16.38	18.94
NRAD 190	A	43054.894	43137.726	44.774	0.20	17.13	18.93
	B	43462.817	43544.557	44.184	0.16	17.48	19.42
0521-36	A	39817.300	40560.300	704.265	0.02	14.60	15.95
	B	43097.0	43221.0	117.536	0.09	15.22	16.22
0735+17	A	42047.323	42148.550	71.090	0.25	15.07	16.56
	B	42717.873	42928.584	147.971	0.51	14.37	16.08
	C	42928.584	43489.702	394.044	0.22	13.90	16.11
0J 287	A	36526.598	36667.301	107.736	0.19	13.12	15.68
	B	41653.639	41822.708	129.456	1.17	13.25	14.65
	C	42341.911	42488.250	112.051	0.87	14.66	15.95
	D	40625.463	42149.566	1167.001	0.50	12.36	16.04
0906+01	A	40862.886	40899.885	18.334	0.44	16.24	17.38
	B	40943.757	41009.590	32.623	0.89	16.44	17.65
	C	41011.667	41041.736	14.900	0.81	16.77	17.58
1156+295	A	44640.708	44729.708	51.505	0.60	13.15	16.78
NGC 4151	A	39505.0	40019.488	512.8	0.10	11.73	14.32
3C 279	A	28279.0	28330.0	33.2	0.45	12.03	13.98
	B	28601.0	28722.0	78.7	0.17	11.27	14.90
	C	27814.0	29028.0	789.3	0.09	11.27	17.32
1308+326	A	43169.877	43310.750	70.578	0.26	15.21	16.95
	B	43543.750	43728.578	92.599	0.63	15.20	17.54
	C	44395.648	44455.578	30.025	0.83	14.95	17.68
	D	44673.806	44754.681	40.519	0.30	15.79	18.82

TABLE 4 (continued)

Event		Julian Date Start End		Duration days	S _e pts/d	B-Magnitude Peak Base
1510-08	A	32671.0	-32800.0	94.8	0.16	11.80-15.00
1545+21	A	40596.920	-40840.580	192.769	0.06	16.06-16.58
4C 38.41	A	41087.4	-41119.5	11.0	0.45	15.85-17.40
NRAD 512	A	40703.4	-40709.5	2.3	2.13	17.00-18.80
	B	40709.5	-40739.4	11.5	0.78	17.60-18.80
	C	40739.4	-40743.621	1.6	2.46	16.67-18.70
	D	40743.621	-40779.769	13.903	1.58	17.76-18.81
	E	41134.742	-41246.518	42.991	0.56	17.30-19.47
	F	41397.890	-41458.875	23.456	0.17	17.39-18.50
	G	41458.875	-41506.709	18.398	0.38	17.52-18.50
	H	41134.742	-41866.726	281.532	0.21	17.30-19.61
3C 345	A	39017.7	-39063.6	28.8	0.97	16.25-17.21
	B	39358.7	-39387.7	18.8	1.01	16.27-17.18
	C	39534.69	-39548.73	8.803	1.14	15.41-16.26
	D	39569.630	-39616.4	29.3	0.48	15.77-16.40
	E	39675.510	-39709.490	21.304	0.76	15.49-16.25
	F	40298.8	-40451.8	95.9	0.96	15.53-17.50
	G	41120.4	-41175.25	34.4	1.13	14.99-16.20
	H	39290.7	-39943.52	409.3	0.62	15.41-17.45
NRAD 530	A	43280.838	-43420.565	73.541	0.20	15.76-18.52
	B	44764.794	-44792.709	23.593	0.68	16.94-18.70
3C 371	A	40827.380	-40879.260	44.824	1.63	14.37-15.53
	B	41471.360	-41518.470	49.363	0.59	14.54-15.62
BL LAC	A	40384.570	-40747.348	83.983	0.83	14.29-16.10
	B	41891.280	-41899.510	7.699	7.27	15.00-16.14
	C	32043.0	-32073.7	28.718	0.45	14.51-16.32
3C 446	A	38944.9	-40127.38	491.9	0.30	15.67-19.00
	B	40500.34	-40918.30	173.86	0.10	16.15-18.94
	C	42301.656	-42687.740	160.606	0.17	15.44-18.80
	D	43018.733	-44550.545	637.205	0.11	15.35-18.57
	E	44572.535	-44792.852	91.646	0.09	16.33-18.35
3C 454.3	A	39856.3	-40150.8	158.4	0.25	16.08-17.21
	B	44057.796	-44246.540	75.214	0.13	16.22-17.62
2345-16	A	40504.691	-41123.864	386.983	0.12	15.87-17.96

TABLE 5
EVENT PARAMETERS II

Event		L_p	L_B	I_p	E_e	R_e
		ergs/sec	Hz		ergs/Hz	
0039+40	A	1.55 [29]	6.78 [28]	8.75 [28]	9.71 [35]	0.44
3C 66A	A	2.18 [31]	9.53 [30]	1.23 [31]	3.31 [37]	0.35
0235+164	A	7.48 [31]	1.65 [30]	7.32 [31]	1.51 [38]	21.26
	B	6.30 [31]	1.65 [30]	6.13 [31]	1.04 [38]	2.92
	C	1.26 [31]	1.65 [30]	1.10 [31]	1.61 [37]	1.24
	D	1.44 [31]	1.45 [30]	1.30 [31]	2.92 [37]	3.03
0420-01	A	1.28 [31]	2.12 [30]	1.06 [31]	1.03 [38]	1.76
	B	1.81 [31]	2.46 [30]	1.57 [31]	2.09 [38]	2.67
	C	2.82 [31]	2.67 [30]	2.55 [31]	8.47 [37]	1.18
NRAD 190	A	1.28 [31]	2.44 [30]	1.04 [31]	1.76 [37]	1.86
	B	9.29 [30]	1.56 [30]	7.73 [30]	1.00 [37]	1.69
0521-36	A	1.40 [29]	4.11 [28]	9.88 [28]	1.99 [36]	0.80
	B	7.91 [28]	3.15 [28]	4.76 [28]	2.67 [35]	0.83
0735+17	A	2.04 [31]	5.16 [30]	1.52 [31]	4.59 [37]	1.45
	B	3.88 [31]	8.04 [30]	3.08 [31]	1.52 [38]	1.48
	C	5.98 [31]	7.82 [30]	5.20 [31]	4.50 [38]	1.69
0J 287	A	3.95 [31]	3.74 [30]	3.58 [31]	1.37 [38]	3.94
	B	3.51 [31]	9.66 [30]	2.54 [31]	1.12 [38]	1.04
	C	9.49 [30]	2.91 [30]	5.57 [30]	2.06 [37]	0.73
	D	9.78 [31]	2.68 [30]	7.69 [31]	2.42 [39]	8.96
0906+01	A	4.32 [31]	1.51 [31]	2.81 [31]	2.81 [37]	1.17
	B	3.60 [31]	1.18 [31]	2.42 [31]	3.00 [37]	0.90
	C	2.65 [31]	1.20 [31]	1.45 [31]	7.44 [36]	0.48
1156+295	A	2.58 [32]	9.12 [30]	2.49 [32]	3.15 [38]	7.77
NGC 4151	A	1.50 [28]	1.38 [27]	1.36 [28]	2.53 [35]	4.13
3C 279	A	3.20 [32]	5.31 [31]	2.67 [32]	2.77 [38]	1.71
	B	6.44 [32]	2.28 [31]	6.21 [32]	8.84 [38]	5.72
	C	6.44 [32]	2.45 [30]	6.42 [32]	3.62 [39]	21.68
1308+326	A	1.45 [32]	1.04 [31]	1.34 [32]	3.70 [38]	5.73
	B	9.25 [31]	1.06 [31]	8.19 [31]	2.45 [38]	2.89
	C	1.15 [32]	9.31 [30]	1.06 [32]	6.94 [37]	2.87
	D	5.31 [31]	3.26 [30]	4.98 [31]	6.23 [37]	5.47

TABLE 5 (continued)

Event		L _p	L _B	l _p	E _e	R _e
		ergs/sec	Hz		ergs/Hz	
1510-08	A	1.89 [32]	9.91 [30]	1.79 [32]	4.84 [38]	5.96
1545+21	A	2.08 [30]	1.26 [30]	8.13 [29]	6.00 [36]	0.29
4C 38.41	A	2.47 [32]	5.93 [31]	1.88 [32]	8.32 [37]	1.47
NRAD 512	A	6.14 [31]	1.17 [31]	4.97 [31]	4.18 [36]	1.78
	B	3.53 [31]	1.17 [31]	2.36 [31]	1.21 [37]	1.05
	C	8.32 [31]	1.28 [31]	7.04 [31]	4.44 [36]	2.73
	D	3.05 [31]	1.16 [31]	1.89 [31]	8.78 [36]	0.63
	E	4.66 [31]	6.31 [30]	4.02 [31]	5.38 [37]	2.30
	F	4.28 [31]	1.54 [31]	2.74 [31]	2.74 [37]	0.88
	G	3.80 [31]	1.54 [31]	2.26 [31]	1.14 [37]	0.47
	H	4.66 [31]	5.55 [30]	4.10 [31]	3.65 [38]	2.53
3C 345	A	8.67 [30]	3.58 [30]	5.09 [30]	4.17 [36]	0.47
	B	8.51 [30]	3.68 [30]	4.83 [30]	2.33 [36]	0.37
	C	1.88 [31]	8.59 [30]	1.02 [31]	3.77 [36]	0.58
	D	1.35 [31]	7.55 [30]	5.94 [30]	7.48 [36]	0.39
	E	1.75 [31]	8.67 [30]	8.79 [30]	8.50 [36]	0.53
	F	1.68 [31]	2.74 [30]	1.41 [31]	2.62 [37]	1.15
	G	2.77 [31]	9.08 [30]	1.86 [31]	1.74 [37]	0.64
	H	1.88 [31]	2.87 [30]	1.59 [31]	1.76 [38]	1.91
NRAD 530	A	1.10 [32]	9.63 [30]	1.01 [32]	8.26 [37]	1.51
	B	3.70 [31]	7.31 [30]	2.97 [31]	2.15 [37]	1.44
3C 371	A	1.26 [29]	4.32 [28]	8.26 [28]	1.64 [35]	1.06
	B	1.08 [29]	3.98 [28]	6.78 [28]	9.43 [34]	0.51
BL LAC	A	8.65 [29]	1.42 [29]	7.23 [29]	2.10 [36]	2.04
	B	4.50 [29]	1.44 [29]	3.06 [29]	1.01 [35]	1.05
	C	7.06 [29]	1.33 [29]	5.73 [29]	9.23 [35]	2.79
3C 446	A	1.83 [32]	8.51 [30]	1.74 [32]	1.72 [39]	4.75
	B	1.18 [32]	9.00 [30]	1.08 [32]	6.23 [38]	4.61
	C	2.26 [32]	1.02 [31]	2.16 [32]	4.03 [38]	2.84
	D	2.46 [32]	1.26 [31]	2.33 [32]	4.38 [39]	6.29
	E	9.95 [31]	1.55 [31]	8.40 [31]	2.57 [38]	2.09
3C 454.3	A	3.11 [31]	1.06 [31]	2.05 [31]	7.97 [37]	0.55
	B	2.73 [31]	7.53 [30]	1.98 [31]	3.80 [37]	0.78
2345-16	A	1.35 [31]	1.97 [30]	1.15 [31]	6.82 [37]	1.04

Table 4--Description

Column 1 gives the event designation by using the object's common name followed by a capital letter suffix.

Column 2 gives the starting and ending Julian Dates.

Column 3 gives the rest frame event duration, T_e , where

$$T_e = [\text{JD}(\text{final}) - \text{JD}(\text{initial})] / (1+z)$$

Column 4 lists the data sampling rate, S_e , where

$$S_e = (\text{number of event points}) / T_e$$

It should be noted here that the actual temporal distribution of measurements is often highly non-uniform.

Column 5 gives the peak and base B-magnitudes.

Table 5--Description

Column 1 gives the event designation by using the object's common name followed by a capital letter suffix.

Column 2 gives the peak total 2500\AA luminosity, L_p .

Column 3 gives the base event 2500\AA luminosity, L_B .

Column 4 gives the peak event 2500\AA luminosity, l_p , where

$$L_p = L_B + l_p$$

Column 5 lists the total event 2500\AA energy, E_e , where E_e is the total energy emitted during the event (corrected for the base level) in a one Hertz bandwidth at 2500\AA . This was determined from a simple point-by-point integration of the event luminosity at point a , l_a , where for an event having m points

$$E_{a,a+1} = (l_a + l_{a+1}) \Delta T_{a,a+1} / 2$$

$$E_e = \sum_{a=1}^{m-1} E_{a,a+1}$$

Column 6 gives the ratio of the event energy to the base energy, R_e , where

$$R_e = E_e / L_B T_e$$

Extreme Luminosity Changes

The change in luminosity, ΔL , was calculated for all possible point pairs. This value was taken to be statistically significant if $\Delta L_{ab}/e_{ab}$ was >2 , where e_{ab} is the sum of the individual root mean square errors associated with L_a and L_b , e_a and e_b respectively. As discussed earlier, for an individual point the positive and the negative errors are not the same. The luminosity at point a is

$$L_{-e_{a-}}^{+e_{a+}} \quad \text{where } |e_{a+}| > |e_{a-}|$$

Thus, for an upward luminosity change from points a to b, the significance condition becomes

$$(L_b - L_a)/(e_{a+} + e_{b-}) > 2$$

whereas for a downward change from points c to d we have

$$(L_c - L_d)/(e_{c-} + e_{d+}) > 2$$

For all statistically significant luminosity changes the following quantities were examined, ΔT , the rest time interval for the change to occur; $\Delta L/\Delta T$, the rate of change of the luminosity, and, most importantly, $\Delta T \bar{L}/\Delta L$, whose application is discussed in the section on emitting region sizes.

Normalized Event Luminosity Curves

In order to examine the general morphology of individual events and groups of events, plots of normalized event luminosity as a function of object event date were created and are shown in Appendix C. The normalized luminosity at a point a is given by

$$l'_a = l_a/l_p$$

The x-axis is the Object Event Date, with divisions being 0.1 of the indicated axis extent. The first and last event points are then at $t=0$ and $t=T_e$. Temporally adjacent points are connected by a dotted line. This aids in following the point-by-point evolution of the event and also better defines the general event shape. The figures in Appendix C show the normalized luminosity curves for the events studied in this work, ordered by right ascension.

Plotting of the rms error bars associated with each point would have resulted in cluttered and confused graphs. The typical size of the error involved in the original luminosity measurement is about 10% (although this can be as small as 2% for photoelectric values or as large as 20% for eye estimates). This percentage, however, is of the total luminosity rather than the base level corrected luminosity.

The "normalized" error for a given point a (at the 10% error level) is:

$$\begin{aligned} e'_a &= 0.10 L_a / l_p \\ &= 0.10 (l'_a + L_B) / l_p \\ &= 0.10 [l'_a + (L_B / l_p)] \end{aligned}$$

For normalized luminosity values of 0.4 and 0.8, respectively, this becomes

$$\begin{aligned} e' &= 0.04 + 0.10 (L_B / l_p) & l' &= 0.4 \\ e' &= 0.08 + 0.10 (L_B / l_p) & l' &= 0.8 \end{aligned}$$

It is evident that, as the ratio of base event luminosity to peak event luminosity becomes small, the value of e' approaches 10% of l' . Values of this ratio range, in the events studied, were between 0.01 and 1.

Event Morphology

The shape of an event, its morphology, describes the way that the energy release took place. This can, hopefully, give some insight into the energy generation mechanism and/or the surrounding macroscopic structure. Before dealing with the individual events, a brief discussion is given below of the so-called supernova-type light curve to illustrate why light curve shapes must be carefully analyzed.

The Supernova-Type Light Curve

Some models for the energy generation mechanisms for compact objects employ the occurrence of one or more supernovae. One of the arguments against this proposition is that few outburst light curves resemble those of classical supernovae. The long "tail" of these events is not seen.

Figure 4 shows a schematic representation of a type I supernova light curve (Zwicky, 1964) given in normalized luminosity. The points span the period of time during which the luminosity is between 16% and 100%. Even without any background contribution to mask the event, it appears quite symmetric. If one were to add observational scatter, less regular data spacing and a background of only 15% of the peak luminosity, the "tail" would be undetectable and the remaining, less pronounced asymmetry would be masked as well. This fabricated event would remain basically smooth in its rise and decline, however, which is not usually observed in compact object events. It should be remembered though that galactic supernovae are relatively isolated, while the physical conditions in the nuclei of Seyfert galaxies and QSO's are not likely to be so quiescent and uniform.

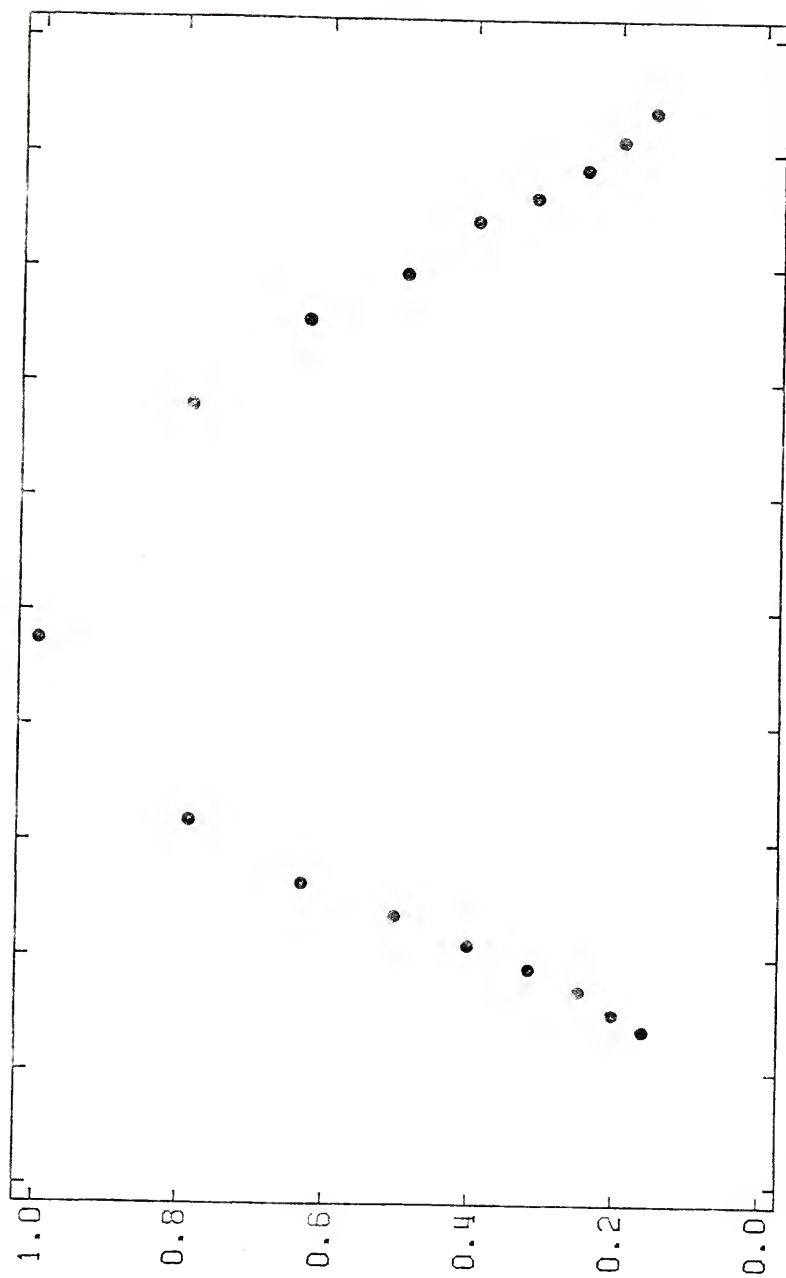


Figure 4. Normalized event luminosity curve for a type I supernova.

Individual Event Morphologies

One qualitative morphological measure of the events shown in Appendix C was made. For luminosities of 20%, 40%, 60%, and 80%, the fraction of the event duration spent at or above each level was determined. In some cases the luminosity dropped below a given level only to rise above it again. In that case the partial durations above that level were summed to obtain the final result.

Table 6 lists, by event, the decimal fraction of the event spent at or above each level. Several events are not included in this table because they are relatively incomplete (i.e., the ingress or decline is not well documented). Values followed by a colon indicate less severe, but still significant incompleteness.

A symmetrical, linear rise and decline would yield values of .80, .60, .40 and .20 for levels of 20%, 40%, 60% and 80%, respectively. It should be mentioned that it is possible to devise more complicated event shapes which would yield these same results, but a glance at their normalized flux curve would quickly reveal their true nature. There are only three well-sampled events in Table 6 which match these values reasonably well (0735+17 A, 3C 345 E and NRAO 512 C). The rates of energy release are thus generally non-linear. The supernova light curve in Figure 4 yields values of .85, .70, .56 and .40 for an event duration of 45 days. Only one event (3C 371 B, .89, .78, .55, .15, 49.363 days) matches these values relatively well, although its 80% duration is rather short. In addition, its light curve shows a pair of peaks (100%, 95%) separated by a decline to below 60%.

TABLE 6
FRACTIONAL FLUX DURATIONS

=====						
Event		Duration	20%	40%	60%	80%
		days	-----			
0039+40	A	375.460	.72	.36	.17	.03
3C 66A	A	115.369	.69	.09	.05	.01
0235+164	A	49.676	.87	.67	.22	.11
	B	175.497	.10	.04	.03	.02
	C	91.093	.15	.11	.07	.04
	D	76.566	.73	.31	.16	.06
0420-01	A	319.263	.71	.31	.17	.07
	B	370.230	.78	.52	.22	.05
	C	310.808	.13	.03	.02	.01
NRAD 190	A	44.774	.69	.52	.35	.17
	B	44.184	.54	.36	.24	.12
0521-36	A	704.265	.50	.41	.19	.11
	B	117.536	.96	.68	.44	.22
0735+17	A	71.090	.82	.57	.40	.16
	B	147.971	.89	.42	.13	.02
	C	394.044	.75	.19	.08	.01
0J 287	A	107.736	.82	.60	.23	.01
	B	129.456	.75	.47	.26	.08
	C	112.051	.76	.47	.20	.08
	D	1167.001	.70	.28	.17	.01
0906+01	A	18.334	.94	.79	.63	.35
	B	32.623	.81	.67	.31	.05
	C	14.900	.65	.42	.27	.18
1156+295	A	51.505	.45	.27	.18	.09
NGC 4151	A	512.849	.94	.53	.18	.04
3C 279	A	33.200	.64	.41	.20	.07
	B	78.700	.29	.20	.14	.04
	C	789.337	.07	.02	.01	.01
1308+326	A	70.578	.95	.71	.14	.07
	B	92.599	.80	.52	.16	.04
	C	30.025	.46	.27	.15	.03
	D	40.519	.65	.33	.21	.12

TABLE 6 (continued)

Event		Duration days	20%	40%	60%	80%
1510-08	A	94.783	.66	.37	.19	.05
1545+21	A	192.769	.79	.55	.29	.14
4C 38.41	A	11.016	.74	.55	.36	.18
NRAO 512	A	2.346	.69	.45	.30	.15
	B	11.500	.82	.64	.43	.07
	C	1.623	.69	.52	.35	.18
	D	13.903	.87	.39	.10	.03
	E	42.991	.68	.41	.28	.01
	F	23.456	.84	.61	.37	.14
	G	18.398	.63	.23	.15	.11
	H	281.532	.80	.35	.15	.01
3C 345	A	28.777	.87	.38	.07	.03
	B	18.909	.52	.34	.21	.10
	C	8.803	.82	.58	.38	.17
	D	29.323	.79	.62	.45	.14
	E	21.304	.89	.55	.43	.28
	F	95.925	.45	.21	.01	.01
	G	34.389	.77	.21	.08	.05
	H	409.292	.63	.25	.06	.03
NRAO 530	A	73.541	.25	.02	.01	.01
	B	23.593	.67	.38	.19	.10
3C 371	A	44.824	.64	.24	.09	.03
	B	49.363	.89	.78	.55	.15
BL LAC	A	83.983	.67	.59	.32	.02
	B	7.699	.68	.58	.42	.26
	C	28.718	.98	.82	.66	.31
3C 446	A	491.880	.46	.22	.09	.01
	B	173.860	.88	.40	.04	.02
	D	637.205	.66	.33	.13	.12
3C 454.3	A	158.436	.62	.25	.07	.03
	B	75.214	.95	.71	.51	.23
2345-16	A	386.983	.30	.17	.05	.01

A careful examination of the light curves presented in Appendix C reveals little to suggest that there is any typical shape to these events. This is borne out as well by the diversity in the duration fractions presented in Table 6. Even for events occurring in the same object, there is no apparent pattern. This is reminiscent of the situation for the long-term light curves of compact objects and suggests that there is little order or regularity in the emission and/or radiation transfer process.

For some events (e.g. 1308+326 C, 3C 345 B and BL Lac B) the decline from maximum luminosity is much steeper than the rise phase. It is difficult to come up with an "explosive" type of energy generation mechanism which will display this characteristic. If the variations are due to the covering and uncovering of a constant source by obscuring clouds of material, this type of behavior could be produced. The edges of the "holes" would have to be rather sharply defined to produce the type of events such as 0235+164 B, 0420-01 C and NRAO 530 A. Large variations in optical depth are required as well to account for such large luminosity changes. In addition, events which are correlated over a large frequency range require "material" which is opaque to that entire range. Delayed correlations would present even larger problems to any obscuration model.

What is the relative position of the point of peak luminosity in these events; that is does the event peak early, late, or is it symmetric? Examination of the light curves by eye gives 8 which peak early, 27 symmetric, 14 late and 18 inconclusive. This again points out the diversity of these events.

Individual Event Comments

Given below are a few descriptive comments for each of the events. The term "consecutive" implies that the end point of one event marks the beginning of the next event.

- 0039+40 A Multiple peaks.
- 3C 66A A Very fast rise, decline to 40%.
- 0235+164 A -
- B Very sharp peak, actual event shorter?
- C Same as above.
- D Multiple peaks.
- 0420-01 A Dual peak.
- B B and C are consecutive.
- C Sharp peak, actual event shorter?
- NRAO 190 A A and B quite similar.
- B -
- 0521-36 A -
- B Very symmetric.
- 0735+17 A Shape similar to type I supernova.
- B Two events?
- C At least two sharp peaks.
- OJ 287 A Multiple peaks, incomplete decline.
- B Fast rise, slow decline.
- C Slow rise, quicker decline, multiple peaks.
- D Longest duration event, contains B
- 0906+01 A -
- B Dual peaks.
- C -

- 1156+295 A Secondary peak.
- NGC 4151 A Ingress incomplete.
- 3C 279 A Triple peak.
- B Actual event shorter?
- C Contains A and B, questionable event.
- 1308+326 A Incomplete ingress, secondary peak.
- B Complex, multiple peaks
- C Very rapid decline.
- D -
- 1510-08 A Two events?
- 1545+21 A -
- NRAO 512 A A,B,C, and D are consecutive.
- B. Incomplete ingress, two events?
- C Shortest event, 1.6 days, 2 magnitudes.
- D Multiple peaks.
- E Incomplete decline, two events?
- F F and G are consecutive.
- G -
- H Extremely complex, contains E,F and G.
- 3C 345 A Sharp decline.
- B Sharp decline.
- C -
- D -
- E -
- F Very sharp peak.
- G Complex multiple peaks.
- H Contains B,C,D and E.

- NRAO 530 A Extremely sharp peak, actual event shorter?
 B Double peak.
- 3C 371 A Sharp rise, slow decline.
 B. Decline incomplete.
- BL LAC A Flat topped event.
 B Flat topped event.
 C Two events?
- 3C 446 A Very active, 6-8 sharp peaks.
 B Multiple peaks, ingress incomplete.
 C Decline only, sharp drop, dual peaks.
 D Late peak, precipitous decline.
 E Ingress only.
- 3C 454.3 A Multiple sharp peaks, ingress poorly defined.
 B Slow ingress, decline incomplete.
- 2345-16 A Dual sharp peaks.

Matese and Whitmire (1978) have discussed the effects of strong gravity on the optical appearance of rapidly fluctuating astronomical sources. In their model of a delta function profile flash occurring in the vicinity of a strong gravitational source, the flash is modified such that the observer (depending on his orientation with respect to the flash position) sees a broadened event. For some orientations a second event is observed as a result of photons initially traveling away from the observer having their paths bent around the mass and back toward the observer. Secondary brightenings are fairly common, but are of a much larger amplitude than the 1% expected from the above model. Satellite observatories, such as the Space Telescope could potentially detect such secondary events.

Variability and Emitting Region Sizes

Knowledge of the absolute physical dimensions of the region where emission occurs in these objects is crucial to the determination of volume dependent quantities such as particle and energy densities. Linear dimension estimations (equated to such quantities as the Schwarzschild radius of a black hole) are extremely important as well. For sources which are not expanding relativistically, upper limits to the emitting region sizes are usually estimated using luminosity variations and light travel time arguments. Often the limiting diameter of the region responsible for an observed variation is given as

$$D < c\Delta T / (1+z)$$

where c is the speed of light, ΔT is the duration of the observed variation and z is the redshift. The use of this approximation has become widespread, but in some cases it has been employed in situations where it is no longer valid. Terrell (1967) derived a more precise expression for this limiting diameter as

$$D < \frac{4c\Delta T}{\pi(1+z)} \frac{\bar{L}}{\Delta L}$$

which reduces to

$$D < 1.2732 \Delta T_0 (\bar{L}/\Delta L)$$

where ΔT_0 is in rest frame days, \bar{L} is the average luminosity during the variation, ΔL is the luminosity change and D is the diameter of the emitting region in light days. This formulation takes into account not only the timescale of the variation, but also the fractional variation as well. For a relatively small luminosity change (a small change in the object's magnitude) the quantity in parentheses can become quite significant. We rewrite the above equation as

$$D < k(\bar{L}, \Delta L) \Delta T_0$$

Table 7 shows the variation of $k(\bar{L}, \Delta L)$, the fractional luminosity factor, for various changes in object magnitude.

TABLE 7
FRACTIONAL LUMINOSITY FACTOR

Δm	L_2/L_1	$k(\bar{L}, \Delta L)$	V
0.01	1.0093	137.5	2.6 [06]
0.02	1.0186	69.1	3.3 [05]
0.05	1.0471	27.7	2.1 [04]
0.10	1.0965	13.8	2.6 [03]
0.20	1.2023	6.9	3.3 [02]
0.50	1.5849	2.8	2.2 [01]
1.00	2.5119	1.5	3.2 [00]
1.63	4.5040	1.0	1.0 [00]
2.00	6.3096	0.9	6.7 [-01]
4.00	39.8107	0.7	3.0 [-01]

For very small magnitude changes the factor k can be larger than 100. An object which is observed to vary 0.02 magnitudes in 5 minutes (0.0035 days) has a maximum emitting region size of 0.24 light days, not 0.0035 light days as the original simple formulation would imply. As shown in the last column of Table 7, this represents a volume factor, V , of 3.3 [05] in the volume of the emitting region. Values of volume dependent quantities based on the simpler diameter estimation will thus be a factor of 3.3 [05] too large. Only for a variation of 1.63 magnitudes will the simpler form be correct, and for very large variations it leads to an overestimation of the emitting region size.

In terms of the object parameters previously discussed, for two measurements a and b , we have

$$\bar{L}_{ab} = (L_a + L_b)/2$$

$$\Delta L_{ab} = |L_a - L_b|$$

Substituting these values into the expression for D gives

$$D < 0.6366 \Delta T_0 (L_a + L_b) / |L_a - L_b|$$

For a given event, the minimum value for the emitting region diameter will occur when $\Delta T_0 \bar{L} / \Delta L$ is a minimum. Table 8 presents this limiting diameter for the emitting region (in light days and in cm) as well as the log of the variability timescale t_v in seconds for each of the objects in this study. The values for certain objects are larger than some previously quoted values. This results, in part, from the effect of the fractional luminosity factor in the expression for D as well as from the fairly strict criterion for a "statistically significant variation."

Bolometric Luminosities

As with physical dimensions, a knowledge of the total energy emitted by these objects is most important in both directly and indirectly distinguishing between potential models for their structure and energy generation and transfer mechanisms.

There are many difficulties involved in the accurate determination of this quantity, which we will refer to as B_L from now on. Two important questions are; what does the complete spectrum of the object look like and how does the shape and level of this spectrum change when an event, such as those under study here, occurs?

There are certain regions of the spectrum which are inaccessible to ground based observations. One is between 1 [12] and 1 [14] Hz and the other is >1 [15] Hz. Satellite observations have begun to fill in the latter, but the former remains relatively unexplored. As indicated by

TABLE 8
 EMITTING REGION SIZES AND VARIABILITY TIMESCALES

Event		Emitting Region Size 1. days	cm	log (t_v) sec.
0039+40	A	12.69	3.29 [16]	6.04
3C 66A	A	4.21	1.09 [16]	5.56
0235+164	A	6.75	1.75 [16]	5.77
	B	0.72	1.87 [15]	4.79
	C	0.79	2.05 [15]	4.83
	D	1.86	4.81 [15]	5.21
0420-01	A	12.22	3.17 [16]	6.02
	B	16.05	4.16 [16]	6.14
	C	3.18	8.25 [15]	5.44
NRAD 190	A	7.70	2.00 [16]	5.82
	B	3.62	9.39 [15]	5.50
0521-36	A	42.03	1.09 [17]	6.56
	B	66.14	1.71 [17]	6.76
0735+17	A	4.09	1.06 [16]	5.55
	B	0.71	1.85 [15]	4.79
	C	2.16	5.59 [15]	5.27
0J 287	A	2.43	6.30 [15]	5.32
	B	0.54	1.39 [15]	4.67
	C	0.38	9.83 [14]	4.54
	D	0.54	1.39 [15]	4.67
0906+01	A	5.32	1.38 [16]	5.66
	B	1.41	3.65 [15]	5.09
	C	5.30	1.37 [16]	5.66
1156+295	A	0.20	5.05 [14]	4.22
NGC 4151	A	10.86	2.82 [16]	5.97
3C 279	A	2.24	5.82 [15]	5.29
	B	2.66	6.90 [15]	5.36
	C	1.40	3.64 [15]	5.08
1308+326	A	5.82	1.51 [16]	5.70
	B	0.23	5.97 [14]	4.30
	C	0.80	2.06 [15]	4.84
	D	4.50	1.16 [16]	5.59

TABLE 8 (continued)

Event		Emitting Region Size l. days	cm	log (t_v) sec.
1510-08	A	2.47	6.40 [15]	5.33
1545+21	A	175.54	4.55 [17]	7.18
4C 38.41	A	3.35	8.69 [15]	5.46
NRAO 512	A	0.62	1.62 [15]	4.73
	B	0.57	1.49 [15]	4.69
	C	0.44	1.13 [15]	4.58
	D	1.77	4.58 [15]	5.18
	E	1.74	4.50 [15]	5.18
	F	16.95	4.39 [16]	6.17
	G	6.67	1.73 [16]	5.76
	H	1.74	4.50 [15]	5.18
3C 345	A	4.28	1.11 [16]	5.57
	B	2.82	7.30 [15]	5.39
	C	1.10	2.84 [15]	4.98
	D	24.75	6.41 [16]	6.33
	E	5.63	1.46 [16]	5.69
	F	0.34	8.82 [14]	4.47
	G	1.90	4.93 [15]	5.22
	H	1.10	2.84 [15]	4.98
NRAO 530	A	0.64	1.67 [15]	4.74
	B	1.07	2.76 [15]	4.97
3C 371	A	2.28	5.90 [15]	5.29
	B	2.71	7.02 [15]	5.37
BL LAC	A	0.49	1.27 [15]	4.63
	B	1.82	4.71 [15]	5.20
	C	2.74	7.11 [15]	5.37
3C 446	A	0.44	1.13 [15]	4.58
	B	2.82	7.32 [15]	5.39
	C	0.79	2.05 [15]	4.83
	D	1.22	3.18 [15]	5.02
	E	45.03	1.17 [17]	6.59
3C 454.3	A	1.27	3.29 [15]	5.04
	B	21.55	5.58 [16]	6.27
2345-16	A	1.70	4.40 [15]	5.17

Oke et al. (1970), estimation of B_L depends strongly on this region and extrapolation to it using the optical and radio spectral indices can lead to quite different results.

Many compact extragalactic objects are known to vary from the radio to the X-ray regions, although not necessarily simultaneously. Thus, to obtain an accurate representation of the instantaneous spectrum, observations at all frequencies must be made at nearly the same time. Because satellite time is limited and usually assigned months in advance, such simultaneity is difficult to achieve. It is even more difficult if one wishes to obtain such a spectrum during a large outburst.

Correlated optical-radio variability has been examined for a large sample of these objects by Pomphrey et al. (1976) and Balonek (1981). Certain OVV's (0235+164, 0420-01, OJ 287 e.g.) have shown a high degree of correlation, but many others have not. During the recent optical outburst of 1156+295 Bregman (1982) observed a similar brightening in the near and far UV regions accessible to the IUE (International Ultraviolet Explorer satellite). No X-ray observations of this event were possible since the Einstein satellite malfunctioned several months earlier. Little is known at present about correlated X-ray-optical variability.

Ground based and airborne investigations in the infrared, such as those of Rieke and Kinman (1974), Rieke et al. (1976), O'Dell et al. (1978) and Moore et al. (1980), suggest that from the optical out to 3-10 microns variations are well correlated and of similar amplitude. For OJ 287 identical rates of decrease of flux at 0.44 and 10.5 microns were found over a two-year period, during which the object's brightness

decreased by a factor of 15. It should be kept in mind that these are observed, rather than emitted, wavelengths.

B_L Lower Limits

From present evidence it is reasonable to assume that when an increase of flux is observed in the B-bandpass (0.44 microns), that a similar increase will be seen, in the rest frame of the object, at least between 0.2 and 2.0 microns. For the object in our sample with the largest redshift, 4C 38.41 at $z=1.814$, the radiation emitted between those limits will be observed between 0.56 and 5.6 microns. This is within the limits of typical correlated variability.

Integration of the flux distribution between 0.2 and 2.0 microns will yield a lower limit to the bolometric luminosity. This limit is actually fairly conservative, excluding radio, far-IR and X-ray regions, but until complete spectra can be obtained during an outburst, the relative contributions of these regions are difficult to assess.

Calculation of B_L

For power-law spectra, calculation of B_L is straightforward. If significant curvature is present, the procedure given below must be modified somewhat. Curvature implies that the spectral index is a function of frequency. For 0235+164, Rieke et al. (1976) pointed out that between 10.6 and 0.36 microns (5.7 and 0.19 microns in the rest frame) the spectral index ranged from 1.49 to 4.14. The spectra of three objects were divided, in this work, into two sections, 0.2-0.6 and 0.6-2.0 microns. The infrared spectral indices were obtained from O'Dell et al. (1978) and were 1.00, 0.64 and 0.86 for 0235+164, 0735+17

and BL Lac, respectively. The spectra of these objects were then treated as two separate power laws between the above defined limits.

For a power-law spectrum we have

$$L(\nu) = k\nu^{-\alpha}$$

The value of the constant k is given by

$$k = (1.199 [15])^\alpha L_{25} \text{ Hz}^\alpha \text{ ergs/sec}$$

where L_{25} is the known luminosity at a rest wavelength of 2500Å, which corresponds to a frequency of 1.199 [15] Hz. The total luminosity over the desired frequency range is then given by

$$\begin{aligned} B_L &= \int_{\nu_1}^{\nu_2} L(\nu) d\nu \\ &= k \int_{\nu_1}^{\nu_2} \nu^{-\alpha} d\nu \\ &= [k/(1-\alpha)](\nu_2^{-\alpha+1} - \nu_1^{-\alpha+1}) \quad \text{for } \alpha \neq 1 \\ &= k(\log \nu_2 - \log \nu_1) \quad \text{for } \alpha = 1 \end{aligned}$$

It is necessary then to supply α and L_{25} and perform the integration. The limits of integration will be taken as 1 [14] to 1 [15] Hz (between 2 and .2 microns).

Table 9 lists the results of these calculations for each of the events. Column 2 gives the peak bolometric luminosity (as we have defined it), in ergs/sec, and column 3 gives the total energy, in ergs, emitted during each event. Listed in columns 4 and 5 are the logs of the variability timescales t_l and t_v which will be discussed later.

The peak luminosity recorded for any object in this sample was 1.23 [49] ergs/sec during the 1975 outburst of 0235+164, and this was

TABLE 9
EVENT LUMINOSITIES AND ENERGIES

=====					
Event		L ergs/sec	E _e ergs	log (t _l) sec.	log (t _v) sec.

0039+40	A	3.71 [44]	2.32 [51]	2.79	6.04
3C 66A	A	8.11 [46]	1.23 [53]	5.13	5.56
0235+164	A	1.23 [49]	2.48 [55]	7.31	5.77
	B	1.05 [49]	1.71 [55]	7.24	4.79
	C	2.09 [48]	2.65 [54]	6.54	4.83
	D	2.40 [48]	4.80 [54]	6.60	5.21
0420-01	A	2.75 [46]	2.20 [53]	4.66	6.02
	B	3.89 [46]	4.45 [53]	4.81	6.14
	C	6.01 [46]	1.81 [53]	5.00	5.44
NRAD 190	A	3.57 [46]	4.91 [52]	4.77	5.82
	B	2.57 [46]	2.79 [52]	4.63	5.50
0521-36	A	1.75 [45]	2.49 [52]	3.46	6.56
	B	9.77 [44]	3.34 [51]	3.21	6.76
0735+17	A	5.13 [46]	1.17 [53]	4.93	5.55
	B	9.77 [46]	3.89 [53]	5.21	4.79
	C	1.53 [47]	1.15 [54]	5.40	5.27
0J 287	A	1.07 [47]	3.71 [53]	5.25	5.32
	B	9.55 [46]	3.03 [53]	5.20	4.67
	C	2.29 [46]	5.58 [52]	4.58	4.54
	D	2.65 [47]	6.56 [53]	5.64	4.67
0906+01	A	9.21 [46]	5.99 [52]	5.18	5.66
	B	7.59 [46]	6.40 [52]	5.10	5.09
	C	5.50 [46]	1.59 [52]	4.96	5.66
1156+295	A	1.05 [48]	1.28 [54]	6.24	4.22
NGC 4151	A	2.08 [43]	3.51 [50]	1.54	5.97
3C 279	A	1.58 [48]	1.36 [54]	6.42	5.29
	B	3.16 [48]	4.34 [54]	6.72	5.36
	C	3.16 [48]	1.78 [55]	6.72	5.08
1308+326	A	5.01 [47]	1.28 [54]	5.92	5.70
	B	3.24 [47]	8.48 [53]	5.73	4.30
	C	3.98 [47]	2.40 [53]	5.82	4.84
	D	1.86 [47]	2.16 [53]	5.49	5.59

TABLE 9 (continued)

Event		L ergs/sec	E _e ergs	log (t _l) sec.	log (t _v) sec.
1510-08	A	4.77 [47]	1.22 [54]	5.90	5.33
1545+21	A	3.25 [45]	9.38 [50]	3.73	7.18
4C 38.41	A	5.27 [47]	1.78 [53]	5.94	5.46
NRAD 512	A	1.32 [47]	8.89 [51]	5.34	4.73
	B	7.59 [46]	2.57 [52]	5.10	4.69
	C	1.77 [47]	9.45 [51]	5.47	4.58
	D	6.46 [46]	1.87 [52]	5.03	5.18
	E	1.00 [47]	1.14 [53]	5.22	5.18
	F	9.12 [46]	5.83 [52]	5.18	6.17
	G	8.13 [46]	2.43 [51]	5.13	5.76
	H	1.00 [47]	7.77 [53]	5.22	5.18
3C 345	A	2.69 [46]	1.28 [52]	4.65	5.57
	B	2.63 [46]	7.14 [51]	4.64	5.39
	C	5.75 [46]	1.16 [52]	4.98	4.98
	D	4.17 [46]	2.29 [52]	4.84	6.33
	E	5.37 [46]	2.61 [52]	4.95	5.69
	F	5.25 [46]	8.03 [52]	4.94	4.47
	G	8.49 [46]	5.33 [52]	5.15	5.22
	H	5.75 [46]	5.39 [53]	4.98	4.98
NRAD 530	A	2.35 [47]	1.76 [53]	5.59	4.74
	B	7.94 [46]	4.59 [52]	5.12	4.97
3C 371	A	2.89 [45]	3.76 [51]	3.68	5.29
	B	2.45 [45]	2.16 [51]	3.61	5.37
BL LAC	A	6.04 [45]	1.47 [52]	4.00	4.63
	B	3.09 [45]	7.05 [50]	3.71	5.20
	C	4.90 [45]	6.44 [51]	3.91	5.37
3C 446	A	1.17 [48]	1.10 [55]	6.29	4.58
	B	7.59 [47]	4.00 [54]	6.10	5.39
	C	1.45 [48]	2.59 [53]	6.38	4.83
	D	1.58 [48]	2.81 [55]	6.42	5.02
	E	6.46 [47]	1.65 [54]	6.03	6.59
3C 454.3	A	1.43 [47]	3.66 [53]	5.38	5.04
	B	1.29 [47]	1.75 [53]	5.33	6.27
2345-16	A	2.88 [46]	1.45 [53]	4.68	5.17

nearly equaled (1.05 [49]) during the subsequent event. Only three other objects have exceeded 1 [48], 1156+295, 3C 279 and 3C 446. Representative of the lower end of the peak luminosities recorded are the compact galaxies NGC 4151 (2.09 [43]), 0039+40 (3.72 [44]) and 0521-36 (1.74 [45]). In terms of peak luminosities the fainter end of the quasar-BL Lac group merges with the brighter end of the compact galaxies. The total range of peak luminosities spans almost six orders of magnitude.

The bolometric event energies give the total energy (in ergs) radiated during the event, corrected for the object's base level. These values range from 3.51 [50] ergs for NGC 4151 A to 2.81 [55] for 3C 446 D. What these luminosities and energies represent in terms of mass conversion will be examined in the next chapter.

The third column of Table 9 gives the log of the minimum variability timescale parameter (t_ℓ) devised by Fabian and Rees (1979) for a spherically symmetric, homogeneous cloud of radiating matter. The shortest timescale for variability occurs when the optical depth of the cloud is unity and is given by

$$t_\ell = 5 [-43] B_L / f \text{ seconds}$$

where B_L is the bolometric luminosity as defined earlier, and f is the mass to energy conversion efficiency factor. Here f was taken as 0.3, a value referred to again in the section on black hole accretion. Reducing f will, of course, increase t_ℓ for a given B_L . Values of the log of t_ℓ for each event are given in column 3 of Table 9. Column 4 gives the log of the variability timescale, t_v , derived from observation.

Thirteen of the sources (27 of the events) show values of $\log(t_v)$ which are more than 0.2 less than their corresponding $\log(t_\lambda)$, with the largest difference being 2.4, that is, 250 times shorter than expected. Significantly, perhaps, none of these discrepant objects are galaxies. The value of t_λ could be lowered a bit by increasing f , but f must remain less than 1 so this does not provide much help. If only one or two objects were involved, one might suspect the values of B_L , but this is not the case. It seems that this simple model of Fabian and Rees (1979) does not apply to a significant number of these sources. At this point we will begin to examine various proposed mechanisms and models for these objects.

CHAPTER VI COMPARISONS WITH THEORETICAL MODELS

Much of the focus of early theoretical studies into the quasar phenomenon was directed towards explaining the enormous energy generation rates, the shapes of the optical and radio continua and the creation of the emission and absorption features. Only more recently has there been an increase in the number of models which attempt to account for variability as well. Given below is a summary of the major past and present models.

(a) Massive Black Holes

- i. Spherical accretion
- ii. Disk accretion-general
- iii. Disk oscillation and accretion
- iv. Disk hot spots and flares
- v. Beamed radiation models

(b) Supermassive Rotating Magnetoplasmonic Bodies

- i. Giant pulsars
- ii. Non-degenerate oblique rotators

(c) Compact Star Clusters (Multiple Supernovae)

(d) Esoteric Models

- i. Matter-antimatter annihilation
- ii. Quark fusion
- iii. White holes
- iv. Plasma laser stars

The presently most accepted category of models is the first one, and this category also provides a majority of the tests applicable to the variability data presented in this work. Categories (b) and (c) will be briefly examined, while the esoteric models given in category (d) are

generally not sufficiently developed to predict variability characteristics.

General Energy and Emission Constraints

Almost all of the present models invoke the mechanism of incoherent synchrotron emission from electrons as the source of the non-thermal continuum. Early on, Hoyle et al. (1966) pointed out that, for the energy densities apparently existing in these objects, inverse Compton scattering could compete with the synchrotron process. The energy densities were determined assuming isotropic emission of radiation, emission region sizes calculated on the basis of variability timescales and cosmological origin of the redshifts. Unless the magnetic energy density exceeds the radiation energy density, inverse Compton losses in these objects would be prohibitive. Field strengths of thousands of gauss were necessary to avoid these losses. The constraints could be eased by "moving" the objects closer than their cosmological z would imply, by invoking non-isotropic emission and bulk relativistic motions. As mentioned earlier, the first of these suggestions is still a source of intense debate.

Columns 2 and 3 of Table 10 list, for each event, the log of the radiation density (in ergs/cm) for the peak event luminosity and for the average event luminosity. Emitting volumes were derived from observed variability timescales. In some cases the values in column 3 exceed 1 [06]. Columns 4 and 5 list the logs of the magnetic field strength in gauss such that the inverse Compton losses just balance the synchrotron emission, that is:

TABLE 10
EVENT ENERGY DENSITIES AND MAGNETIC FIELDS

Event		Energy Densities		Magnetic Fields	
		Log Peak	Log Avg.	Log Peak	Log Avg.
		- - - ergs/sec - - -	- - -	- - - gauss - - -	- - -
0039+40	A	0.44	0.24	0.92	0.82
3C 66A	A	3.74	3.51	2.57	2.45
0235+164	A	5.50	5.19	3.45	3.30
	B	7.39	6.55	4.40	3.98
	C	6.61	6.07	4.01	3.74
	D	5.91	5.51	3.66	3.46
0420-01	A	2.35	2.01	1.88	1.70
	B	2.26	1.95	1.83	1.68
	C	3.85	3.17	2.63	2.28
NRAD 190	A	2.86	2.60	2.13	2.00
	B	3.36	3.02	2.38	2.21
0521-36	A	0.07	-0.21	0.74	0.60
	B	-0.58	-0.71	0.41	0.34
0735+17	A	3.56	3.36	2.48	2.38
	B	5.36	5.08	3.38	3.24
	C	4.59	4.14	3.00	2.77
DJ 287	A	4.34	4.01	2.87	2.70
	B	5.59	5.34	3.50	3.37
	C	5.23	5.01	3.32	3.20
	D	6.03	4.47	3.72	2.93
0906+01	A	3.59	3.48	2.50	2.44
	B	4.65	4.45	3.03	2.93
	C	3.37	3.21	2.39	2.31
1156+295	A	7.53	7.02	4.47	4.21
NGC 4151	A	-0.67	-1.00	0.37	0.20
3C 279	A	5.57	5.25	3.49	3.32
	B	5.73	5.10	3.57	3.25
	C	6.29	5.23	3.85	3.31
1308+326	A	4.25	3.94	2.83	2.67
	B	6.86	6.50	4.13	3.95
	C	5.87	5.37	3.64	3.38
	D	4.04	3.63	2.72	2.52

TABLE 10 (continued)

Event	Energy Densities		Magnetic Fields	
	Log Peak	Log Avg.	Log Peak	Log Avg.
	- - ergs/sec - - -		- - - gauss - - -	
1510-08 A	4.97	4.53	3.18	2.97
1545+21 A	-0.90	-2.01	0.25	-0.31
4C 38.41 A	4.75	4.53	3.08	2.96
NRAO 512 A	5.61	5.33	3.51	3.37
B	5.45	5.27	3.43	3.34
C	6.04	5.76	3.72	3.58
D	4.40	4.20	2.90	2.80
E	4.59	4.23	3.00	2.82
F	2.57	2.40	1.99	1.90
G	3.34	2.11	2.37	1.75
H	4.59	4.24	3.00	2.82
3C 345 A	3.24	3.02	2.32	2.21
B	3.59	3.38	2.50	2.39
C	4.75	4.61	3.08	3.00
D	1.91	1.80	1.66	1.60
E	3.30	3.18	2.35	2.29
F	5.73	5.27	3.57	3.33
G	4.44	4.17	2.92	2.79
H	4.75	4.36	3.08	2.88
NRAO 530 A	5.84	5.13	3.62	3.27
B	4.91	4.59	3.16	3.00
3C 371 A	2.83	2.65	2.12	2.02
B	2.60	2.39	2.00	1.89
BL LAC A	4.47	4.17	2.94	2.78
B	3.04	2.87	2.22	2.13
C	2.90	2.76	2.15	2.08
3C 446 A	6.86	6.29	4.13	3.84
B	5.05	4.68	3.23	3.04
C	6.45	5.80	3.93	3.60
D	6.11	4.31	3.76	2.86
E	2.58	----	1.99	----
3C 454.3 A	5.03	4.75	3.22	3.07
B	2.52	----	1.96	----
2345-16 A	4.07	3.54	2.74	2.47

$$\rho_R = \rho_M = B^2/8\pi$$

Average magnetic field strengths often reached 1 [03] gauss, on the same order of magnitude as that found in sunspots, but over a vastly larger region.

A second, recently determined, constraint concerns an analog for electrons of the optical depth for photons. Cavaliere and Morrison (1980) point out that when

$$L_{45}/R_{15} > 1$$

(where L_{45} is the bolometric luminosity in units of $1 [45]$ ergs and R_{15} is the emitting region size in units of $1 [15]$ cm) electrons will undergo repeated scatterings as they traverse the emission region. Strong replenishment of the electron energies is then crucial for highly variable sources, independently of the nature of their non-thermal radiation emission mechanism.

Table 11 lists the values of L_{45}/R_{15} for each event. The values range from 1 [-03] to 5 [03], indicating that re-acceleration mechanisms are required in some but not all of these objects. Cavaliere and Morrison point out that constant injection of new, high energy electrons results in a density of "spent" electrons which would wash out rapid variability, high polarization and even power-law spectral shapes.

Reduction of the implied luminosity by employing radiating needle beam models (e.g. Blandford and Rees, 1979) would lower the values of L_{45}/R_{15} . For the largest determined values of L_{45}/R_{15} in Table 11 this directivity would have to be very large. One consequence of this type of model, an implied correlation between shorter variability timescales and higher luminosity, is examined later in this chapter.

TABLE 11
EVENT PARAMETERS III

Event		L_{45} / R_{15}	$\text{Log } (T_e / t^{3/2})$
0039+40	A	1.12 [-02]	--
3C 66A	A	7.41 [00]	--
0235+164	A	7.08 [02]	-6.96
	B	5.62 [03]	-4.94
	C	1.02 [03]	-5.29
	D	5.01 [02]	-5.93
0420-01	A	8.71 [-01]	-6.53
	B	9.33 [-01]	-6.64
	C	7.24 [00]	-5.67
NRAD 190	A	1.78 [00]	-7.08
	B	2.75 [00]	-6.60
0521-36	A	1.58 [-02]	-6.99
	B	5.75 [-03]	-8.07
0735+17	A	4.79 [00]	-6.47
	B	5.25 [01]	-5.01
	C	2.69 [01]	-5.31
0J 287	A	1.70 [01]	-5.95
	B	6.92 [01]	-4.89
	C	2.34 [01]	-4.76
	D	1.91 [02]	-3.94
0906+01	A	6.61 [00]	-7.23
	B	2.09 [01]	-6.12
	C	3.98 [00]	-7.32
1156+295	A	2.09 [03]	--
NGC 4151	A	7.41 [-04]	--
3C 279	A	2.75 [02]	-6.41
	B	4.57 [02]	-6.14
	C	8.71 [02]	-4.72
1308+326	A	3.31 [01]	-6.70
	B	5.37 [02]	-4.48
	C	1.95 [02]	-5.78
	D	1.62 [02]	-6.78

TABLE 11 (continued)

Event		L_{45} / R_{15}	$\text{Log } (T_e / t^{3/2})$
1510-08	A	7.41 [01]	--
1545+21	A	7.08 [-03]	--
4C 38.41	A	6.03 [01]	--
NRAD 512	A	8.13 [01]	-6.73
	B	5.13 [01]	-5.97
	C	1.58 [02]	-6.83
	D	1.41 [01]	-6.63
	E	2.24 [01]	-6.14
	F	2.09 [00]	-7.88
	G	4.68 [00]	-7.38
	H	2.24 [01]	-5.32
3C 345	A	2.40 [00]	-6.90
	B	3.63 [00]	-6.81
	C	2.04 [01]	-6.53
	D	6.46 [-01]	-8.03
	E	3.72 [00]	-7.21
	F	5.89 [01]	-4.72
	G	1.74 [01]	-6.29
	H	2.04 [01]	-4.86
NRAD 530	A	1.41 [02]	-5.24
	B	2.88 [01]	-6.08
3C 371	A	4.90 [-01]	-6.28
	B	9.12 [-01]	-6.36
BL LAC	A	4.79 [00]	-5.02
	B	6.61 [-01]	-6.91
	C	6.92 [-01]	-6.60
3C 446	A	1.05 [03]	-4.18
	B	1.05 [02]	-5.84
	C	7.08 [02]	-5.04
	D	5.01 [02]	-4.73
	E	5.49 [00]	--
3C 454.3	A	4.37 [01]	-5.36
	B	2.29 [00]	--
2345-16	A	6.61 [00]	--

Black Hole Models

Accretion of matter onto a supermassive black hole has been and remains the most popular model for compact sources. Various models of this type have been examined by Salpeter (1964), Lynden-Bell (1969), Lynden-Bell and Rees (1971), Hills (1975), Shields and Wheeler (1976), Young et al. (1977), Vila (1979) and Pineault (1980). The major variable among these models is the nature and structure of the accreting material. We will begin by examining the general black hole accretion process and then look in detail at more specialized cases.

Mass Accretion

For matter accreting onto a black hole, the resulting rate of energy release is given by.

$$L = f \dot{M} c^2$$

where f is the efficiency factor for the energy conversion process, \dot{M} is the mass accretion rate and c is the speed of light. Values of f for three types of black holes are given by Thorne (1974) as 0.06 for a Schwarzschild configuration, 0.30 when the hole is torqued by accretion and damped by radiation and 0.42 for a maximal Kerr condition. Altering the above equation somewhat gives

$$L = 1.70 [46] \dot{M}_{\odot} \text{ ergs/sec}$$

where \dot{M}_{\odot} is in solar masses per year and f is equal to 0.30. A second relation of interest is

$$\begin{aligned} E &= f M c^2 \\ &= 5.37 [53] M_{\odot} \text{ ergs} \end{aligned}$$

This expression gives the total energy released during the accretion of M solar masses of material where f is, again, equal to 0.3.

Table 12 presents, for all 24 event objects, the mass accretion rates in solar masses per year which correspond to each object's lowest base and highest peak bolometric luminosities. In Table 13 the total mass accreted during each event is shown.

The peak accretion rate was for 0235+164, corresponding to 7.2 [02] M_{\odot} /year. It should be kept in mind that this peak rate was maintained for only a small fraction of the duration of the event. The largest base rate seen, again in 0235+164, was about 14 M_{\odot} /year. Only seven objects had base accretion rates greater than 1 M_{\odot} /year.

Table 13 details the total converted mass for each of the events, which ran from about 0.001 to 50 solar masses. These values closely approximate the lower and upper bounds for the masses of normal stars. This result will be discussed in detail in the section on accretion of stars by black holes.

Black Hole Masses and Eddington Luminosities

The luminosity of an accreting black hole must be less than the Eddington luminosity (L_{EDD}), determined by the condition that the radiation pressure on the infalling matter cannot exceed the gravitational force (Eddington, 1921). We find that

$$L_{\text{EDD}} = 3.2 [04] L_{\odot} M_{\text{Ho}}$$

where L_{\odot} is the luminosity of the sun and M_{Ho} is the mass of the black hole in solar masses. The bolometric luminosity of an object thus sets a lower limit on the mass of the black hole.

The minimum variability timescale, based on the black hole model, is related to the gravitational radius of the hole, given by

TABLE 12
MASS ACCRETION RATES

Object	L ergs/sec	M M _⊙ /yr	L ergs/sec	M M _⊙ /yr
0039+40	3.71 [44]	2.18 [-02]	1.62 [44]	9.53 [-03]
3C 66A	8.11 [46]	4.77 [-02]	3.55 [45]	2.09 [00]
0235+164	1.23 [49]	7.24 [02]	2.38 [47]	1.40 [01]
0420-01	6.01 [46]	3.54 [00]	4.52 [45]	2.66 [-01]
NRAO 190	3.57 [46]	2.10 [00]	4.35 [45]	2.56 [-01]
0521-36	1.75 [45]	1.03 [-01]	3.94 [44]	2.32 [-02]
0735+17	1.53 [47]	9.00 [00]	1.32 [46]	7.76 [-01]
OJ 287	2.65 [47]	1.56 [01]	7.26 [45]	4.27 [-01]
0906+01	9.21 [46]	5.42 [00]	2.51 [46]	1.48 [00]
1156+295	1.05 [48]	6.18 [01]	3.71 [46]	2.18 [00]
NGC 4151	2.08 [43]	1.22 [-03]	1.92 [42]	1.13 [-04]
3C 279	3.16 [48]	1.86 [02]	1.20 [46]	7.06 [-01]
1308+326	3.98 [47]	2.34 [01]	1.13 [46]	6.65 [-01]
1510-08	4.75 [47]	2.81 [01]	2.50 [46]	1.47 [00]
1545+21	3.25 [45]	1.91 [-01]	1.97 [45]	1.16 [-01]
4C 38.41	5.27 [47]	3.10 [01]	1.26 [47]	7.41 [00]
NRAO 512	1.77 [47]	1.04 [01]	1.18 [46]	6.94 [-01]
3C 345	8.49 [46]	4.99 [00]	1.10 [46]	6.47 [-01]
NRAO 530	2.35 [47]	1.38 [01]	1.56 [46]	9.18 [-01]
3C 371	2.89 [45]	1.70 [-01]	9.11 [44]	5.36 [-02]
BL Lac	6.04 [45]	3.55 [-01]	9.28 [44]	5.46 [-02]
3C 446	1.58 [48]	9.29 [01]	5.46 [46]	3.21 [00]
3C 454.3	1.43 [47]	8.41 [00]	3.46 [46]	2.04 [00]
2345-16	2.88 [46]	1.69 [00]	4.20 [45]	2.47 [-01]

TABLE 13
EVENT ENERGIES AND CONVERTED MASSES

Event		E_e ergs	Conv. Mass M_o
0039+40	A	2.32 [51]	4.32 [-03]
3C 66A	A	1.23 [53]	2.29 [-01]
0235+164	A	2.48 [55]	4.62 [01]
	B	1.71 [55]	3.18 [01]
	C	2.65 [54]	4.93 [00]
	D	4.80 [54]	8.94 [00]
0420-01	A	2.20 [53]	4.10 [-01]
	B	4.45 [53]	8.29 [-01]
	C	1.81 [53]	3.37 [-01]
NRAD 190	A	4.91 [52]	9.14 [-02]
	B	2.79 [52]	5.20 [-02]
0521-36	A	2.49 [52]	4.64 [-02]
	B	3.34 [51]	6.22 [-03]
0735+17	A	1.17 [53]	2.18 [-01]
	B	3.89 [53]	7.24 [-01]
	C	1.15 [54]	2.14 [00]
OJ 287	A	3.71 [53]	6.91 [-01]
	B	3.03 [53]	5.64 [-01]
	C	5.58 [52]	1.04 [-01]
	D	6.56 [53]	1.22 [00]
0906+01	A	5.99 [52]	1.12 [-01]
	B	6.40 [52]	1.19 [-01]
	C	1.59 [52]	2.96 [00]
1156+295	A	1.28 [54]	2.38 [00]
NGC 4151	A	3.51 [50]	6.54 [-04]
3C 279	A	1.36 [54]	2.53 [00]
	B	4.34 [54]	8.08 [00]
	C	1.78 [55]	3.31 [01]
1308+326	A	1.28 [54]	2.38 [00]
	B	8.48 [53]	1.58 [00]
	C	2.40 [53]	4.47 [-01]
	D	2.16 [53]	4.02 [-01]

TABLE 13 (continued)

Event		E_0 ergs	Conv. Mass M_\odot
1510-08	A	1.22 [54]	2.27 [00]
1545+21	A	9.38 [50]	1.75 [-03]
4C 38.41	A	1.78 [53]	3.31 [-01]
NRAD 512	A	8.89 [51]	1.66 [-02]
	B	2.57 [52]	4.79 [-02]
	C	9.45 [51]	1.76 [-02]
	D	1.87 [52]	3.48 [-02]
	E	1.14 [53]	2.12 [-01]
	F	5.83 [52]	1.09 [-01]
	G	2.43 [51]	4.53 [-03]
	H	7.77 [53]	1.45 [00]
3C 345	A	1.28 [52]	2.38 [-02]
	B	7.14 [51]	1.33 [-02]
	C	1.16 [52]	2.16 [-02]
	D	2.29 [52]	4.26 [-02]
	E	2.61 [52]	4.86 [-02]
	F	8.03 [52]	1.50 [-01]
	G	5.33 [52]	9.93 [-02]
	H	5.39 [53]	1.00 [00]
NRAD 530	A	1.76 [53]	3.28 [-01]
	B	4.59 [52]	8.55 [-02]
3C 371	A	3.76 [51]	7.00 [-03]
	B	2.16 [51]	4.02 [-03]
BL LAC	A	1.47 [52]	2.74 [-02]
	B	7.05 [50]	1.31 [-03]
	C	6.44 [51]	1.20 [-02]
3C 446	A	1.10 [55]	2.05 [01]
	B	4.00 [54]	7.45 [00]
	C	2.59 [53]	4.82 [-01]
	D	2.81 [55]	5.23 [01]
	E	1.65 [54]	3.07 [00]
3C 454.3	A	3.66 [53]	6.82 [-01]
	B	1.75 [53]	3.26 [-01]
2345-16	A	1.45 [53]	2.70 [-01]

$$\begin{aligned}
 R_g &= G M_H / c^2 \\
 &= 1.5 [05] M_{H\odot} \text{ cm}
 \end{aligned}$$

The variability timescale will then be

$$\begin{aligned}
 t_v &= n R_g / c \quad (n \geq 1) \\
 &= 1.5 [05] n M_{H\odot} / c
 \end{aligned}$$

We note that the minimum variability timescale sets an upper limit on the mass of the black hole. Assuming that the object, at its peak luminosity L_p , is radiating at the Eddington limit, and relating t_v and L_p gives

$$\begin{aligned}
 t_v &= \frac{1.5 [05] L_p n}{3.2 [04] L_\odot c} \\
 &= 4.0 [-44] n L_p \text{ seconds}
 \end{aligned}$$

$$\log t_v = \log n + \log L_p - 43.4$$

Figure 5 is a plot of $\log t_v$ versus $\log L_p$ for each of the events studied in this work, and parallels the plot of Young et al. (1977). The lines represent the relation between minimum variability timescales and luminosities for $n = 1, 2, 6$ and $20 R_g$. Values of $n = 1$ and 6 correspond to the last stable orbits for maximal Kerr and Schwarzschild black holes respectively, while $n = 2$ is the value used by Elliot and Shapiro (1974) in a similar investigation. The last case, $n = 20$, is based on Lynden-Bell's (1969) value of $22R_g$ for the radius of greatest luminosity of the accretion disk. The filled circles, empty circles and triangles represent events occurring in BL Lac objects, QSO's and compact galaxies, respectively.

All but two of the events lie near or above the $n = 1$ line, making their variability timescales at least marginally consistent with the

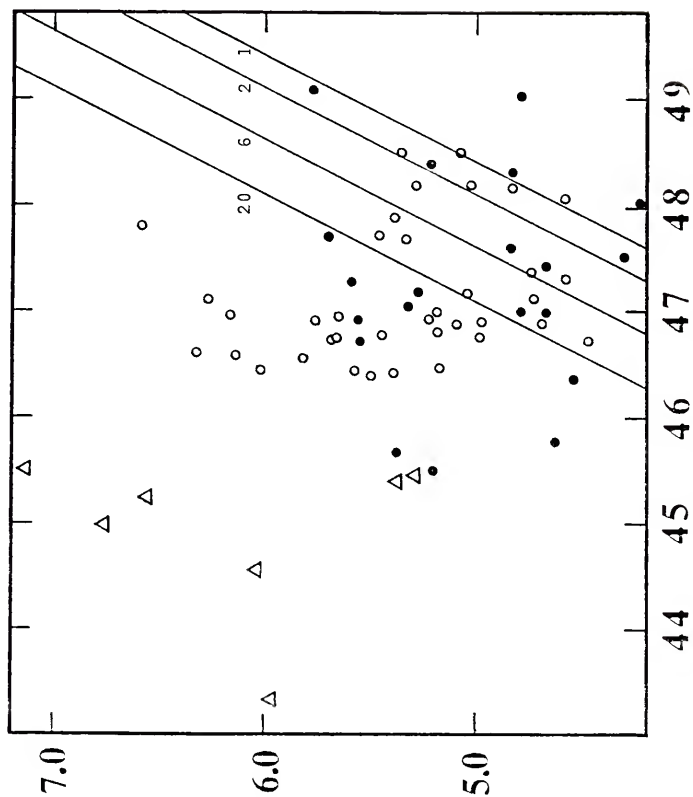


Figure 5. Log of the variability timescale in seconds versus the log of the bolometric luminosity in ergs/sec.

general black hole model. Two events (0235+164 B and 1156+295 A) lie well below the $n = 1$ line. There are many possible reasons for this.

If there is bulk relativistic motion, then the physical size of the emitting region can be larger than that indicated by variability arguments (Rees, 1966). There does not seem to be any problem with the original photometry; in fact there are other pairs of measurements which yield only slightly larger values of t_v for these events. Any of the earlier mentioned factors which work to reduce the actual luminosity could come into play. The emission directivity factor in a beaming model for 0235+164 would have to be 0.15 to sufficiently lower its luminosity.

In this regard, it was mentioned earlier that for beaming models there should be a correlation between shorter variability timescales and higher luminosities. cursory examination of Figure 5 reveals some indication of such a correlation between t_v and L_p . The faint end of the luminosity range is undersampled, however, which should be remedied in the future by more vigorous observations of intrinsically faint sources. Scatter will be introduced into the correlation mentioned above if there is a wide range in the directivity factors for objects of similar intrinsic luminosities.

A final comment concerning the position of the points on Figure 5 should be made. The actual bolometric luminosities of these objects may be greater than that used here, if the contributions from the parts of the spectrum not included in its calculation contribute significantly to the total luminosity. If this were indeed the case, then the points on Figure 5 will be shifted to the right, perhaps resulting in more objects lying below the $R_g = 1$ line.

Upper and lower mass limits of the black holes involved can be determined as indicated earlier from the shortest observed variability timescale and the assumption that the peak luminosity equals the Eddington luminosity. This differs slightly from the method used to create Figure 5, in that these two conditions may not appear during the same event.

Table 14 presents these lower and upper mass limits. For three objects, 0235+164, 1156+295 and 3C 446, the lower limit exceeds the upper limit by factors of 7, 2 and 1.5 respectively. One also notes that the mass of the central object associated with 3C 279 seems rather well determined.

Accretion of Stars

In the models of Hills (1975) and Young et al. (1977) matter accreted onto a black hole was assumed to be from stars which were tidally disrupted. Both investigators found that once the central mass exceeded about 3 [08] solar masses it would swallow stars whole, with a resulting decline in the luminosity from its peak value of about 8 [45] ergs/sec. This result, of course, assumes no other source of accreting material. Examination of the base luminosities for the event objects given in Table 13 shows thirteen objects whose base luminosities exceed 8 [45] ergs/sec. Of these, however, only three (0235+164, 4C 38.41 and 3C 446) exceed this value by a factor of 5 or more. Consequently, accretion of tidally disrupted stars seems able to account for the base luminosities in most of these objects.

If the base energy emission is due to tidally disrupted stars, what is the source of the discrete event energy? Assuming the event energy is

TABLE 14
UPPER AND LOWER MASS LIMITS

Object	Lower Limit M_{Ho}	Upper Limit M_{Ho}
0039+40	2.85 [06]	2.19 [11]
3C 66A	6.24 [08]	7.27 [10]
0235+164	9.46 [10]	1.25 [10]
0420-01	4.62 [08]	5.50 [10]
NRAD 190	2.75 [08]	6.26 [10]
0521-36	1.35 [07]	7.27 [11]
0735+17	1.18 [09]	1.23 [11]
OJ 287	2.04 [09]	6.55 [09]
0906+01	7.08 [08]	2.43 [10]
1156+295	8.08 [09]	3.37 [09]
NGC 4151	1.60 [05]	1.88 [11]
3C 279	2.43 [10]	2.43 [10]
1308+326	3.06 [09]	3.98 [09]
1510-08	3.67 [09]	4.27 [10]
1545+21	2.50 [07]	3.03 [12]
4C 38.41	4.05 [09]	5.79 [10]
NRAD 512	1.36 [09]	7.53 [09]
3C 345	6.53 [08]	5.88 [09]
NRAD 530	1.81 [09]	1.11 [10]
3C 371	2.22 [07]	3.93 [10]
BL Lac	4.65 [07]	8.47 [09]
3C 446	1.22 [10]	7.53 [09]
3C 454.3	1.10 [09]	2.19 [10]
2345-16	2.22 [08]	2.93 [10]

released as the result of mass accreted onto the black hole, then this mass has two potential origins. It may be material which has never been in stellar form and thus does not require disruption. Alternatively, it may be material from stars which have been disrupted in some manner other than tidally by the black hole. This seems the more likely of the two possibilities. Such a process would provide discrete "bursts" of accretable material, rather than an amorphous source of "free" mass. In addition, as pointed out earlier in this chapter, the equivalent converted masses for the energies emitted during these events lie almost exactly within the range of known stellar masses.

Two processes for stellar disruption (other than tidal effects) may be occurring in these objects. If the concentration of stars is high, collisions between them become more likely. This collision process can lead to the mechanical disruption of one or both stars or may even initiate a supernova, the former producing accretable mass and the latter both accretable mass and emitted radiation. Judging by the typical frequency of these events one would require only a few such collisions per year. Supernovae resulting from stellar evolution, rather than collisions, could also contribute radiation and accretable material.

Accretion Disk Timescales

The formation of accretion disks around the black holes in these objects has been modeled by a number of people. Paczynski (1978) presented a model where turbulence is driven by local disk instabilities and the accompanying viscosity makes possible the accretion onto the central object. He also found, however, that the timescale for such

accretion was on the order of 10 million years, but that local gravitational instabilities could decrease this to hundreds of years. This is still much too long to explain the known variations in these objects.

Pulsation of the accretion disk has been examined by Ledoux (1951), Goldreich and Lynden-Bell (1965), Stewart (1975) and others. Vila (1980) examined adiabatic oscillations in these disks and found that

$$P M^{1/2} r^{-3/2} = 0.035 \text{ days}$$

where P is the oscillation period, M is the mass of the central object (in grams) and r is the radius of the disk (in cm) at which the oscillation occurred.

Table 15 shows the oscillation periods in days expected for various typical combinations of r and M , where M is in solar masses.

TABLE 15
DISK PULSATION PERIODS

M_{Ho}	Disk Radius (cm)			
	1 [14]	1 [15]	1 [16]	1 [17]
1 [07]	2.5 [-01]	7.8 [00]	2.5 [02]	7.8 [03]
1 [09]	2.5 [-02]	7.8 [-01]	2.5 [01]	7.8 [02]
1 [11]	2.5 [-03]	7.8 [-02]	2.5 [00]	7.8 [01]

These values are in the same range as the durations of the events studied here. Could these events represent a cycle of one of these oscillations? If so, then for multiple events in a given object (so that M is the same in all cases) we would find

$$P r^{-3/2} = \text{constant}$$

which also means that

$$T_e/t^{3/2} = \text{constant}$$

Table 11 lists the log of $T_e/t^{3/2}$ for all objects with more than one event. For some objects (e.g. 0420-01) the values for each of the events are quite similar, but for many objects the ratio varies by several orders of magnitude from event to event. This result does not preclude the possibility that some of these events are due to this type of oscillation, but certainly not all of the events are so created.

Accretion Disk Flares

Few, if any, models prior to that of Pineault (1980) have suggested that the origin of the background luminosity is significantly different than that of the flare luminosity. Pineault proposes that the background (or base luminosity as we have referred to it) is a result of the central object accreting at or below its Eddington luminosity, while the outburst energy results from scaled up versions of solar flares occurring on the accretion disk and resulting from the release of stored magnetic energy. Models of this type are quite attractive because, for all of the objects in this study, their base level luminosities are well below their Eddington luminosities. This obviates the need to invoke beamed radiation, at least for the base luminosity.

Pineault has applied his model to the 1975 outburst of 0235+164. Following his procedures we will calculate similar parameters for the events in this study. We find from his scaling laws that

$$R_F = R_S T_e/T_S$$

$$B_F = B_S (E_F/E_S)^{1/2} (T_e/T_S)^{-3/2}$$

where R_F is the flare region size, T_e is the flare duration and E_F is the energy in the flare. The laboratory scaling values are $R_S = 1$ [01] cm, $T_S = 1$ [-06] seconds, $B_S = 1$ [04] gauss and $E_S = 1$ [08] ergs. Substituting these values in the above two equations gives

$$R_F = 1 \text{ [07]} T_e \text{ cm}$$

$$B_F = 1 \text{ [-09]} E_F^{1/2} / T_e^{3/2} \text{ gauss}$$

where

$$E_F = E_{RF} g(\theta) / j$$

where E_{RF} is the radiative flare energy, j is the fraction of the flare energy given off as radiation, and $g(\theta)$ is the correction factor allowing for non-isotropic emission of the flare energy. Values of R_F and $B_F j^{1/2} / g(\theta)^{1/2}$ are given in Table 16. All of the values of R_F are smaller than their emission region size counterparts calculated from variability timescales.

We can compare the size of the flare region to the thickness of the accretion disk using the model of a thin disk by Novikov and Thorne (1973) in which the thickness H is given by

$$H = 1.34 \text{ [14]} M_\odot \text{ cm}$$

where M_\odot is in solar masses per year. The base level values of M_\odot were given in Table 12. The third column of Table 16 lists (next to the first object event) the value of H obtained using M_\odot .

In a majority of cases $H > R_F$, indicating that, even in the extreme case of the viewing the disk edge on, the flare region solid angle will be less than that of the disk. In the cases where $R_F > H$, the disk could be being viewed at a non-zero inclination. Also the

TABLE 16
MAGNETIC FLARE MODEL PARAMETERS

Event		Flare Extent R_F (cm)	Disk Thickness H (cm)	B_F (j/g(0)) gauss
0039+40	A	3.24 [14]	1.28 [12]	2.61 [05]
3C 66A	A	9.97 [13]	2.80 [14]	1.11 [07]
0235+164	A	4.29 [13]	1.88 [15]	5.60 [08]
	B	1.52 [14]		7.00 [07]
	C	7.87 [13]		7.37 [07]
	D	6.62 [13]		1.29 [08]
0420-01	A	2.76 [14]	3.56 [13]	3.24 [06]
	B	3.20 [14]		3.69 [06]
	C	2.69 [14]		3.06 [06]
NRAD 190	A	3.87 [13]	3.43 [13]	2.91 [07]
	B	3.82 [13]		2.24 [07]
0521-36	A	6.08 [14]	3.11 [12]	3.32 [05]
	B	1.02 [14]		1.79 [06]
0735+17	A	6.14 [13]	1.04 [14]	2.25 [07]
	B	1.28 [14]		1.36 [07]
	C	3.40 [14]		5.40 [06]
0J 287	A	9.31 [13]	5.72 [13]	2.14 [07]
	B	1.12 [14]		1.47 [07]
	C	9.68 [13]		7.84 [06]
	D	1.01 [15]		8.00 [05]
0906+01	A	1.58 [13]	1.98 [14]	1.23 [08]
	B	2.82 [13]		5.35 [07]
	C	1.29 [13]		8.63 [07]
1156+295	A	4.45 [13]	2.92 [14]	1.21 [08]
NGC 4151	A	4.43 [14]	1.51 [10]	6.35 [04]
3C 279	A	2.87 [13]	9.46 [13]	2.40 [08]
	B	6.80 [13]		1.17 [08]
	C	6.82 [14]		7.49 [06]
1308+326	A	6.10 [13]	8.91 [13]	7.51 [07]
	B	8.00 [13]		4.07 [07]
	C	2.59 [13]		1.17 [08]
	D	3.50 [13]		7.10 [07]

TABLE 16 (continued)

Event		Flare Extent R_F (cm)	Disk Thickness H (cm)	B_F (j/g(θ)) gauss
1510-08	A	8.19 [13]	1.97 [14]	4.71 [07]
1545+21	A	1.67 [14]	1.55 [13]	4.51 [05]
4C 38.41	A	9.50 [12]	9.93 [14]	4.55 [08]
NRAO 512	A	1.99 [12]	9.30 [13]	1.06 [09]
	B	9.94 [12]		1.62 [08]
	C	1.38 [12]		1.89 [09]
	D	1.20 [13]		1.04 [08]
	E	3.71 [13]		4.72 [07]
	F	2.03 [13]		8.37 [07]
	G	1.59 [13]		2.46 [07]
	H	2.43 [14]		7.35 [06]
3C 345	A	2.49 [13]	8.67 [13]	2.88 [07]
	B	1.62 [13]		4.08 [07]
	C	7.61 [12]		1.62 [08]
	D	2.53 [13]		3.76 [07]
	E	1.84 [13]		6.47 [07]
	F	8.29 [13]		1.19 [07]
	G	2.97 [13]		4.51 [07]
	H	3.54 [14]		3.49 [06]
NRAO 530	A	6.35 [13]	1.23 [14]	2.62 [07]
	B	2.04 [13]		7.36 [07]
3C 371	A	3.87 [13]	7.18 [12]	8.05 [06]
	B	4.26 [13]		5.28 [06]
BL LAC	A	7.26 [13]	7.32 [12]	6.20 [06]
	B	6.65 [12]		4.89 [07]
	C	2.48 [13]		2.05 [07]
3C 446	A	4.25 [14]	4.30 [14]	1.20 [07]
	B	1.50 [14]		3.44 [07]
	C	1.39 [14]		9.85 [06]
	D	5.51 [14]		1.30 [07]
	E	---		---
3C 454.3	A	1.37 [14]	2.73 [14]	1.19 [07]
	B	---		---
2345-16	A	3.34 [14]	3.31 [13]	1.97 [06]

value of M_0 (and thus H) goes inversely as the mass to energy conversion efficiency factor, which for these calculations was 0.30, but which certainly could be much lower.

This magnetic flare model seems to be able to account for many of the properties seen in these objects and does not suffer so badly from energetics problems as do others. It would be extremely useful if the model could be developed in such a way as to predict the time dependence of the flare emission process so that it could be compared to the events studied here.

Supermassive Rotating Magnetoplasmic Body

The model of compact objects as supermassive rotating magnetoplasmic bodies is summarized by Ginzburg and Ozneroy (1977). The radiation is a combination of thermal and synchrotron contributions, generated by the rotator in the course of collapse and rotational braking. One of the main points of this type of model is its ability to explain certain quasi-periodic behavior in the observed light curves. These periodicities, determined by Fourier analysis of light curves, generally do not persist for many cycles, require phase drift and seem rather questionable at best as to their reality. Many false periods can arise from observational selection effects. We note that in the table of periodicities of Ginzburg and Ozneroy (1977) three of the periods are within 20 days or so of one year, while the period of 29.5 days listed for NGC 1275 is exactly the synodic period of the moon. Because the observing seasons for objects vary as a function of the object's declination combined with the observer's latitude, checks for this type of false period must be done as well.

No predictions of the shapes or parameters of events have been made. In terms of total luminosity, thermal plus non-thermal, the energy requirements do seem satisfied.

Multiple Supernovae

This model assumes that both the luminosity and its fluctuations are the result of supernovae and their remnant pulsars in a dense star cluster. These supernovae result from the frequent collisions between stars. As shown earlier, one would not expect to detect a classical supernova light curve as was often thought if a single (rather than superimposed multiple) event of this type occurred. Ginzburg and Ozneroy (1977) point out as well that, without some sort of coherence process in the cluster, it is difficult to produce sufficient energy to power a quasar without a prohibitively large number of events per year.

Final Comments and Suggestions for Future Work

This work has, for the first time, gathered together data on and analyzed the collective properties of a group of compact extragalactic objects which have exhibited discrete optical outbursts. In addition, every attempt was made to keep the analysis as internally consistent and physically meaningful as possible.

It is evident that these optical events are very diverse in terms of their morphology and their energetics. Indications of the validity of certain models have arisen. The correlation between variability timescales and luminosity points toward beaming models, which also have the advantage of reducing the energetics involved in these objects. More objects need to be placed on Figure 5 employing both old and new observations.

That the total energy in the events corresponds to the conversion of stellar-size masses lends support to the accretion of stars as the source of the event energies, provided that a suitable process of stellar disruption exists. If events are detected in the future whose converted masses exceeded $100 M_{\odot}$, then this method of providing accretable material would become less attractive. One of the most important concepts to keep in mind when modeling these objects is that the sources of the base luminosity and event luminosity may be completely different. Indeed, the processes of stellar accretion, disk accretion, disk magnetic flares and supernovae seem in no way to be mutually exclusive. If some combination of these processes is functioning in these objects, then individual characteristics may become distorted beyond simple recognition.

An accurate determination of the behavior of the entire spectrum of these objects during large optical outbursts is crucial to calculate a firm limit to their peak bolometric luminosities. Such investigations will as well provide information on such things as correlated optical-X-ray variability. If the scenario of Cavaliere and Morrison (1980) is correct then little such correlation is expected. Marscher (1980) points out that, for his relativistic jet models, the variations should occur first at higher frequencies and with correspondingly shorter characteristic timescales. Simultaneous short-timescale monitoring in the optical and infrared during short (< 1 week) events is proposed as a test.

Continuous very short timescale monitoring (resolution of tens of seconds) during violent events is needed to pin down minimum

variability timescales and to examine the exact behavior of the energy release mechanisms. Calculation of these variability timescales from relatively small flux changes must take into account the fractional luminosity factor to avoid drastic underestimation of emitting region diameters and volumes.

For a long time variability observations of compact objects were well ahead of the theories attempting to describe the nature of these objects. Newer models are now requiring variability data which are obtainable with presently available instrumentation, but which will require more dedication of telescope and satellite time and more co-operation between various observing groups. It is now the responsibility of observationalists to provide the information necessary to distinguish further between competing models for these remarkable astronomical objects.

LIST OF REFERENCES

- Angione R.J., 1973, Ap. J., 78, 353.
- Arp H.A., 1961, Ap. J., 133, 869.
- Balonek T., 1981, Doctoral dissertation, University of Massachusetts.
- Barbieri C., Romano G., and Rosino L., 1976, Ast. and Ap., 47, 153.
- Blandford R.D., and Rees M.J., 1979, Proc. Pittsburgh Conference on BL Lacertae Objects, ed. A. Wolfe, University of Pittsburgh Press.
- Bregman J., 1982, private communication.
- Burbidge G., 1979, Ap. J. Supp., 40, 583.
- Cannon R.D., Penston M.F., and Brett R.A., 1971, M.N.R.A.S., 152, 79.
- Cavaliere A., and Morrison P., 1980, Ap. J. Ltrs., 238, L63.
- Dorschner J.V., and Gurtler J., 1963, Ast. Nach., 225, 23.
- Eddington A.S., 1921, Zs. fur Phys., 7, 351.
- Eggen O.J., 1970, Ap. J. Ltrs., 159, L95.
- Elliot J.L., and Shapirio S.L., 1974, Ap. J. Ltrs., 192, L3.
- Fabian A.C., and Rees M.J., 1979, COSPAR, X-ray Astronomy, Pergamon Press.
- Ginzburg V.L., and Ozneroy L.M., 1977, Ap. and Space Sci., 54, 23.
- Goldreich P., and Lynden-Bell D., 1965, M.N.R.A.S., 130, 97.
- Hewitt A., and Burbidge G., 1980, Ap. J. Supp., 43, 57.
- Hills J.G., 1975, Nature, 254, 295.
- Hoyle, F., Burbidge G.R., and Sargent W.L.W., 1966, Nature, 209, 751.
- Johnson H.L., 1966, Ann. Rev. Ast., and Ap., 4, 193.
- Kinman T.D., Lamla E., Ciurla T., Harlan E., and Wirtanen C.A., 1968, Ap. J., 152, 357.
- Ledoux P., 1951, Ann. d'Ap., 14, 438.

- Liller M.H., and Liller W., 1975, *Ap. J. Ltrs.*, 199, L133.
- Lu P.K., 1972, *Ast. J.*, 77, 829.
- Lynden-Bell D., 1969, *Nature*, 223, 690.
- Lynden-Bell D., and Rees M.J., 1971, *M.N.R.A.S.*, 152, 461.
- Marscher A., 1980, *Ap. J.*, 235, 386.
- Matese J.J., and Whitmire D.P., 1978, *Ap. J.*, 226, 501.
- Matthews T., and Sandage A., 1963, *Ap. J.*, 138, 30.
- Moore R.L., Angel J.P.R., Rieke G.H., Lebofsky M.J., Wisniewski W.Z., Mufson S.L., Vrba F.J., Miller H.R., McGimsey B.Q., and Williamon R.M., 1980, *Ap. J.*, 235, 717.
- Morrison P., 1969, *Ap.J. Ltrs.*, 157, L73.
- Novikov I.D., and Thorne K.S., 1973, *Black Holes*, ed., B. Dewitt, Gordon and Breech Publishers.
- O'Dell S.L., Puschell J.J., Stein W.A., and Warner J.W., 1978, *Ap. J. Supp.*, 38, 767.
- Oke J.B., Neugebauer G., and Becklin E.E., 1970, *Ap. J.*, 159, 341.
- Paczynski B., 1978, *Acta. Astr.*, 28, 91.
- Penston M.V., and Cannon R.D., 1970, *Roy. Obs. Bull.*, 159, 85.
- Penston M.V., Penston M.J., Neugebauer G., Tritton K.P., Becklin E.E., and Visvanathan N., 1971, *M.N.R.A.S.*, 153, 29.
- Pica A.J., Pollock J.T., Smith A.G., Leacock R.J., Edwards P.L., and Scott R.L., 1980, *Ast. J.*, 85, 1442.
- Pineault S., 1980, *Ap. J.*, 241, 528.
- Pollock J.T., 1975, *Penn. State Sci. Rep.* 029.
- Pollock J.T., 1982, in preparation.
- Pollock J.T., Pica A.J., Smith A.G., Leacock R.L., Edwards P.L., and Scott R.L., 1979, *Ast. J.*, 84, 1658.
- Pomphrey R.B., Smith A.G., Leacock R.L., Olssen C.N., Scott R.L., Pollock J.T., Edwards P.L., and Dent W.A., 1976, *Ast. J.*, 81, 489.

- Rees M.J., 1966, *Nature*, 211, 468.
- Richstone D.O., and Schmidt M., 1980, *Ap. J.*, 235, 361.
- Rieke G.H., Grasdalen G.L., Kinman T.D., Hintzen P., Wills B.J., and Wills D., 1976, *Nature*, 260, 754.
- Rieke G.H., and Kinman T.D., 1974, *Ap. J. Ltrs.*, 192, L115.
- Salpeter E.E., 1964, *Ap. J.*, 140, 796.
- Schmidt M., 1963, *Nature*, 197, 1040.
- Schmidt M., 1968, *Ap. J.*, 151, 393.
- Seyfert C., 1943, *Ap. J.*, 97, 28.
- Shen B.S.P., Usher P.D., and Barrett J.W., 1972, *Ap. J.*, 171, 457.
- Shields G.A., and Wheeler J.C., 1976, *Ap. Ltrs.*, 17, 69.
- Smith H.J., and Hoffleit D., 1963, *Nature*, 198, 650.
- Stewart J.M., 1975, *Ast. and Ap.*, 42, 95.
- Stock J., and Williams A.D., 1962, *Stars and Stellar Systems*, Volume II, page 374, University of Chicago Press.
- Tapia S., Craine E.R., and Johnson K., 1976, *Ap. J.*, 203, 291.
- Terrell J., 1967, *Ap. J.*, 147, 829.
- Thorne K.S., 1974, *Ap. J.*, 191, 507.
- Vila S.C., 1980, *Ap. J.*, 234, 636.
- Wyndham J.D., 1966, *Ap. J.*, 144, 459.
- Young P.J., Shields G.A., and Wheeler J.C., 1977, *Ap. J.*, 212, 367.
- Zwicky F., 1964, *Ann. d'Ap.*, 27, 300.
- Zwicky F., Oke J.B., Neugebauer G., Sargent W.L.W., and Fairall A.P., 1969, *P.A.S.P.*, 82, 93.

APPENDICES

APPENDIX A
LIST OF SYMBOLS

α	spectral index
B	Johnson blue magnitude
B_C	blue magnitude corrected for galactic absorption and emission lines
B_F	flare magnetic field strength
B_S	magnetic field strength scaling factor
B_L	bolometric luminosity
c	speed of light
D	emitting region diameter
e_{a+}	upward error on luminosity at point a
e_{a-}	downward error on luminosity at point a
e'_a	error on normalized luminosity at point a
E_e	total energy emitted during the event in a one hertz band at 2500Å
E_F	energy in magnetic flare
E_S	magnetic flare energy scaling factor
f	mass to energy conversion efficiency factor
f_{25}	emitted flux at 2500Å
f_{44}	received flux at 4400Å
$f(\nu)$	flux as a function of frequency
$f_B(D'')$	galaxy flux contribution through aperture of D arc seconds in the B bandpass
$g(\theta)$	non-isotropic emission factor

G	universal gravitational constant
H	accretion disk thickness
H_0	Hubble's constant
j	fraction of magnetic flare energy given off as radiation
k	power law spectrum proportionality constant
$k(\bar{L}, \Delta L)$	fractional luminosity factor
l_a	2500 \AA event luminosity at point a
l'_a	normalized event luminosity at point a
l_p	2500 \AA peak event luminosity
\bar{L}	average luminosity over some time interval
L_{25}	total luminosity at 2500 \AA
L_{45}	luminosity in units of $1 [45]$ ergs/sec
L_B	event base luminosity at 2500 \AA
L_{EDD}	Eddington luminosity
L_p	peak total 2500 \AA luminosity
L_\odot	luminosity in units of solar luminosities
$L(\nu)$	rest frame luminosity as a function of frequency
ΔL	change in luminosity over some time interval
M_H	mass of black hole
M_{H_0}	mass of black hole in units of solar masses
M	mass accretion rate
M_\odot	mass accretion rate in units of solar masses/year
P	photographic magnitude
P	accretion disk oscillation period
q_0	cosmological constant

R_{15}	radius of emitting region in units of 1 [15] cm
R_e	ratio of base to event energy
R_F	magnetic flare region size
R_S	magnetic flare size scaling factor
R_g	gravitational radius of a black hole
ρ_M	magnetic energy density
ρ_R	radiation energy density
S_e	data sampling rate for an event
t_ℓ	variability timescale for a homogeneous, spherical radiating cloud
t_v	variability timescale established from observations
T_e	rest frame event duration
T_S	magnetic flare duration scaling factor
$\Delta T_{a,a+1}$	interval between two successive event points
ΔT_O	time interval in rest frame
U	Johnson ultraviolet magnitude
V	fractional luminosity volume factor
V	Johnson visual magnitude
z	redshift

APPENDIX B
REFERENCES TO OPTICAL VARIABILITY DATA

- Adam G., 1978, *Ast. and Ap. Supp.* 31, 151.
- Alksnis A., and Duncans L., 1973, *Ast. Circ.*, #763.
- Andrews P.J., Glass I.S., and Hawarden T.G., 1974, *M.N.R.A.S.*, 168, 1P.
- Angione R.J., 1971, *Ast. J.*, 76, 25.
- Angione R.J., 1973, *Ast. J.*, 78, 353.
- Arp H., Sargent W.L.W., Willis A.G., and Oosterbaan C.E., 1979, *Ap. J.*, 230, 68.
- Arp H., Sulentic J.W., Willis A.G., and deRuiter H.R., 1976, *Ap. J. Ltrs.*, 207, L13.
- Babadzhanjanz M.K., 1971, *Ast. Circ.*, #614.
- Babadzhanjanz M.K., 1973, *Pub. Trudy Obs. Leningrad*, 29, 72.
- Babadzhanjanz M.K., 1974, *Pub. Trudy Obs. Leningrad*, 30, 69.
- Babadzhanjanz M.K., 1975, *Pub. Trudy Obs. Leningrad*, 31, 100.
- Babadzhanjanz M.K., 1975, *Pub. Trudy Obs. Leningrad*, 32, 52.
- Babadzhanjanz M.K., Gager-Torn V.A., and Lyutyi V., 1972, *Astrophys.*, 8, 300.
- Barbieri C., 1973, *Ap. Ltrs.*, 14, 231.
- Barbieri C., and Abati-Erculiani L., 1968, *Mem. Ast. Soc. Ital.*, 39, 421.
- Barbieri C., and Romano G., 1976, *Ast. and Ap.*, 50, 15.
- Barbieri C., and Romano G., 1977, *Acta Ast.*, 27, 195.
- Barbieri C., and Romano G., 1981, *Ast. and Ap. Supp.*, 44, 159.
- Barbieri C., Romano G., di Serego S., and Zambon M., 1977, *Ast. and Ap.*, 59, 419.
- Barbieri C., Romano G., di Serego S., and Zambon M., 1977, *Nature*, 268, 318.

- Barbieri C., Romano G., and Rosino L., 1976, *Ast. and Ap.*, 47, 153.
- Barbieri C., Romano M., and Zambon M., 1978, *Ast. and Ap. Supp.*, 31, 401.
- Barbieri C., and Rosino L., 1970, *Mem. Ast. Soc. Ital.*, 41, 507.
- Barnes T.G., 1968, *Ap. Ltrs.*, 1, 171.
- Baumert J.H., 1980, *P.A.S.P.*, 92, 156.
- Belokon E.T., Babadzanjan M.K., and Lyutyi V.M., 1978, *Ast. and Ap. Supp.*, 31, 383.
- Bertaud Ch., Dumortier B., and Pollas C., 1975, *I.B.V.S.*, 970.
- Bertaud Ch., Wlerick G., Veron P., Dumortier B., Bigjay J., Paturel G., Duruy M., and de Saevisky P., 1973, *Ast. and Ap.*, 24, 357.
- Bertaud Ch., Wlerick G., Veron P., Dumortier B., Duruy M., and de Saevisky P., 1973, *Ast. and Ap. Supp.*, 11, 77.
- Biraud F., 1971, *Nature*, 232, 178.
- Bolton J.G., and Kinman T.D., 1966, *Ap. J.*, 145, 951.
- Bolton J.G., Kinman T.D., and Wall J.V., 1968, *Ap. J. Ltrs.*, 154, L105.
- Bonoli F., Bracesi A., Fererici L., Zitelli V., and Formiggini L., 1979, *Ast. and Ap. Supp.*, 35, 391.
- Carswell R.F., Strittmatter P.A., Williams R.E., Kinman T.D., and Serkowski K., 1974, *Ap. J. Ltrs.*, 190, L101.
- Cannon R.D., and Penston M.V., 1967, *Nature*, 214, 256.
- Cannon R.D., Penston M.V., and Brett R.A., 1971, *M.N.R.A.S.*, 152, 79.
- Craine E.R., Johnson K., and Tapia S., 1975, *P.A.S.P.*, 87, 123.
- Craine E.R., and Warner J.W., 1973, *Ap. J. Ltrs.*, 179, L53.
- Crovisier J., LeSqueren A.M., Pollock J.T., and Usher P.D., 1974, *Ast. and Ap.*, 30, 175.
- de Vaucouleurs G., and de Vaucouleurs A., 1972, *Ap. Ltrs.*, 12, 1.
- Dibia E.A., Zaitseva G.V., and Lyutyi V.M., 1969, *Sov. Ast. J.*, 13, 187.
- Dubjago I.A., and Ourassine L.A., 1976, *I.B.V.S.*, 1134.

- Dubjago I.A., Tokhtasjeo S.S., and Fomin C.K., 1974, *Ast. Circ.*, #822.
- Dumortier B., 1976, PhD Dissertation, University of Paris.
- Dupay D., Schmitt J., McClure R., van den Bergh S., and Racine R., 1969, *Ap. J. Ltrs.*, 156, L135.
- Dyck H.M., Kinman T.D., Lockwood G.W., and Landolt A.U., 1971, *Nature Phys. Sci.*, 234, 71.
- Eachus L.J., and Liller W., 1975, *Ap. J. Ltrs.*, 200, L61.
- Eggen O.J., *Ap. J. Ltrs.*, 159, L95.
- Eggen O.J., 1973, *Ap. J. Ltrs.*, 186, L1.
- Folsom G.H., Miller H.R., Wingert D.W., and Williamon R.M., 1976, *Ast. J.*, 81, 145.
- Ford W.K., and Rubin V.C., 1966, *Ap. J. Ltrs.*, 145, L357.
- Frohlich A., Goldsmith S., and Weistrop D., 1974, *M.N.R.A.S.*, 168, 417.
- Gager-Torn V.A., 1977, *Pub. Trudy Obs. Lenningrad*, 33, 15.
- Gager-Torn V.A., 1978, *Pub. Trudy Obs. Lenningrad*, 34, 16.
- Gilmore G., 1979, *M.N.R.A.S.*, 187, 389.
- Gilmore G., 1980, *M.N.R.A.S.*, 190, 649.
- Ginzburg V.L., and Ozneroy L.M., 1977, *Ap. and Spa. Sci.*, 50, 23.
- Goldsmith D.W., and Kinman T.D., 1965, *Ap. J.*, 142, 1693.
- Goldsmith S., and Weistrop D., 1973, *Ap. J.*, 180, 661.
- Gottlieb E.W., and Liller W., 1978, *Ap. J. Ltrs.*, 222, L1.
- Grandi S., and Tifft W.G., 1974, *P.A.S.P.*, 86, 873.
- Green R.F., Huchra J.P., and Bond H.E., 1977, *P.A.S.P.*, 89, 255.
- Griffiths R.E., Tapia S., Briel U., and Chaisson L., 1979, *Ap. J.*, 234, 810.
- Hall D.L., and Usher P.D., 1973, *Nature Phys. Sci.*, 241, 31.
- Hunter J.H., and Lu P.K., *Nature*, 223, 1045.
- Jackisch G., 1971, *Ast. Nach.*, 292, 271.

- Jackish G., 1971, *Ast. Nach.*, 293, 175.
- Jurkevich I., 1972, *Ap. J. Ltrs.*, 172, L29.
- Jurkevich I., Usher P.D., and Shen B.S.P., 1971, *Ap. and Spa. Sci.*, 10, 402.
- Kikuchi M., Yoshitaka M., Konno M., and Inoue M., *P.A.S.J.*, 28, 117.
- Kingham K.A., and O'Connell R.W., 1979, *Ast. J.*, 84, 1537.
- Kinman T.D., 1968, *Science*, 162, 1081.
- Kinman T.D., Bolton J.G., Clarke R.W., and Sandage A., 1967, *Ap. J.*, 147, 848.
- Kinman T.D., Lamla E., Ciurla T., Harlan E., and Wirtanen C.A., 1968, *Ap. J.*, 152, 357.
- Kinman T.D., Lamla E., and Wirtanen C.A., 1966, *Ap. J.*, 146, 964.
- Krautter J., and Appenzeller I., and Mollenhoff C., 1976, *Ast. and Ap.*, 52, 149.
- Kurochkin N.E., 1971, *Ast. Circ.*, #644.
- Kurochkin N.E., 1974, *Ast. Circ.*, #844.
- Lyutyi V.M., 1971, *Ast. Circ.*, #620.
- Lyutyi V.M., 1971, *Ast. Circ.*, #627.
- Lyutyi V.M., 1973, *Ast. Circ.*, #777.
- Lyutyi V.M., 1973, *Sov. Ast. J.*, 16, 763.
- Lyutyi V.M., 1976, *Ast. Circ.*, #920.
- Lyutyi V.M., 1977, *Sov. Ast. J.*, 21, 655.
- Lyutyi V.M., 1979, *Sov. Ast. J.*, 23, 518.
- Lanning H.H., 1976, *P.A.S.P.*, 88, 198.
- Liller M.H., and Liller W., 1975, *Ap. J. Ltrs.*, 199, L133.
- Liller W., 1974, *Ap. J. Ltrs.*, 189, L101.
- Low F.J., and Johnson H.L., 1965, *Ap. J.*, 141, 336.

- Lu P.K., 1972, *Ast. J.*, 77, 829.
- Lu P.K., 1977, *Ast. J.*, 82, 773.
- Lu P.K., and Hunter J.H., 1969, *Nature*, 221, 755.
- Lucchetti S.C., and Usher P.D., 1971, *Nature*, 232, 622.
- MacPherson G.J., 1972, *P.A.S.P.*, 84, 392.
- Markova L.T., Fomin S.K., and Zhukov G.V., 1973, *Ast. Circ.*, #791.
- Markova L.T., and Zhukov G.V., 1974, *Ast. Circ.*, #843.
- Markova L.T., and Zhukov G.V., 1975, *Ast. Circ.*, #862.
- Matthews T.A., and Sandage A., 1963, *Ap. J.*, 138, 30.
- McGimsey B.Q., and Miller H.R., 1978, *Ast. and Ap. Supp.*, 31, 147.
- Miller H.R., 1975, *Ap. J. Ltrs.*, 201, L109.
- Miller H.R., 1977, *Ast. and Ap.*, 54, 537.
- Miller H.R., 1977, *Ap. J. Ltrs.*, 212, L53.
- Miller H.R., 1977, *Ap. J.*, 212, 34.
- Miller H.R., 1978, *Ap. J. Ltrs.*, 223, L67.
- Miller H.R., 1978, *P.A.S.P.*, 90, 661.
- Miller H.R., 1979, *Ast. and Ap. Supp.*, 35, 387.
- Miller H.R., 1979, *Ap. J.*, 227, 52.
- Miller H.R., 1980, *Ast. J.*, 85, 99.
- Miller H.R., Clonts S.L., and Folsom G.H., 1974, *Ast. J.*, 79, 1352.
- Miller H.R., and McGimsey B.Q., 1978, *Ap. J.*, 220, 19.
- Miller J.S., and Hawley S.A., 1977, *Ap. J. Ltrs.*, 212, L47.
- Milone E.F., 1972, *P.A.S.P.*, 84, 723.
- Milone E.F., 1974, *P.A.S.P.*, 86, 899.
- Moore R.L., Angel J.R.P., Rieke G.H., Lebofsky M.J., Wisniewski W.Z., Mufson S.L., Vrba F.J., Miller H.R., McGimsey B.Q., and Willamon R.M., 1980, *Ap. J.*, 235, 717.

- Mullikin T.L., and Miller H.R., 1977, P.A.S.P., 89, 639.
- O'Dell S.L., Stein W.A., and Warner J.W., 1978, Ap. J. Supp., 38, 267.
- Oke J.B., 1966, Ap. J., 145, 669.
- Oke J.B., 1967, Ap. J., 147, 901.
- Ourassine L., 1975, Nature 254, 125.
- Pacholczyk A.G., 1971, Ap. J., 163, 449.
- Pacholczyk A.G., and Wisniewski W.Z., 1967, Ap. J., 147, 394.
- Peach J.V., 1969, Nature, 222, 439.
- Penston M.V., Penston M.J., Neugebauer G., Tritton K.P., Becklin E.E., and Visvanathan N., 1971, M.N.R.A.S., 153, 29.
- Penston M.V., Penston M.J., Selmes R.A., Becklin E.E., and Neugebauer G., 1974, M.N.R.A.S., 169, 357.
- Peterson B.A., and Bolton J.G., 1972, Ap. Ltrs., 10, 105.
- Pica A.J., 1977, Ast. J., 82, 935.
- Pica A.J., Pollock J.T., Smith A.G., Leacock R.J., Edwards P.L., and Scott R.L., 1980, Ast. J., 85, 1442.
- Pollock J.T., 1975, Ap. J. Ltrs., 198, L53.
- Pollock J.T., Hall D.L., Ambruster C., and Usher P.D., 1974, Ast. and Ap., 30, 41.
- Pollock J.T., Pica A.J., Smith A.G., Leacock R.J., Edwards P.L., and Scott R.L., 1979, Ast. J., 84, 1658.
- Pronik V.I., and Shcherbakov A.G., 1970, Astrophys., 6, 287.
- Puschell J.J., Stein W.A., Jones T.W., Owen F., Rudnick L., Aller H., and Hodge P., 1979, Ap. J. Ltrs., 227, L11.
- Quintana H., Kaufmann P., and Sersic J.L., M.N.R.A.S., 173, 57P.
- Richter G.A., 1978, Ast. Nach., 293, 233.
- Richter G.A., and Richter N.B., 1978, Ast. Nach., 292, 133.
- Rieke G.H., Grasdalen G.L., Kinman T.D., Hintzen P., Wills B.J., and Wills D., 1976, Nature, 260, 754.
- Rieke G.H., and Kinman T.D., 1974, Ap. J. Ltrs., 192, L115.

- Rieke G.H., Lebofsky M.J., Kemp J.C., Coyne G.V., and Tapia S., 1977, *Ap. J. Ltrs.*, 218, L37.
- Romano G., 1971, *Mem. Ast. Soc. Ital.*, 42, 57.
- Romano G., 1972, *Mem. Ast. Soc. Ital.*, 43, 309.
- Romano G., and Minello S., 1977, *Ap. and Spa. Sci.*, 50, 421.
- Nebelitskij V.B., 1972, *Ast. Circ.*, #732.
- Nebelitskij V.B., 1972, *Ast. Circ.*, #764.
- Netzer H., 1974, *M.N.R.A.S.*, 167, 1P.
- Sandage A., 1964, *Ap. J.*, 139, 416.
- Sandage A., 1966, *Ap. J.*, 144, 1234.
- Sandage A., Westphal J.A., and Strittmatter P.A., 1966, *Ap. J.*, 146, 322.
- Sandage A., and Wyndham J.D., 1965, *Ap. J.*, 141, 328.
- Schaefer B.E., 1980, *P.A.S.P.*, 92, 255.
- Selmes R.A., Tritton K.P., and Wordsworth R.W., 1975, *M.N.R.A.S.*, 170, 15.
- Selove D.M., 1969, *Ap. J. Ltrs.*, 158, L19.
- Sharov A.S., and Efremov Y.N., 1964, *Sov. Ast. J.*, 7, 727.
- Shen B.S.P., Usher P.D., and Barrett J.W., 1972, *Ap. J.*, 171, 457.
- Smith H.J., and Hoffleit D., 1963, *Nature*, 198, 650.
- Smyth M.J., and Wolstencroft R.D., 1970, *Ap. and Spa. Sci.*, 8, 471.
- Strittmatter P.A., and Burbidge G.R., 1967, *Ap. J.*, 147, 13.
- Tapia S., Craine E.R., Gearhart M.R., Pacht E., and Kraus J., 1977, *Ap. J. Ltrs.*, 215, L71.
- Tritton K.P., and Brett R.A., 1970, *Observatory*, 90, 110.
- Tritton K.P., and Selmes R.A., 1971, *M.N.R.A.S.*, 153, 453.
- Urassin L.A., and Lavrova N.V., 1972, *Ast. Circ.*, #744.
- Usher P.D., Cannon R.D., and Penston M.V., *Observatory*, 89, 198.
- Usher P.D., Kolpanen D., and Pollock J.T., 1975, *Nature*, 252, 365.

- Usher P.D., Shen B.S.P., and Barrett J.W., 1971, *Ap. J.*, 165, 647.
- Usher P.D., Shen B.S.P., Wright F.W., Shapley H., and Hanley C.M., 1969, *Ap. J.*, 158, 535.
- Veron M.P., 1975, *Ast. and Ap.*, 41, 423.
- Veron P., and Veron M.P., 1975, *Ast. and Ap.*, 39, 281.
- Veron P., and Veron M.P., 1976, *Ast. and Ap.*, 47, 319.
- Visvanathan N., *Ap. J.*, 179, 1.
- Wampler E.J., 1967, *Ap. J.*, 147, 1.
- Wampler E.J., 1967, *Ap. J. Ltrs.*, 148, L101.
- Weistrop D., and Goldsmith S., 1973, *Ap. Ltrs.*, 14, 225.
- Wesselink A.J., and Hunter J.H., 1967, *Science*, 156, 103.
- Westerlund B.E., and Stokes N.R., 1966, *Ap. J.*, 145, 354.
- Westerlund B.E., and Wall J.V., 1969, *Ast. J.*, 74, 335.
- Wills B.J., and Wills D., 1974, *Ap. J. Ltrs.*, 190, L97.
- Wills D., and Lynds R., 1978, *Ap. J. Supp.*, 36, 317.
- Wing R.F., 1973, *Ast. J.*, 78, 684.
- Zaitseva G.V., and Lyutyi V.M., 1969, *Sov. Ast. J.*, 13, 184.
- Zink J., Pica A.J., Pollock J.T., Kolpanen D., and Usher P.D., 1978, *I.B.V.S.*, 1441.
- Zwicky F., Oke J.B., Neugebauer G., and Sargent W.L.W., 1970, *P.A.S.P.*, 82, 93.

APPENDIX C
NORMALIZED EVENT LUMINOSITY CURVES

Appendix C contains plots of the normalized event luminosity versus the object event date for each event. X-axis divisions are each one-tenth of the interval indicated.

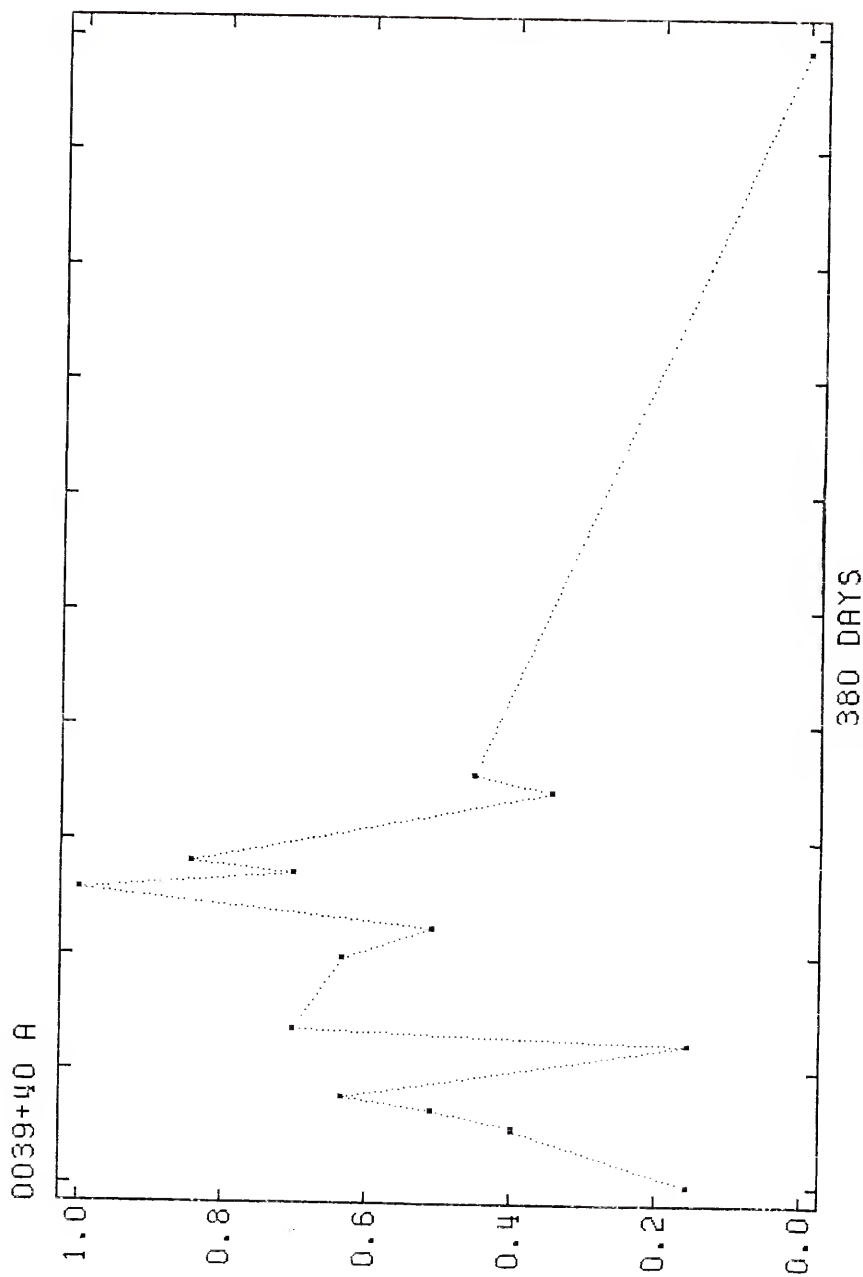


Figure 6. Event 0039+40 A, J.D. 41513 to 41927.

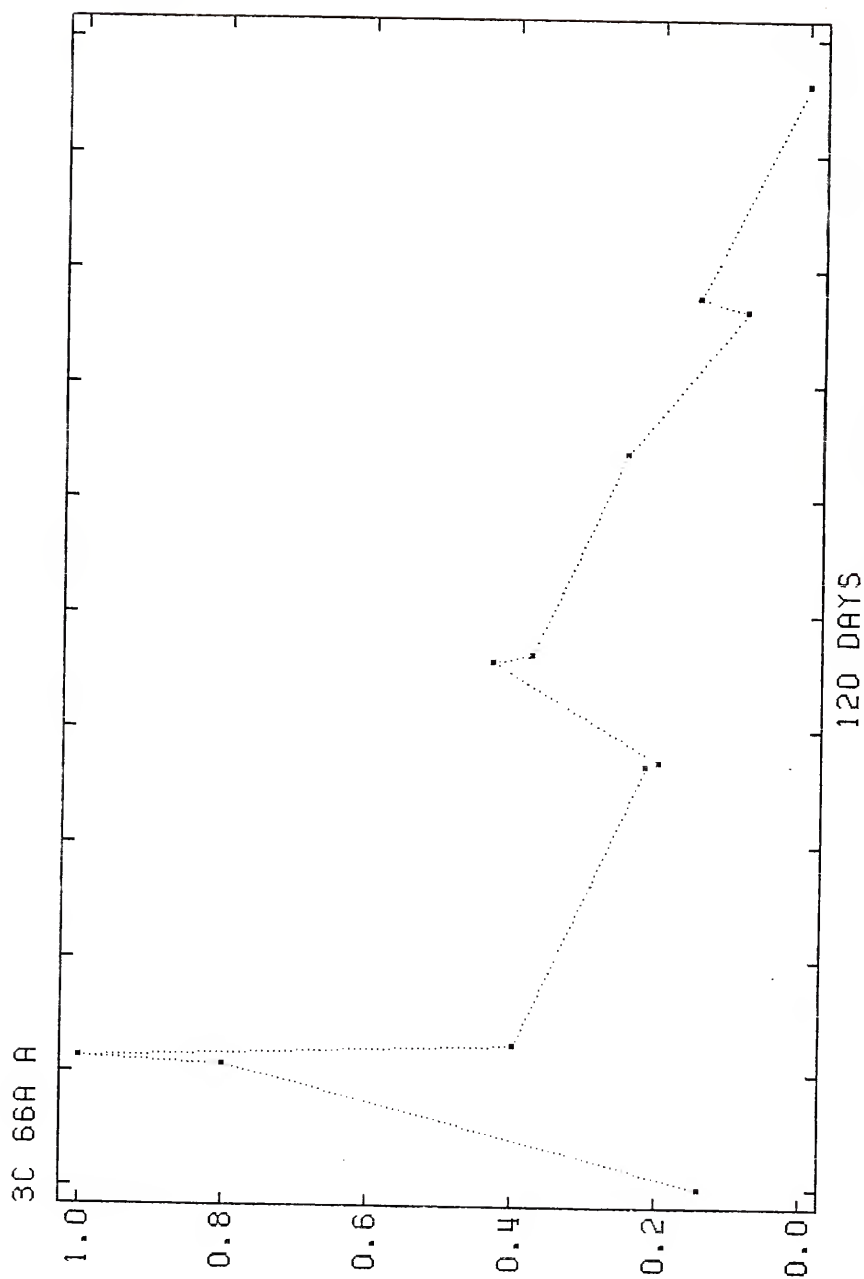


Figure 7. Event 3C 66A A, J.D. 42667 to 42834.

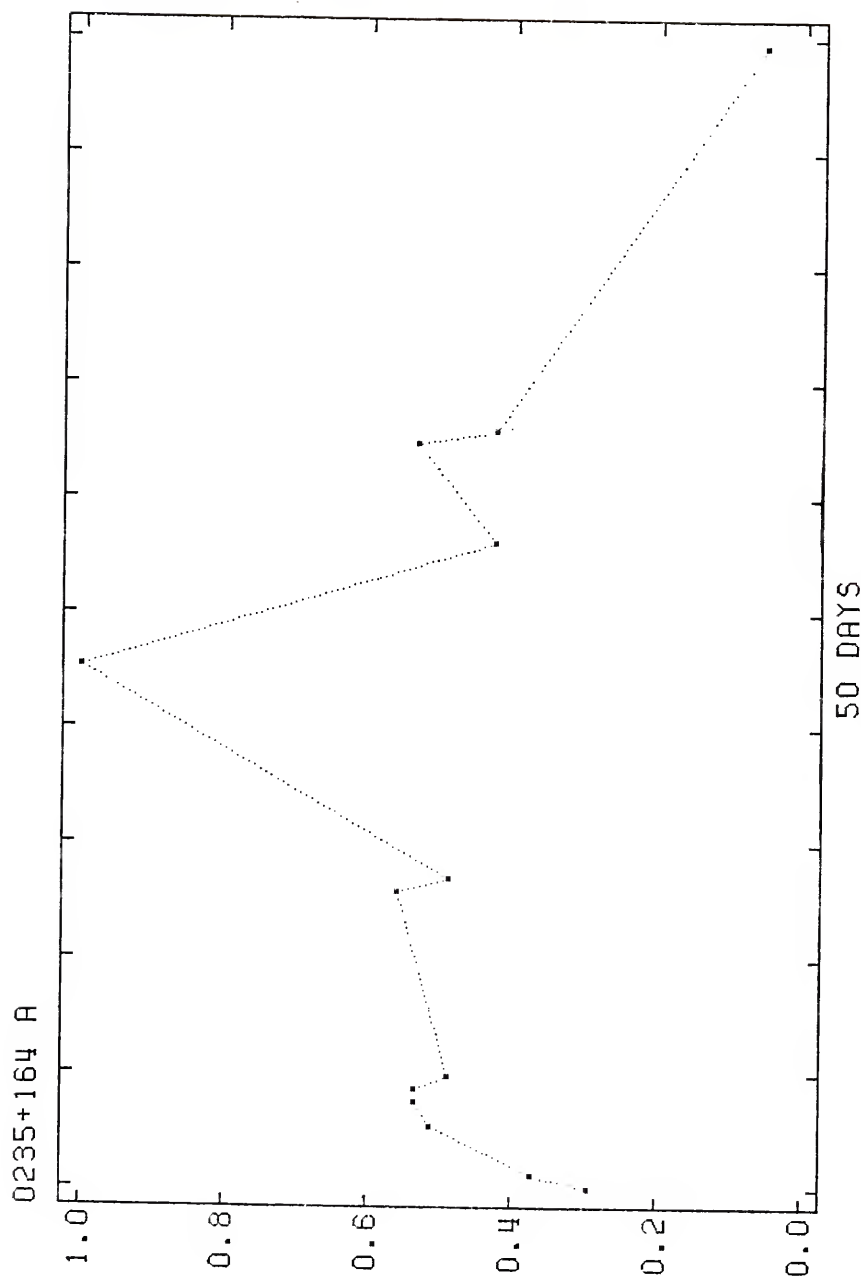


Figure 8. Event 0235+164 A, J.D. 42688 to 42780.

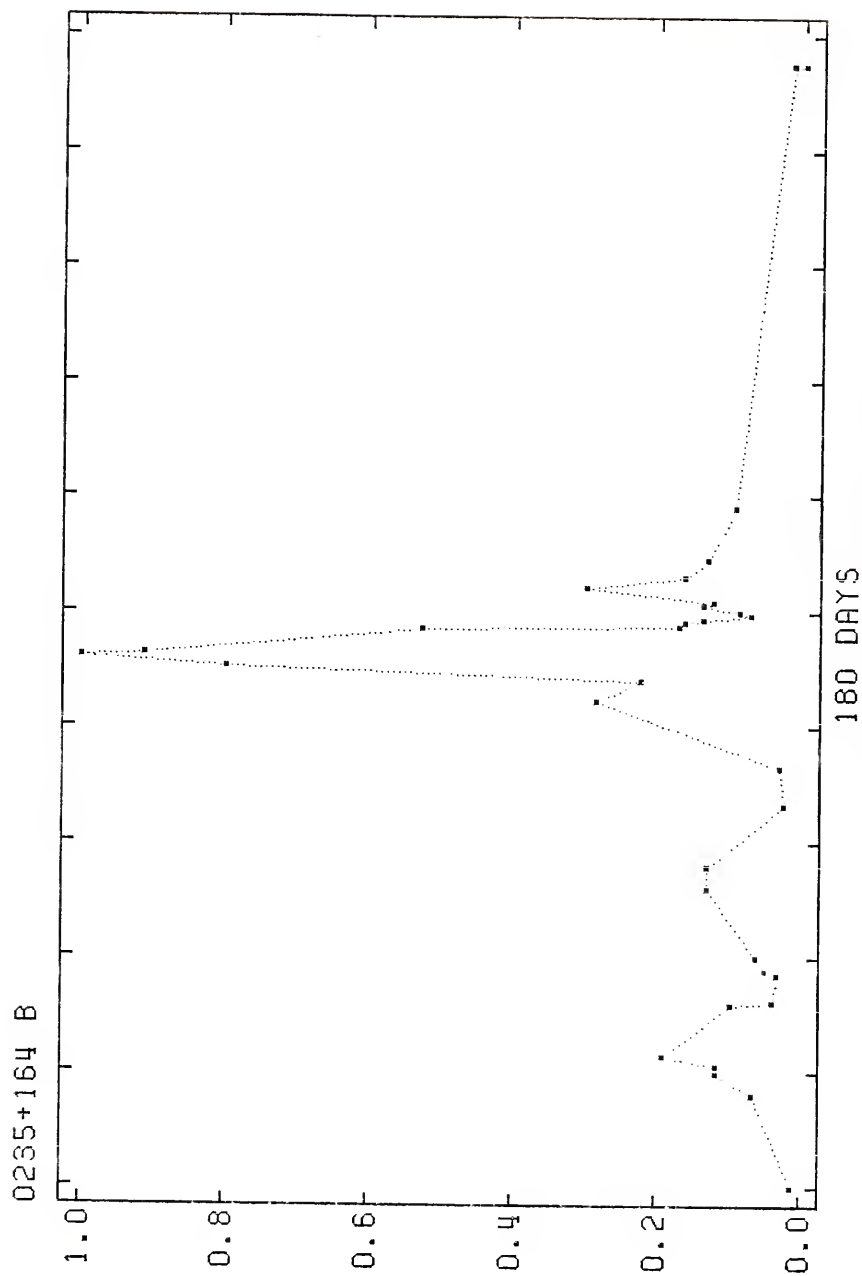


Figure 9. Event 0235+164 B, J.D. 43751 to 44136.

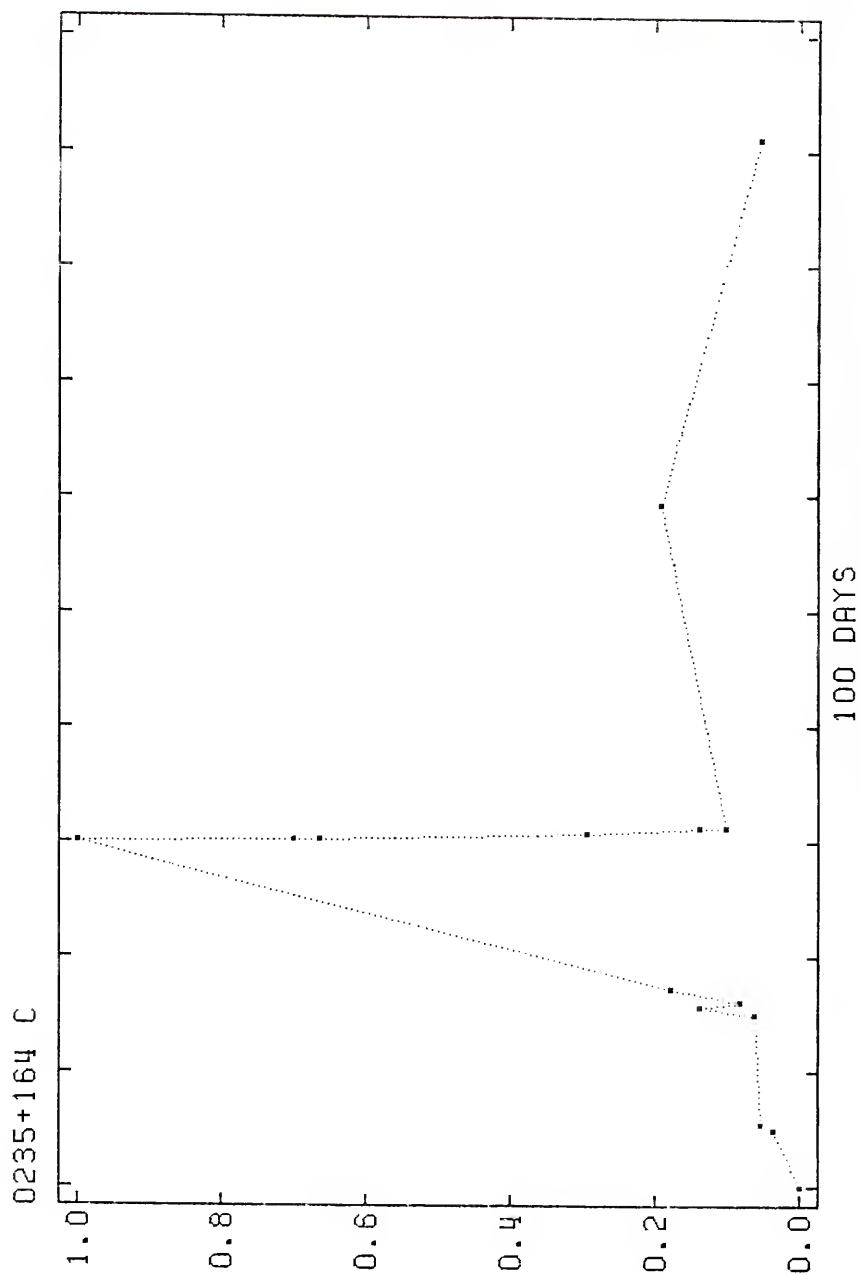


Figure 10. Event 0235+164 C, J.D. 44136 to 44305.

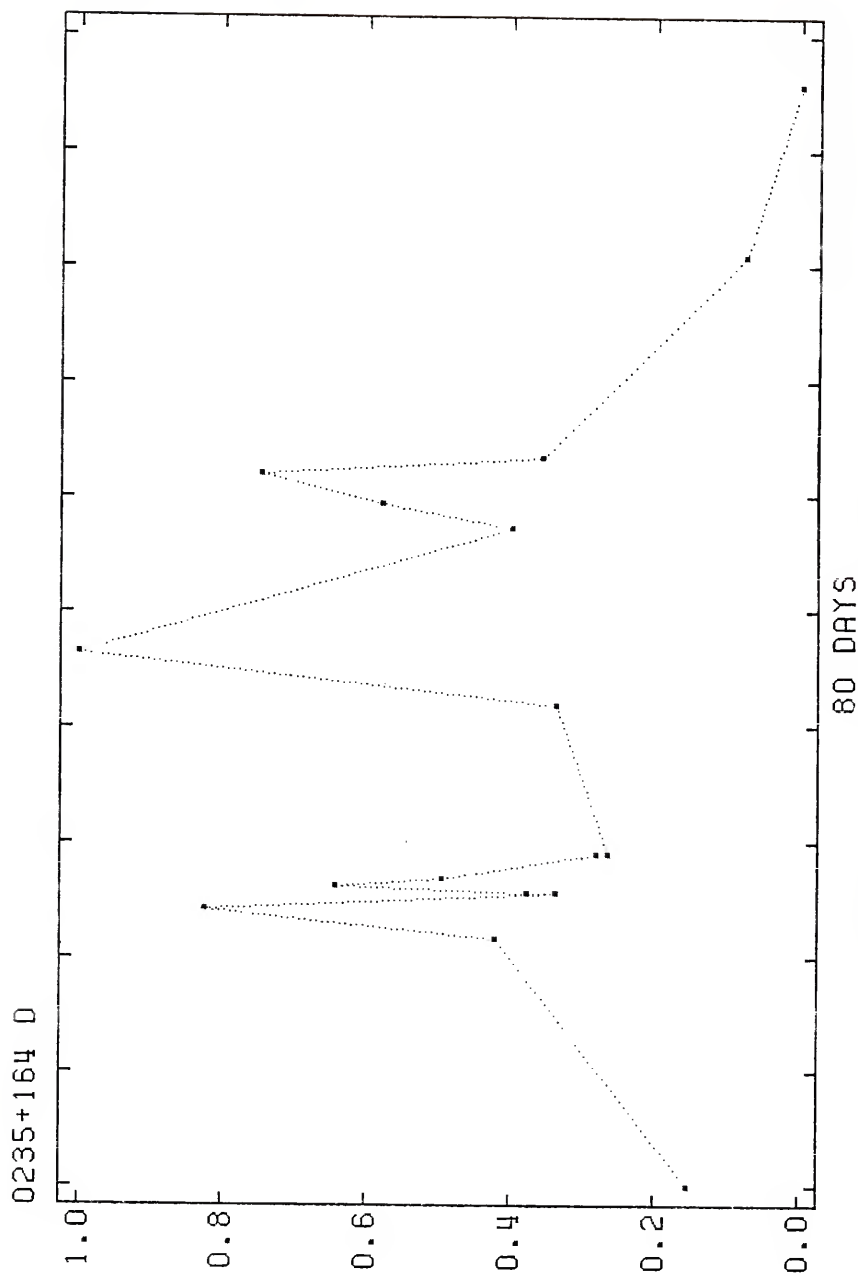


Figure 11. Event 0235+164 D, J.D. 44487 to 44629.

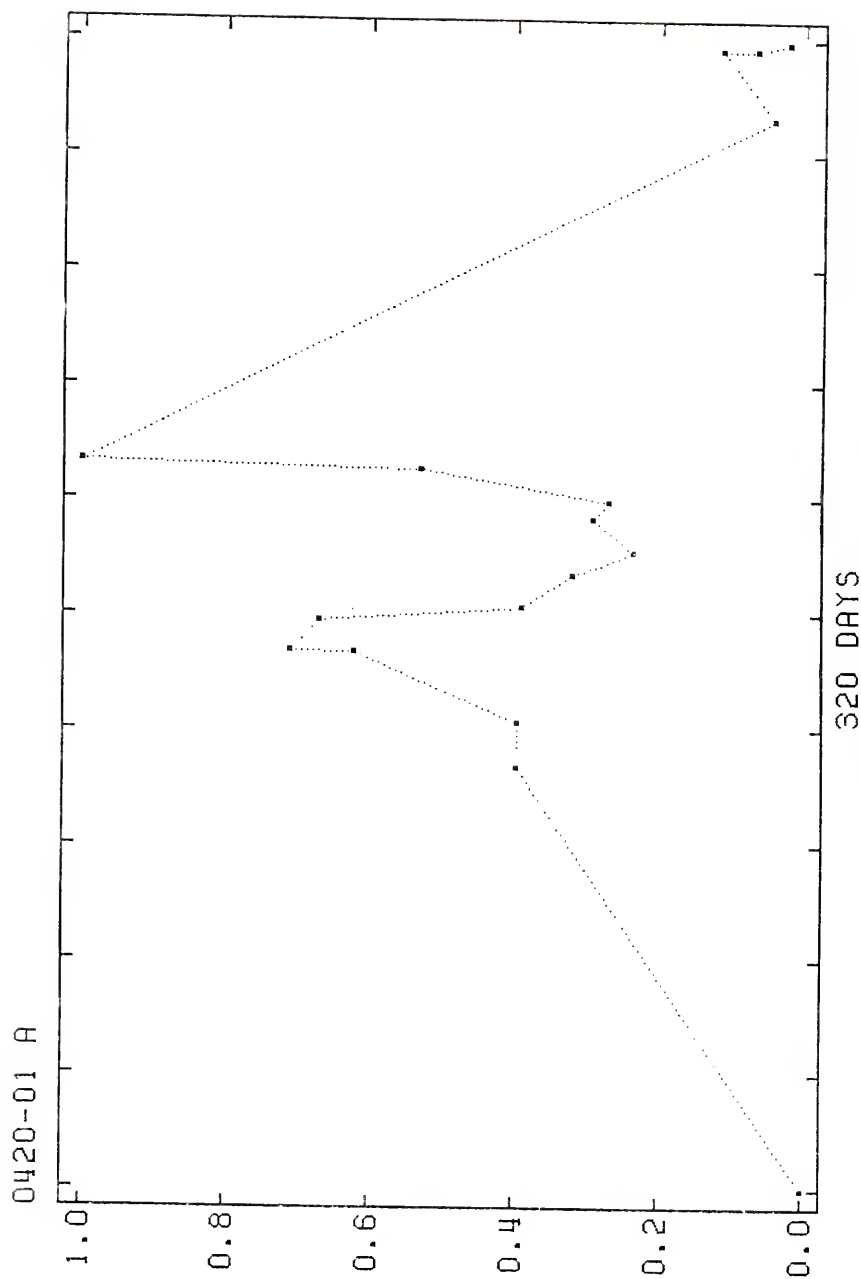


Figure 12. Event 0420-01 A, J.D. 42039 to 42700.

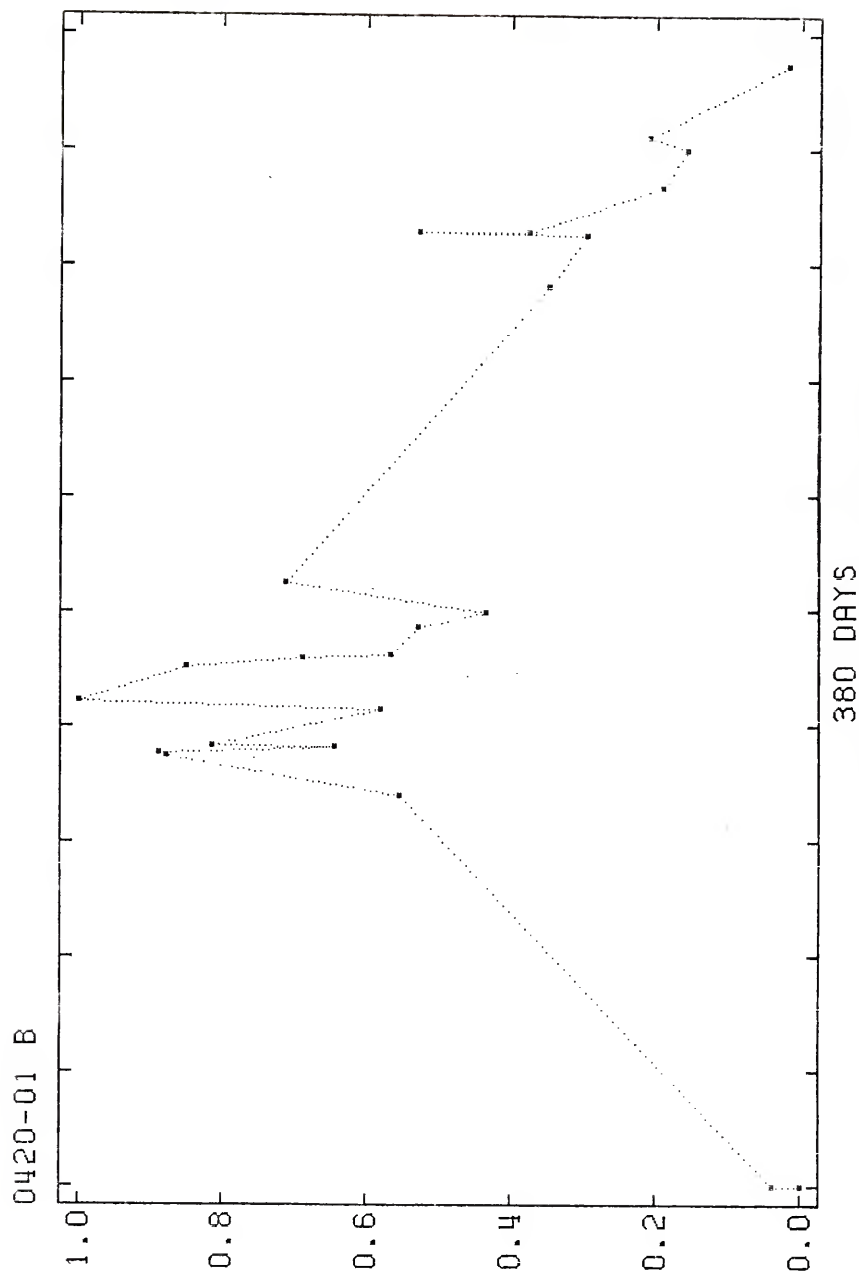


Figure 13. Event 0420-01 B, J.D. 43183 to 43892.

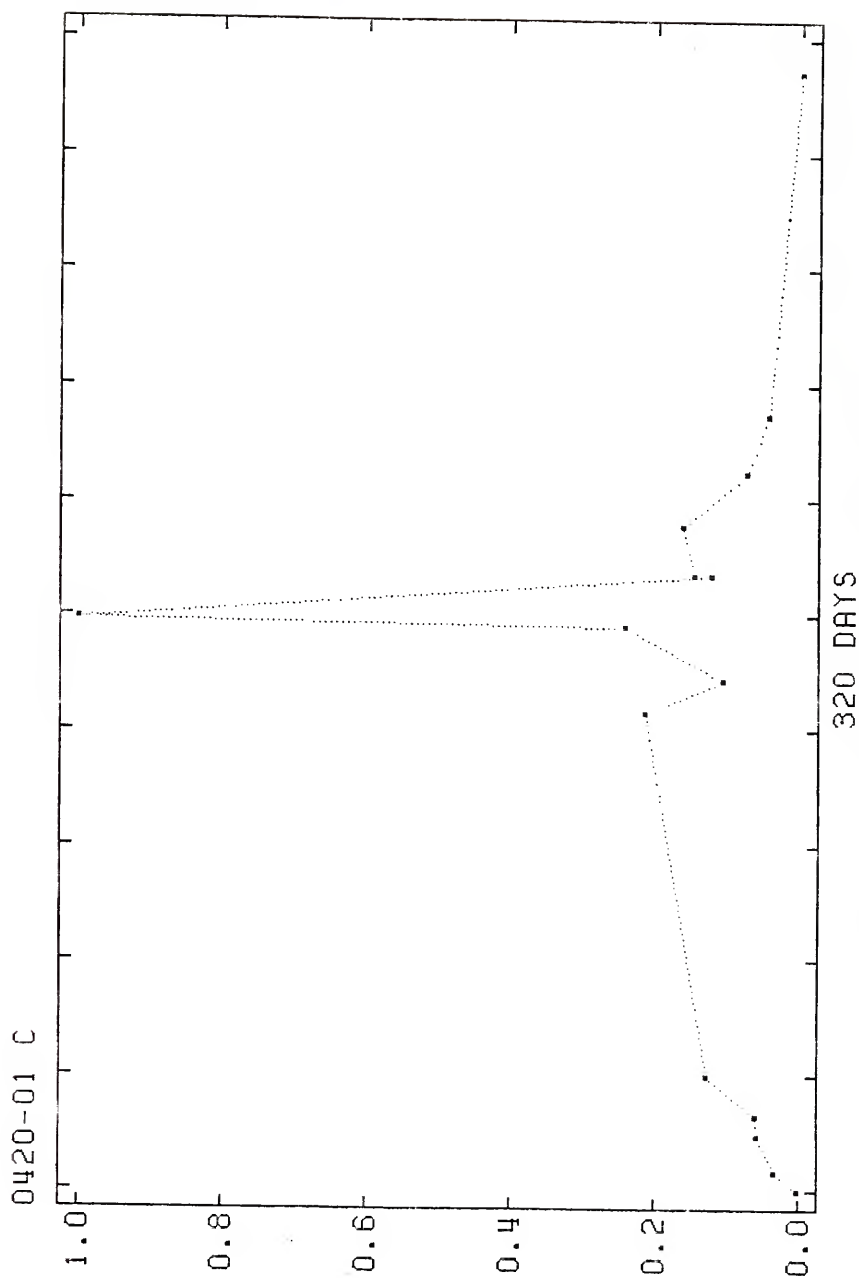


Figure 14. Event 0420-01 C, J.D. 43892 to 44487.

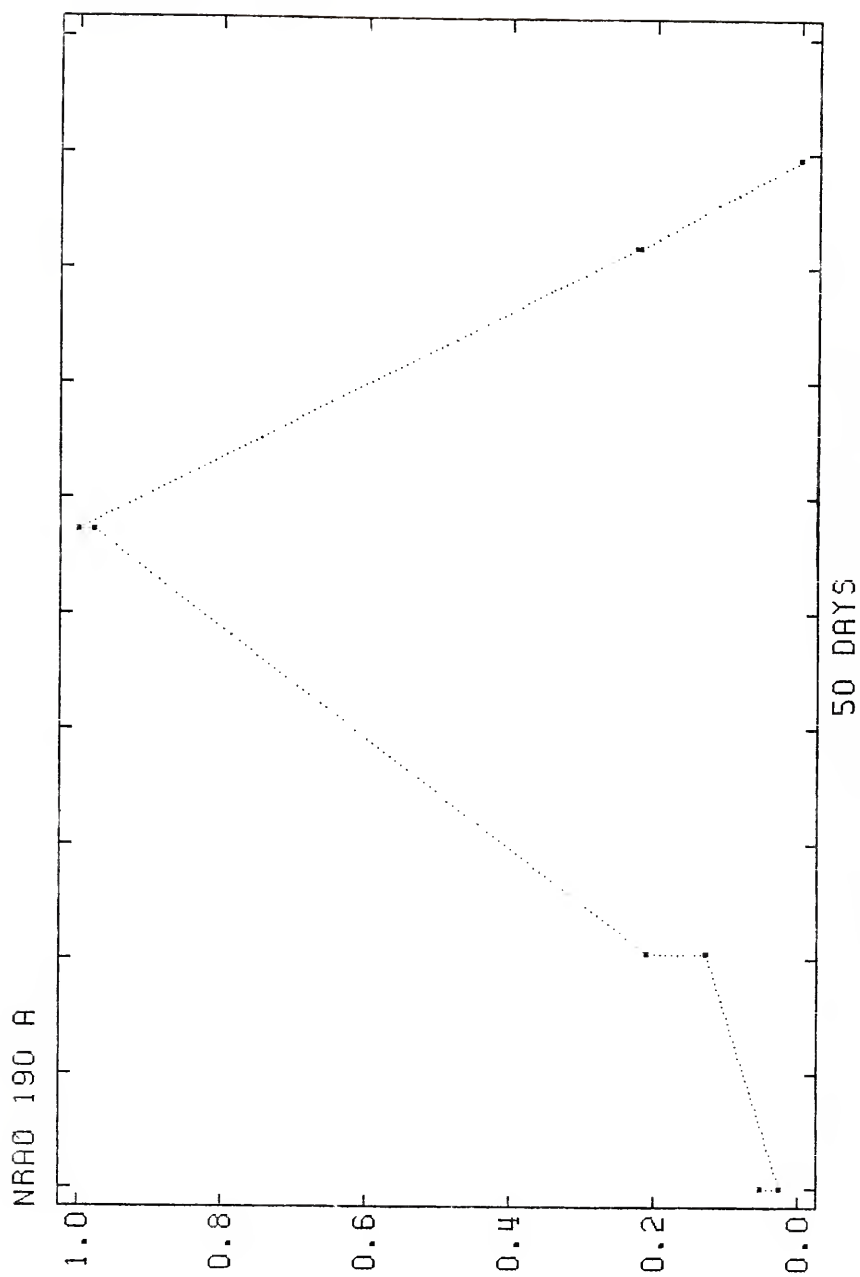


Figure 15. Event NRAO 190 A, J.D. 43054 to 43137.

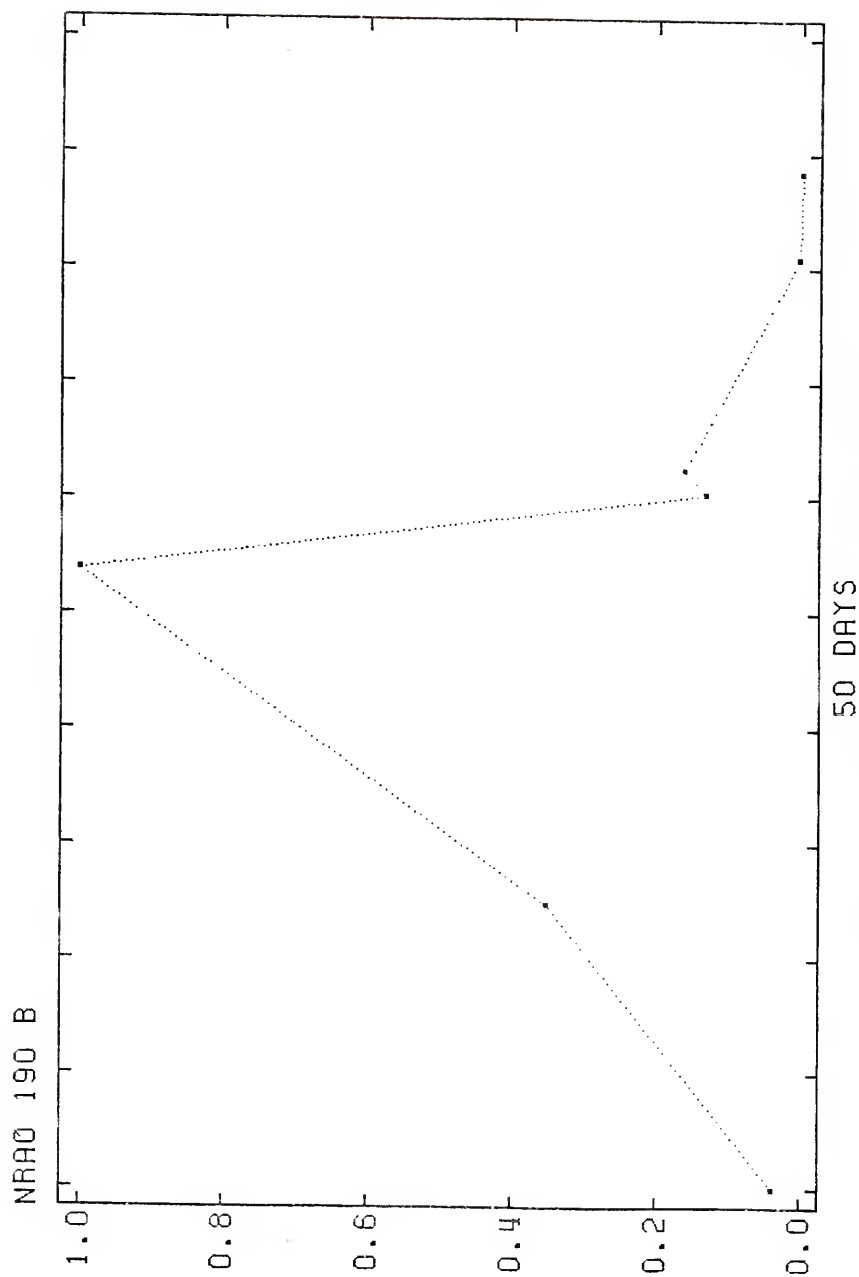


Figure 16. Event NRAO 190 B, J.D. 43462 to 43544.

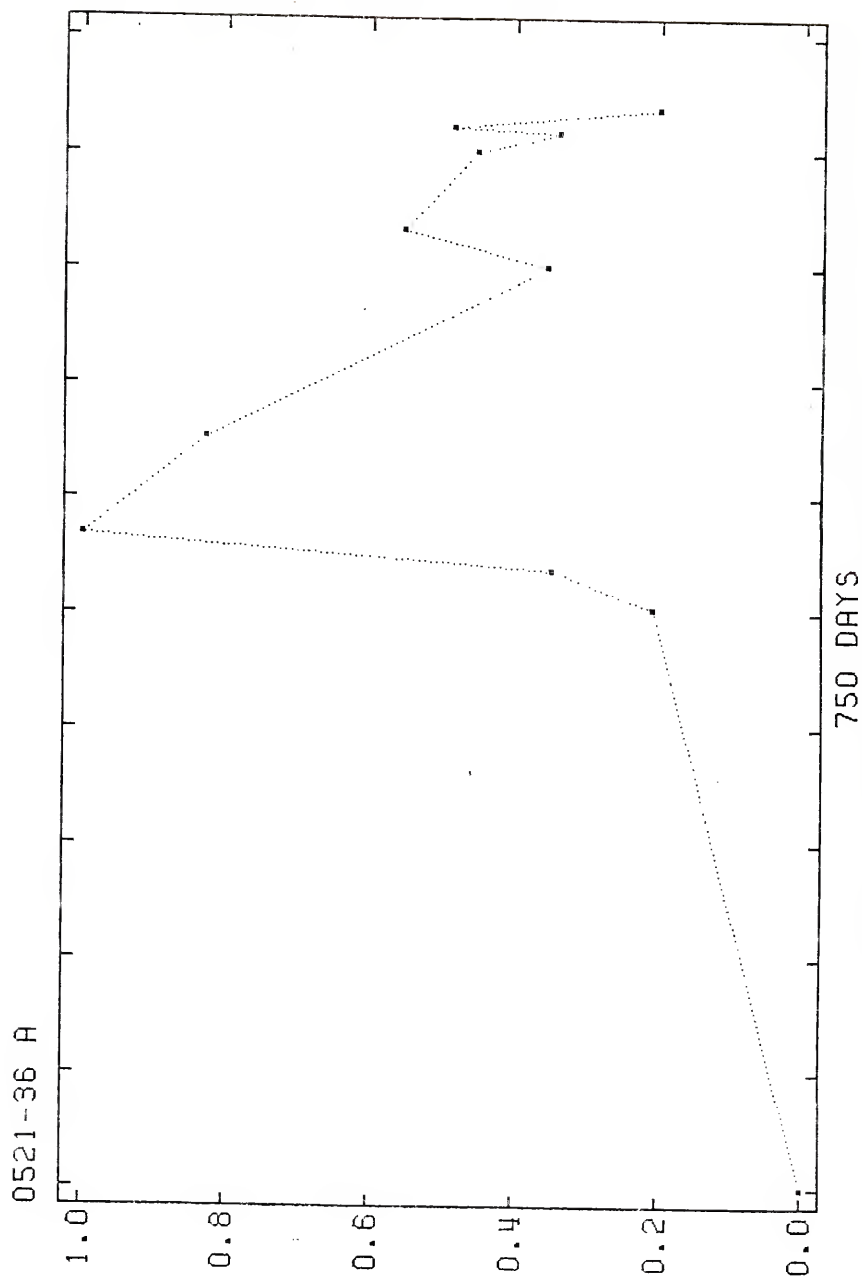


Figure 17. Event 0521-36 A, J.D. 39817 to 40560.

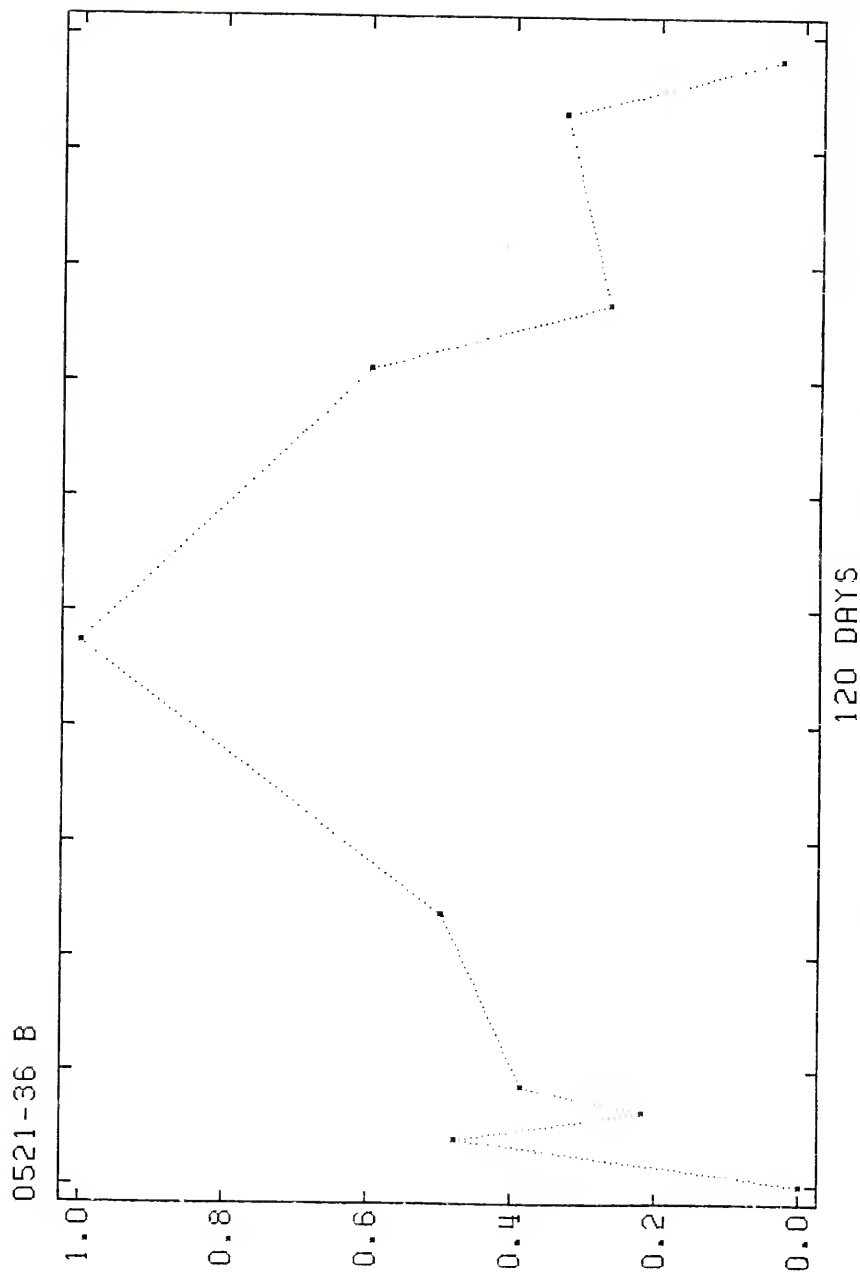


Figure 18. Event 0521-36 B, J.D. 43097 to 43221.

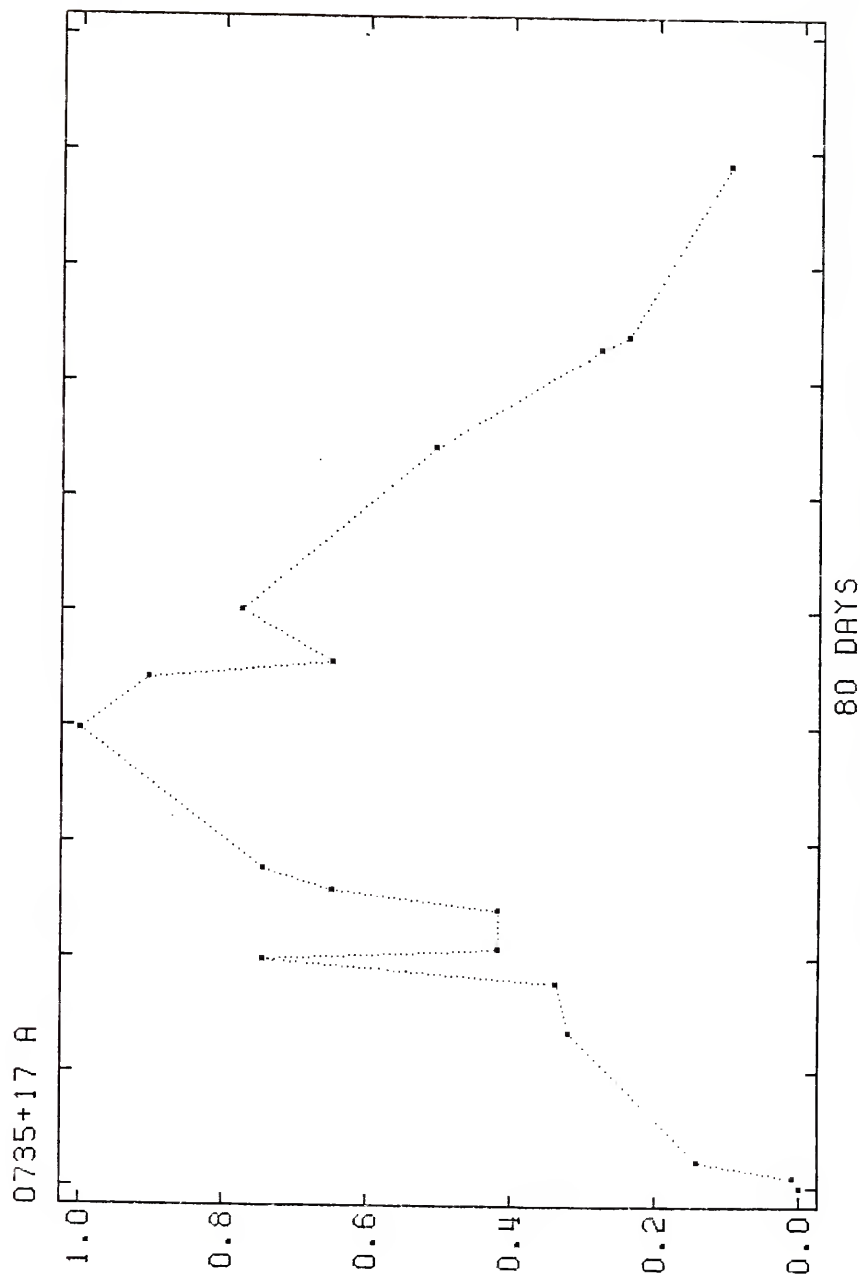


Figure 19. Event 0735+17 A, J.D. 42074 to 42148.

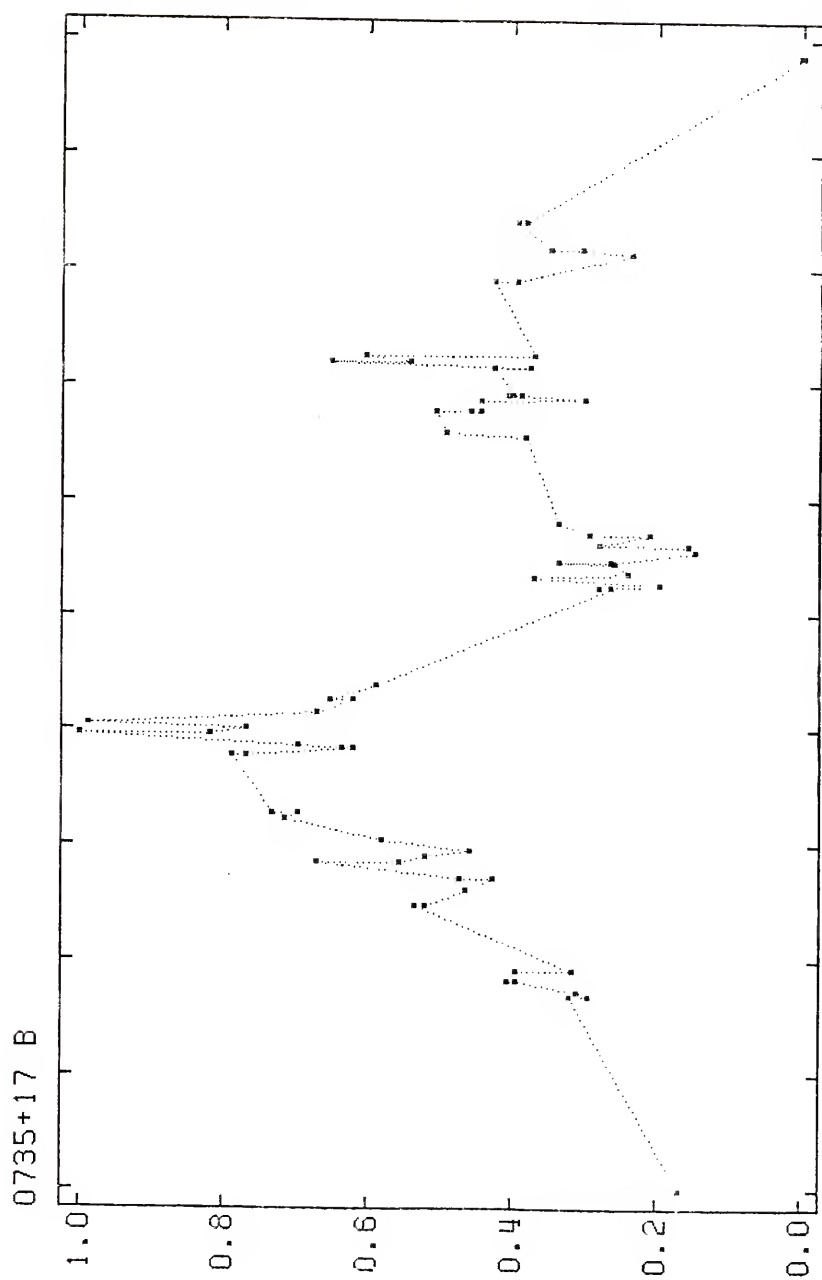


Figure 20. Event 0735+17 B, J.D. 42717 to 42928.

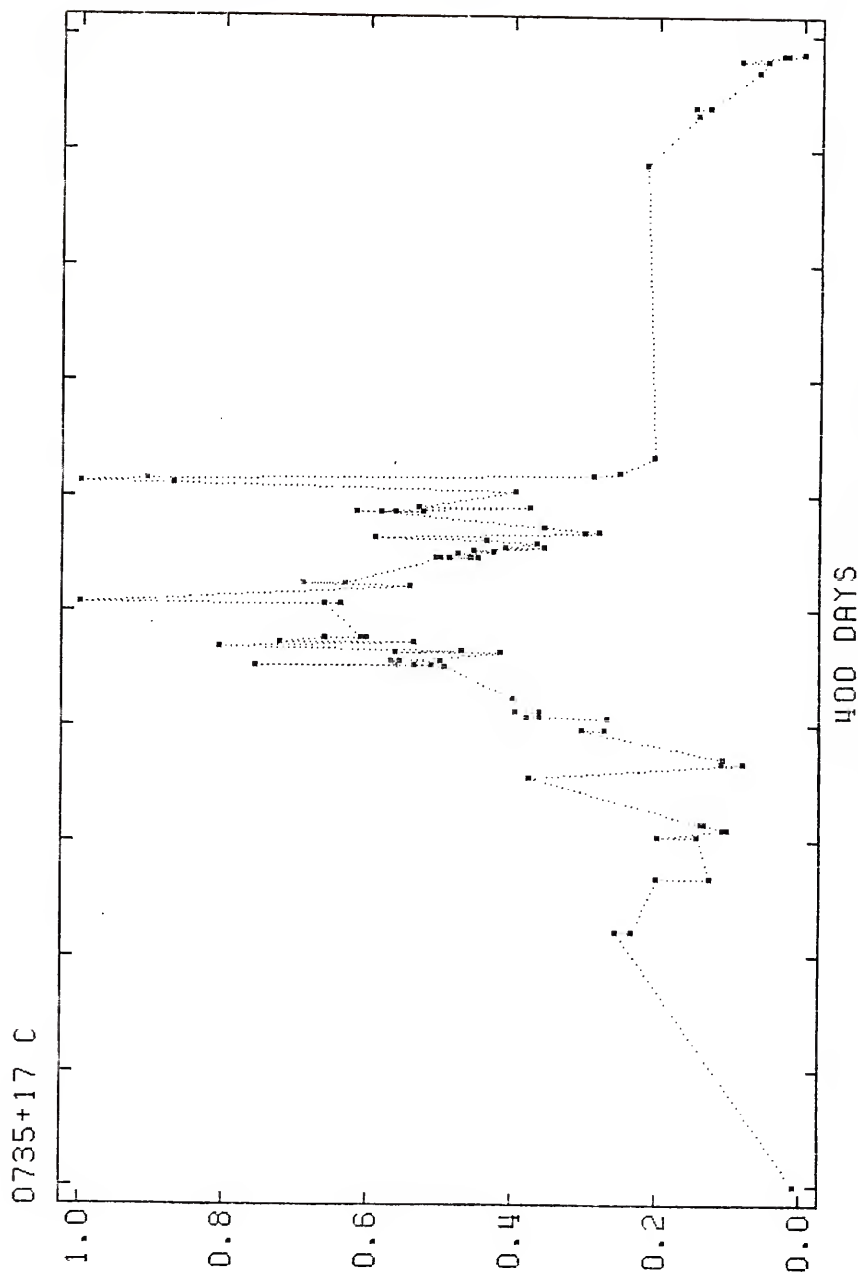


Figure 21. Event 0735+17 C, J.D. 42928 to 43489.

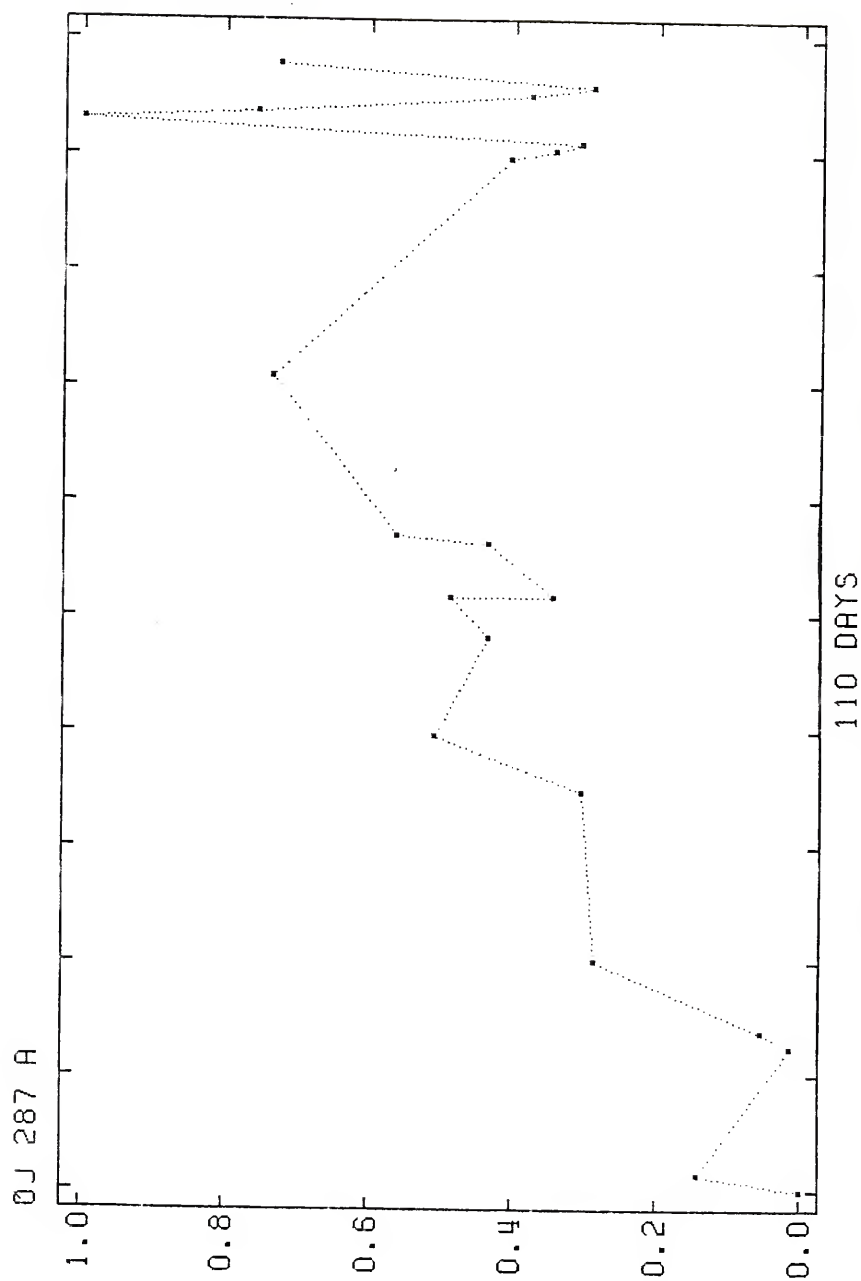


Figure 22. Event 0J 287 A, J.D. 36526 to 36667.

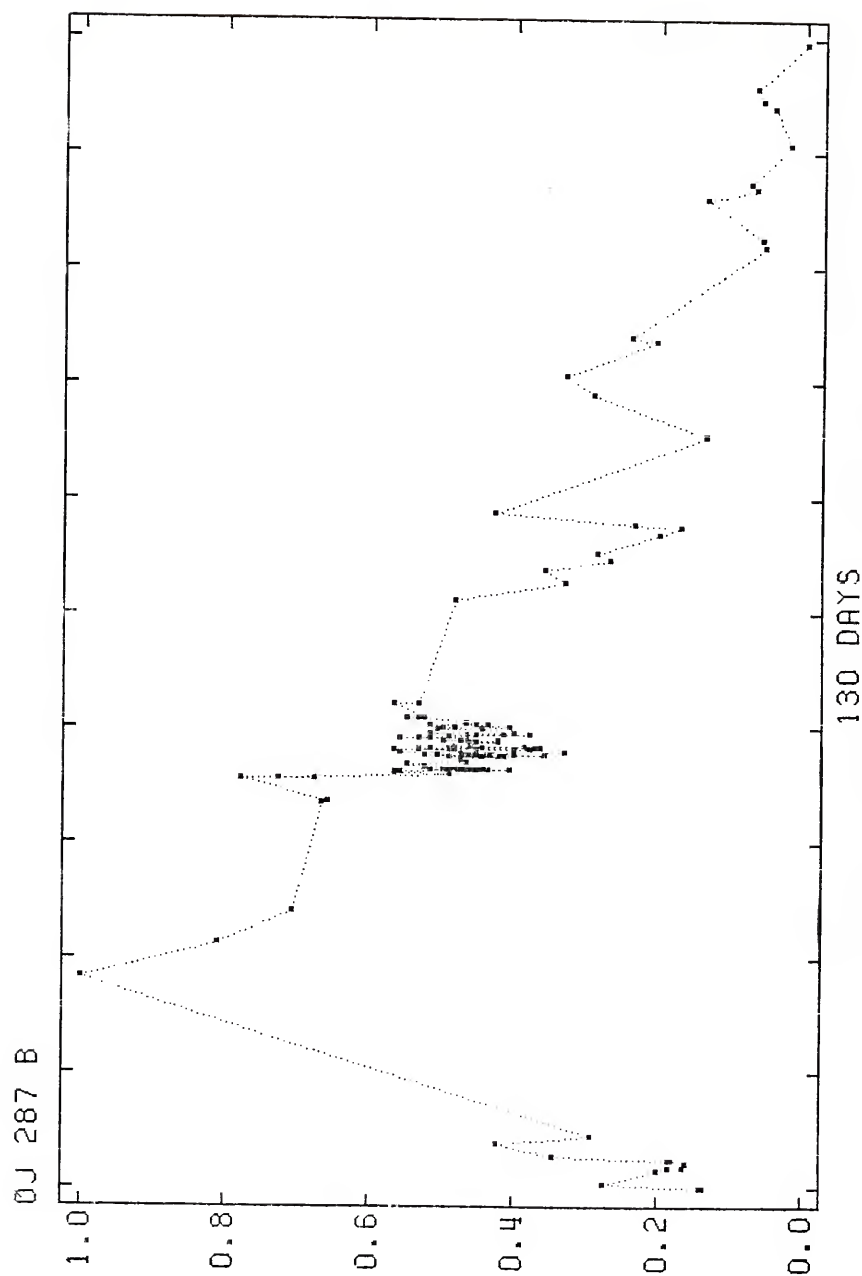


Figure 23. Event OJ 287 B, J.D. 41653 to 41822.

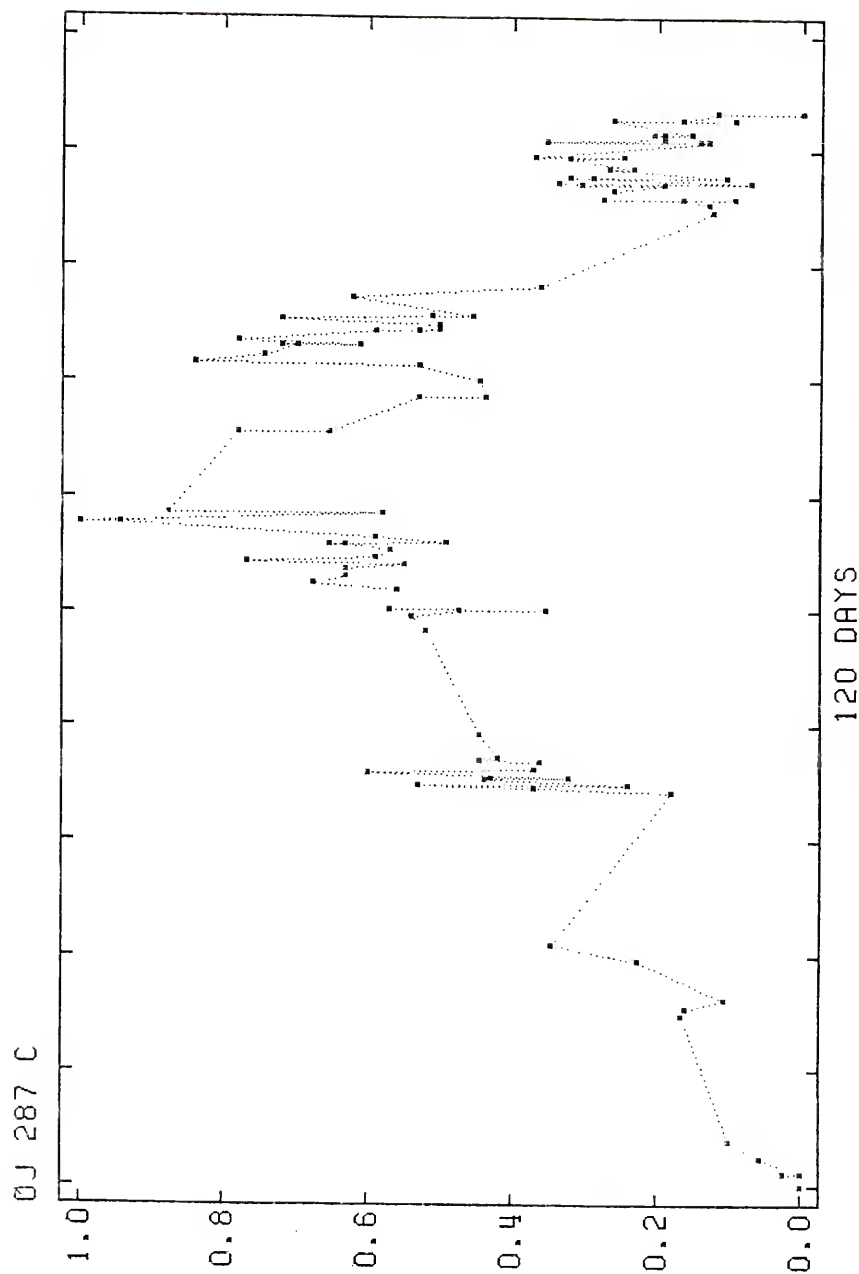


Figure 24. Event OJ 287 C, J.D. 42341 to 42488.

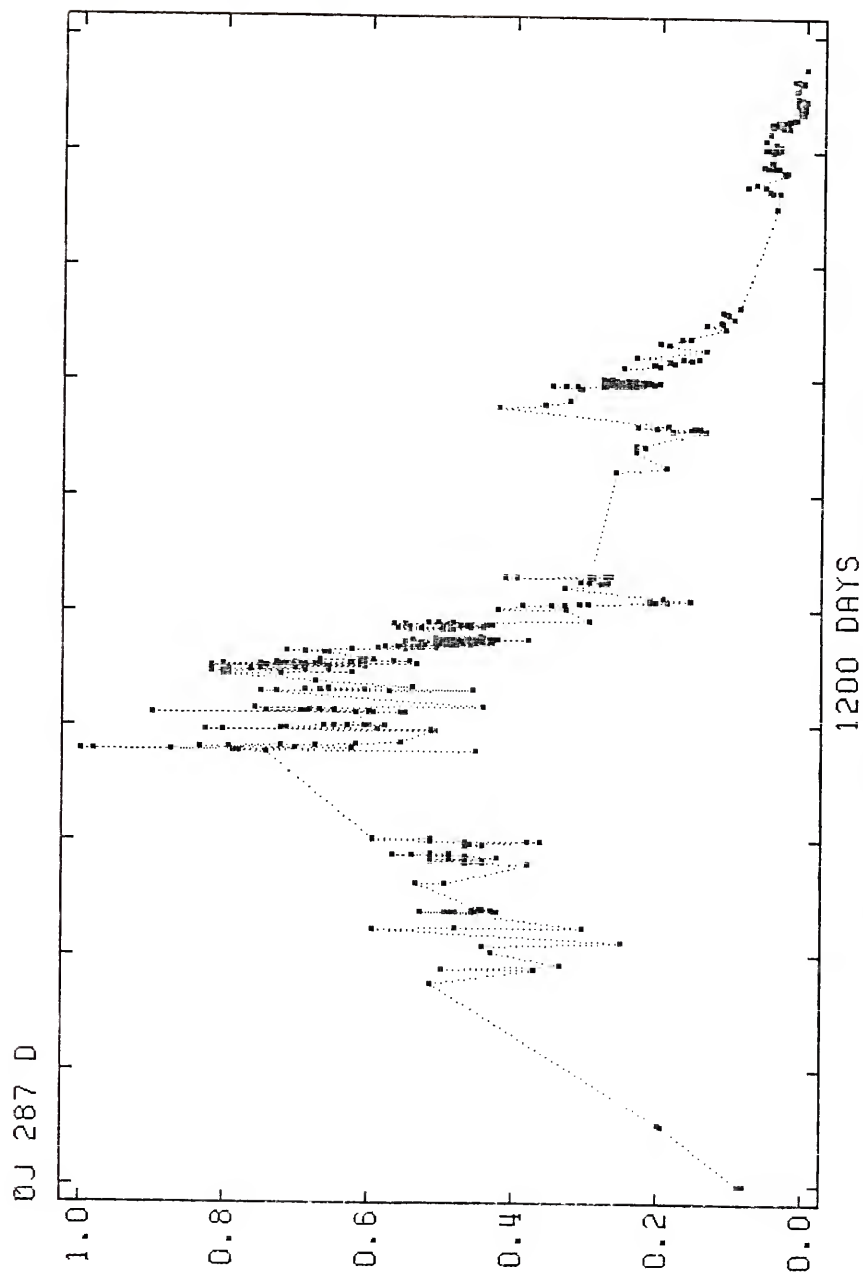


Figure 25. Event OJ 287 D, J.D. 40625 to 42149.

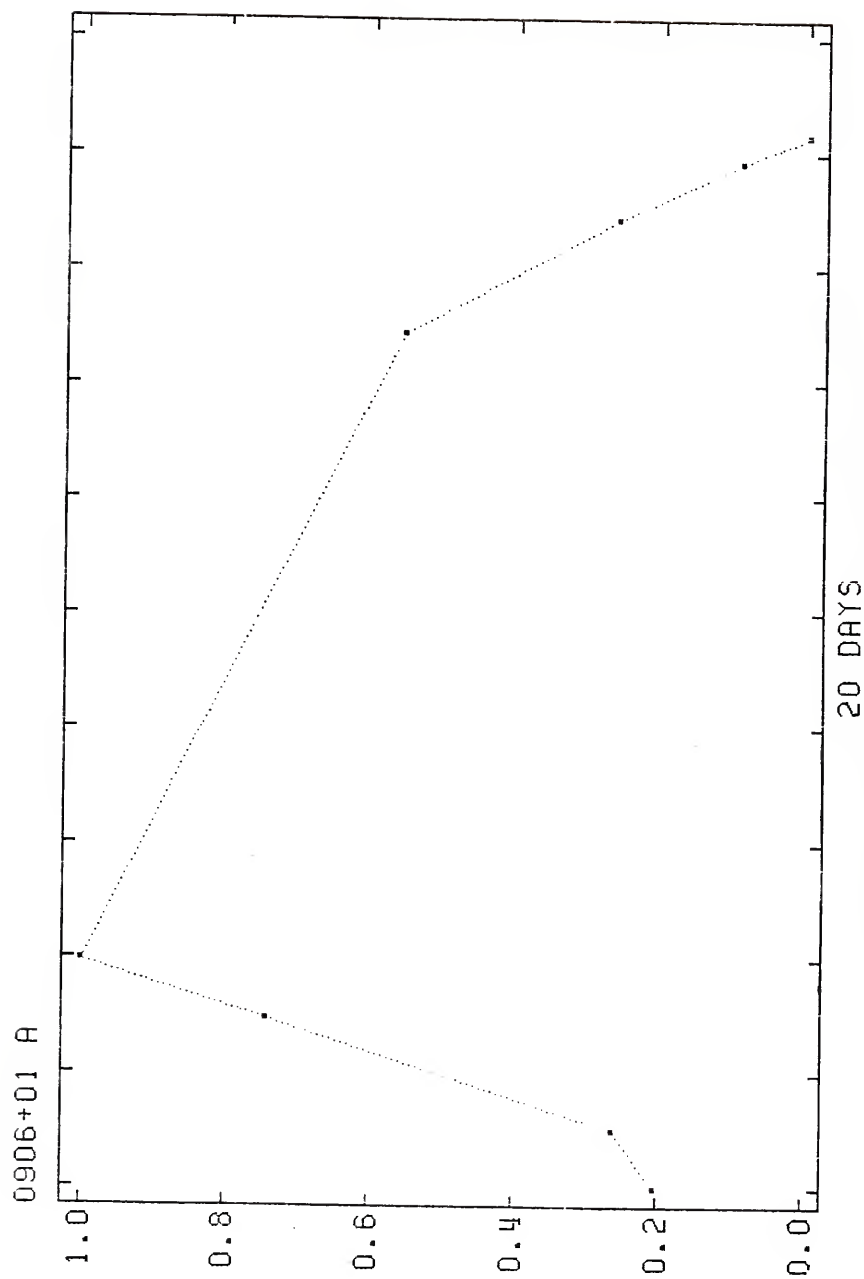


Figure 26. Event 0906+01 A, J.D. 40862 to 40899.

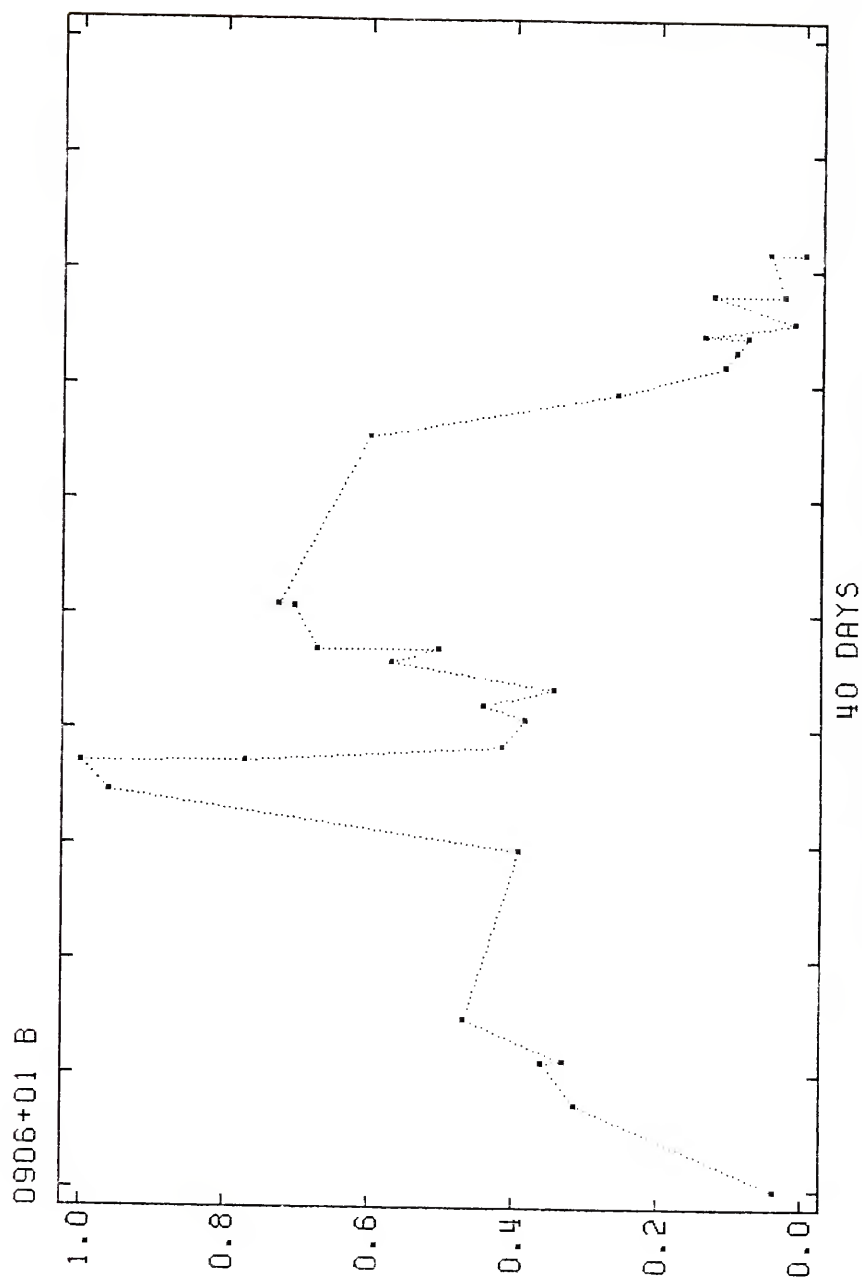


Figure 27. Event 0906+01 B, J.D. 40943 to 41009.

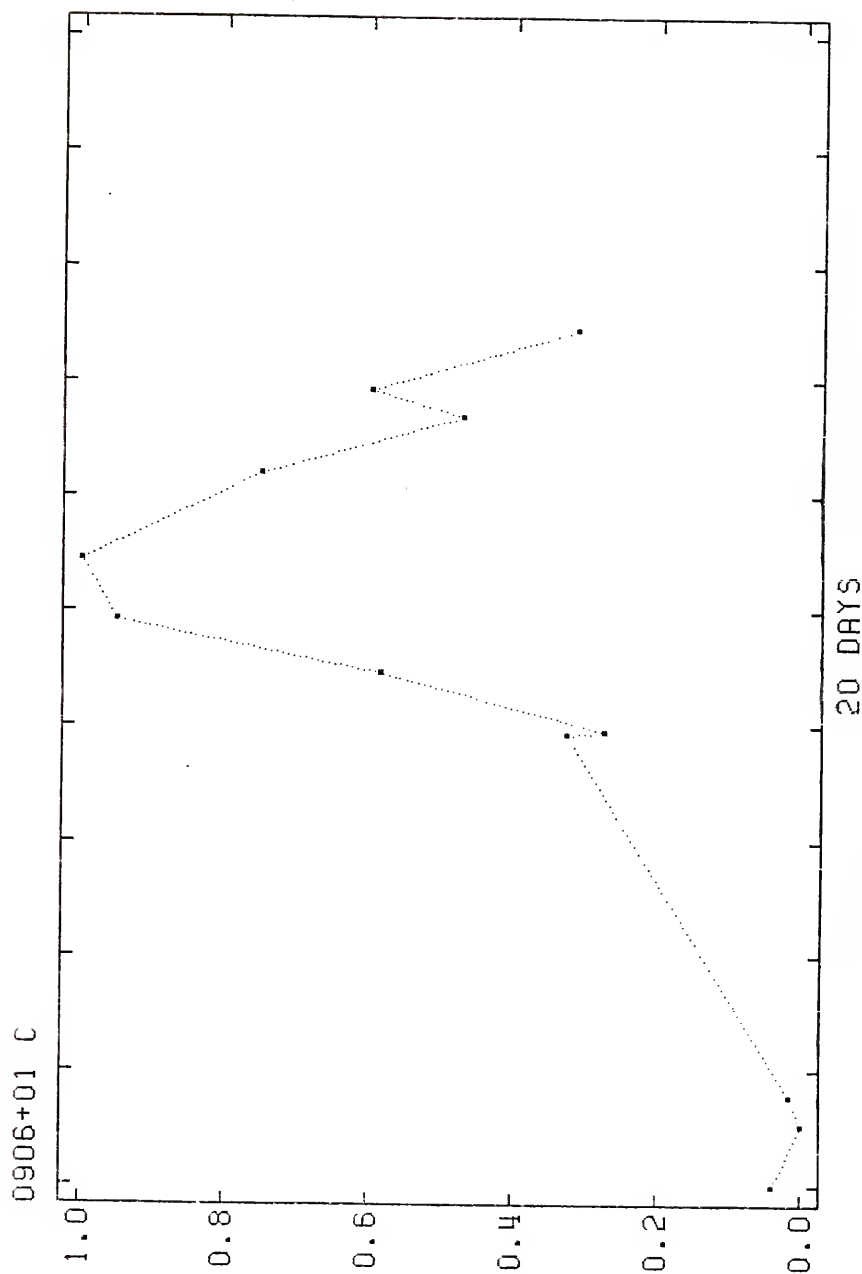


Figure 28. Event 0906+01 C, J.D. 41011 to 41041.

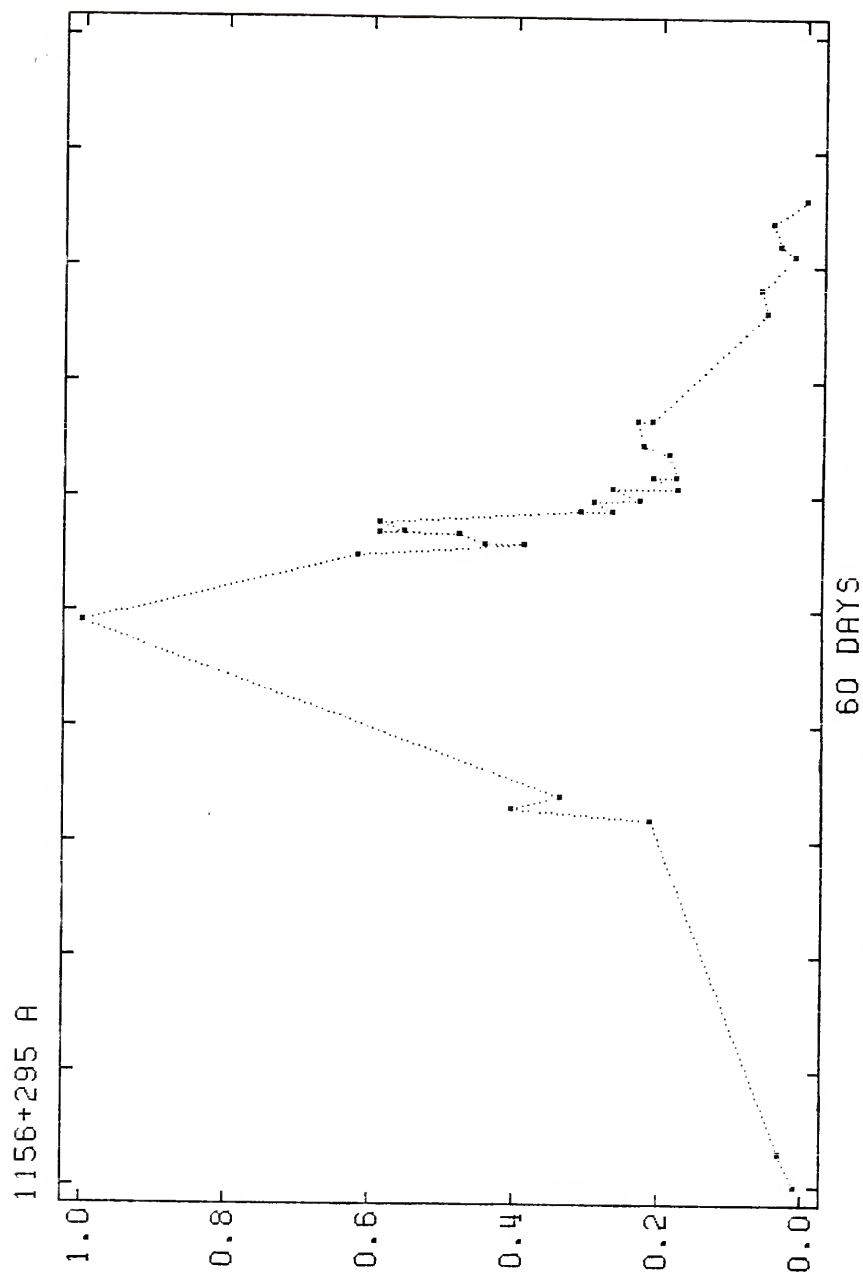


Figure 29. Event 1156+295 A, J.D. 44640 to 44729.

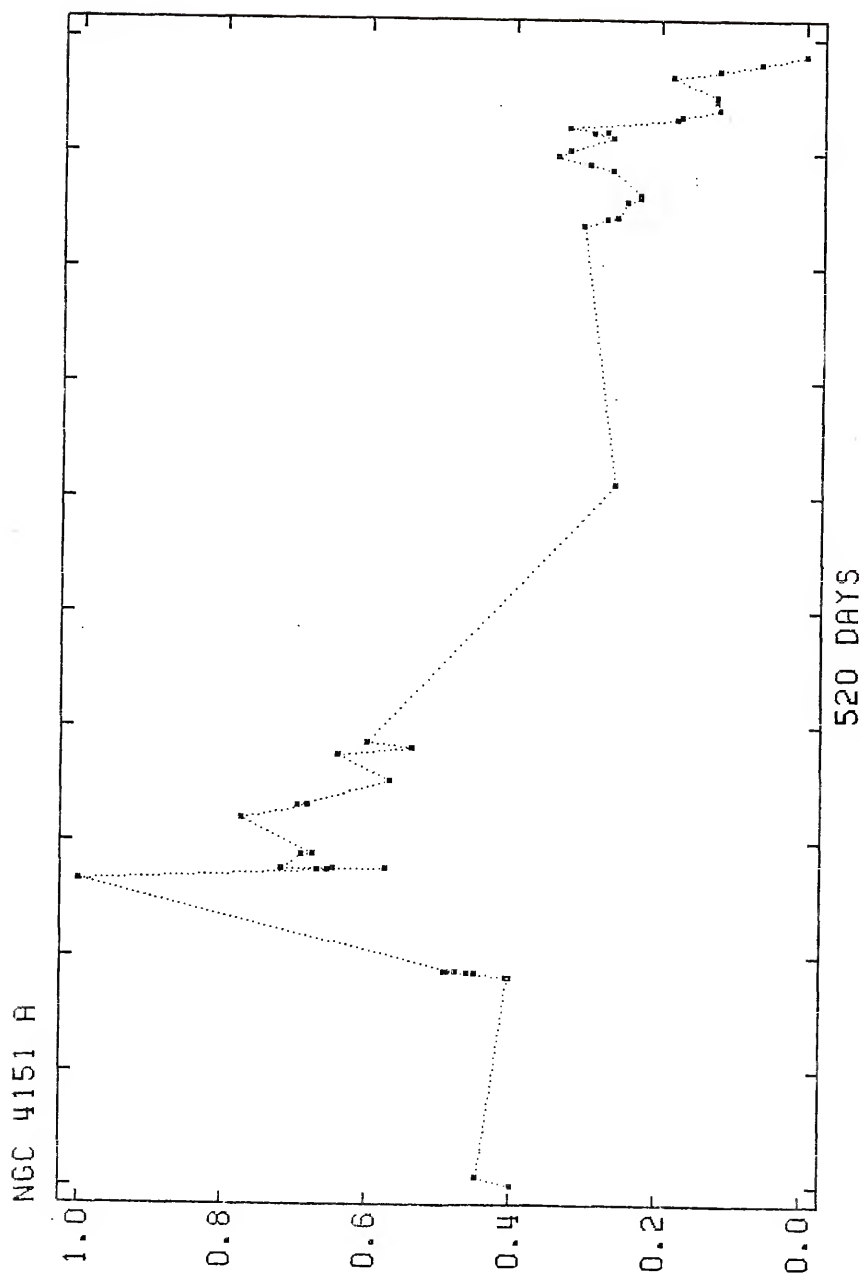


Figure 30. Event NGC 4151 A, J.D. 39505 to 40019.

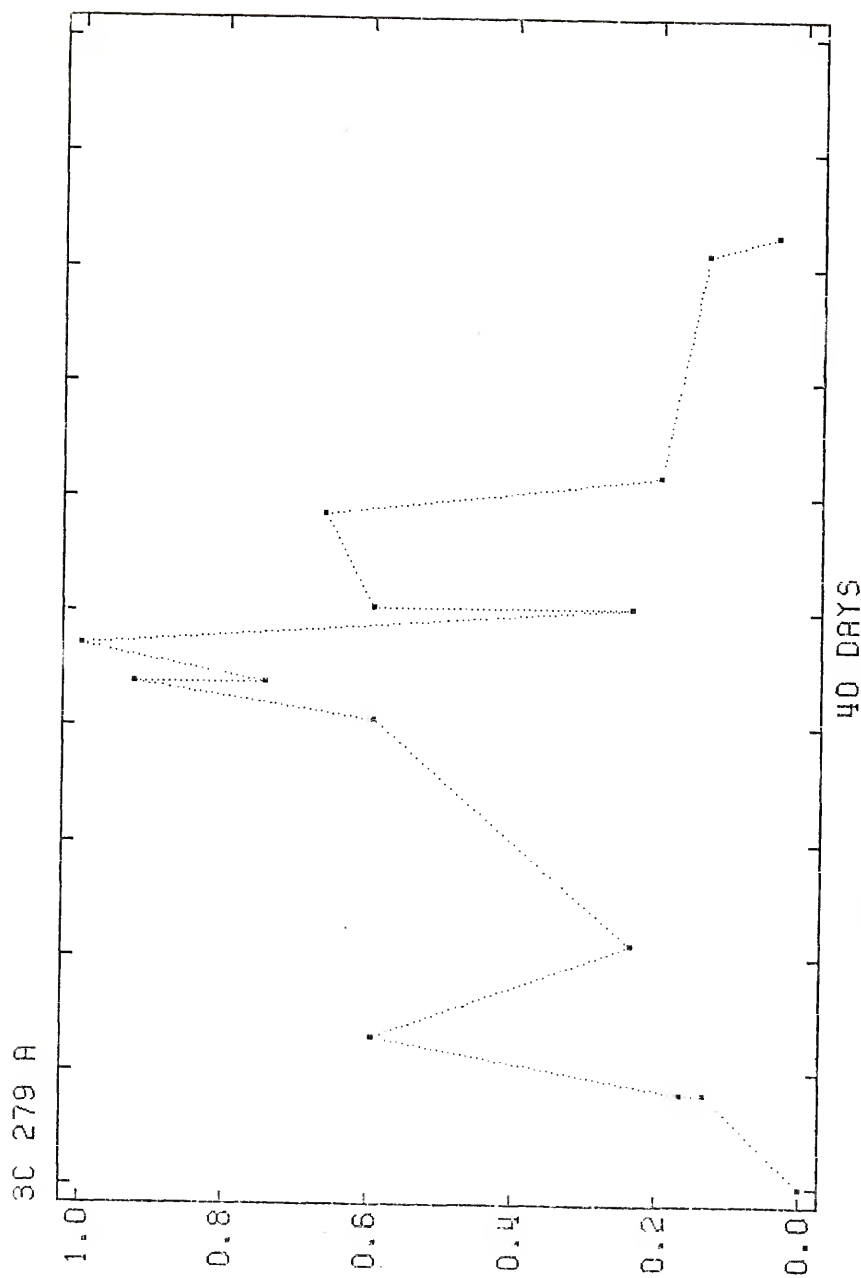


Figure 31. Event 3C 279 A, J.D. 28279 to 28330.

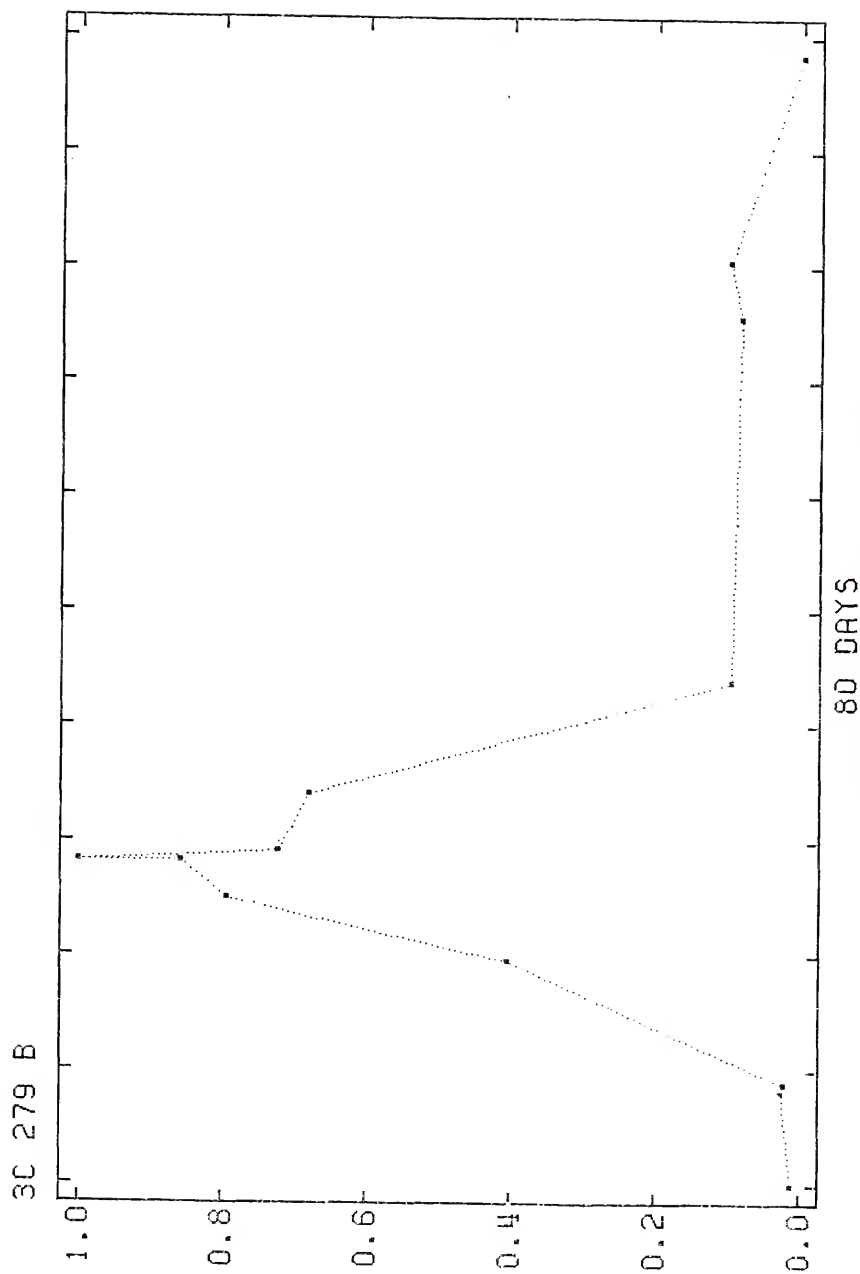


Figure 32. Event 3C 279 B, J.D. 28601 to 28722.

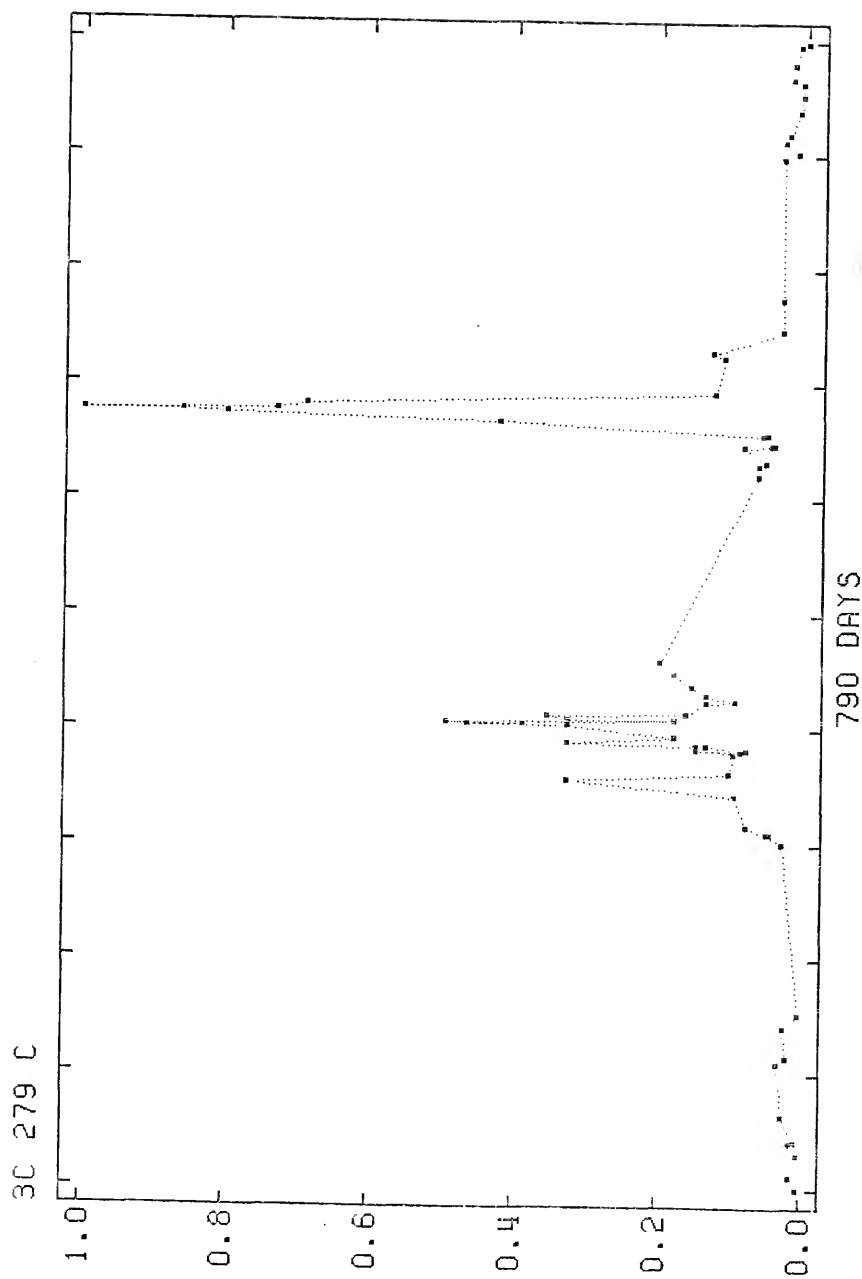


Figure 33. Event 3C 279 C, J.D. 27814 to 29028.

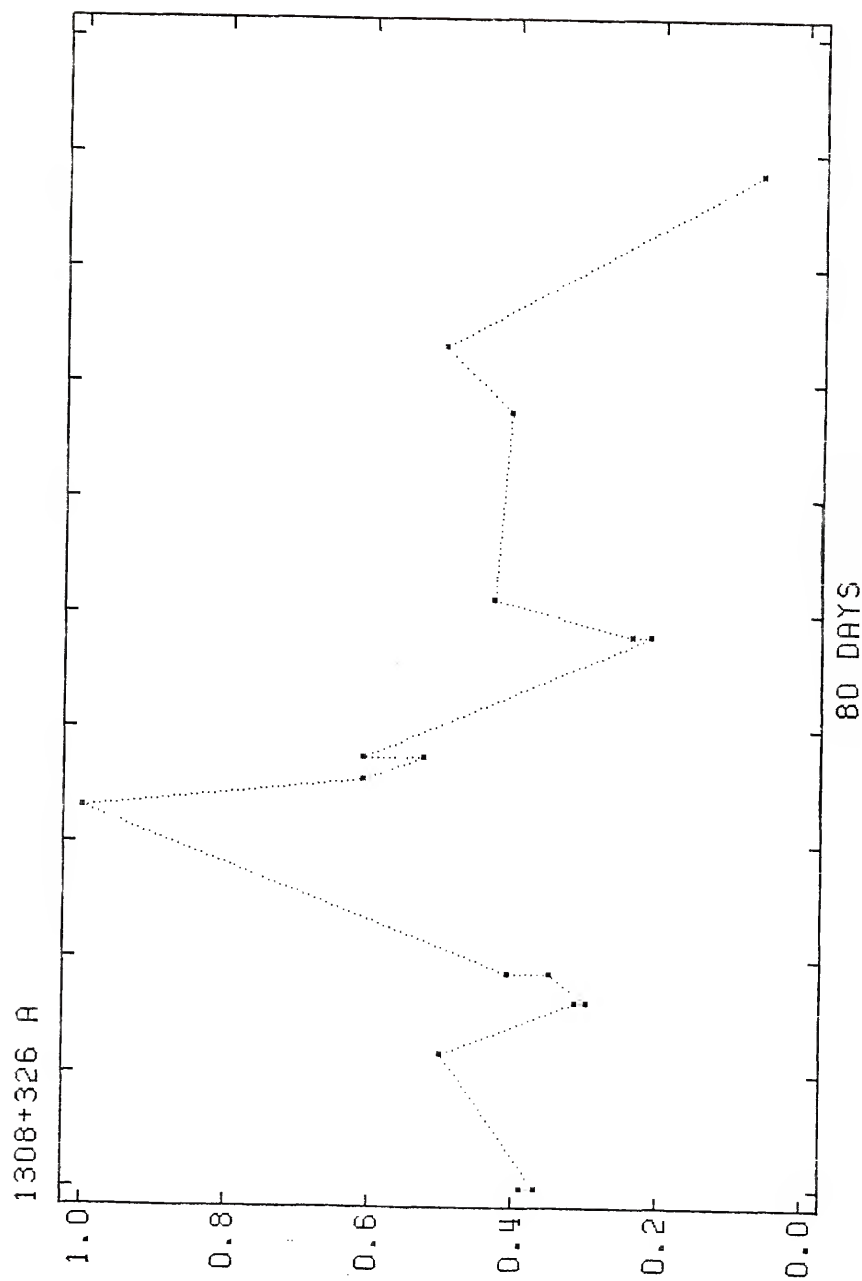


Figure 34. Event 1308+326 A, J.D. 43169 to 43310.

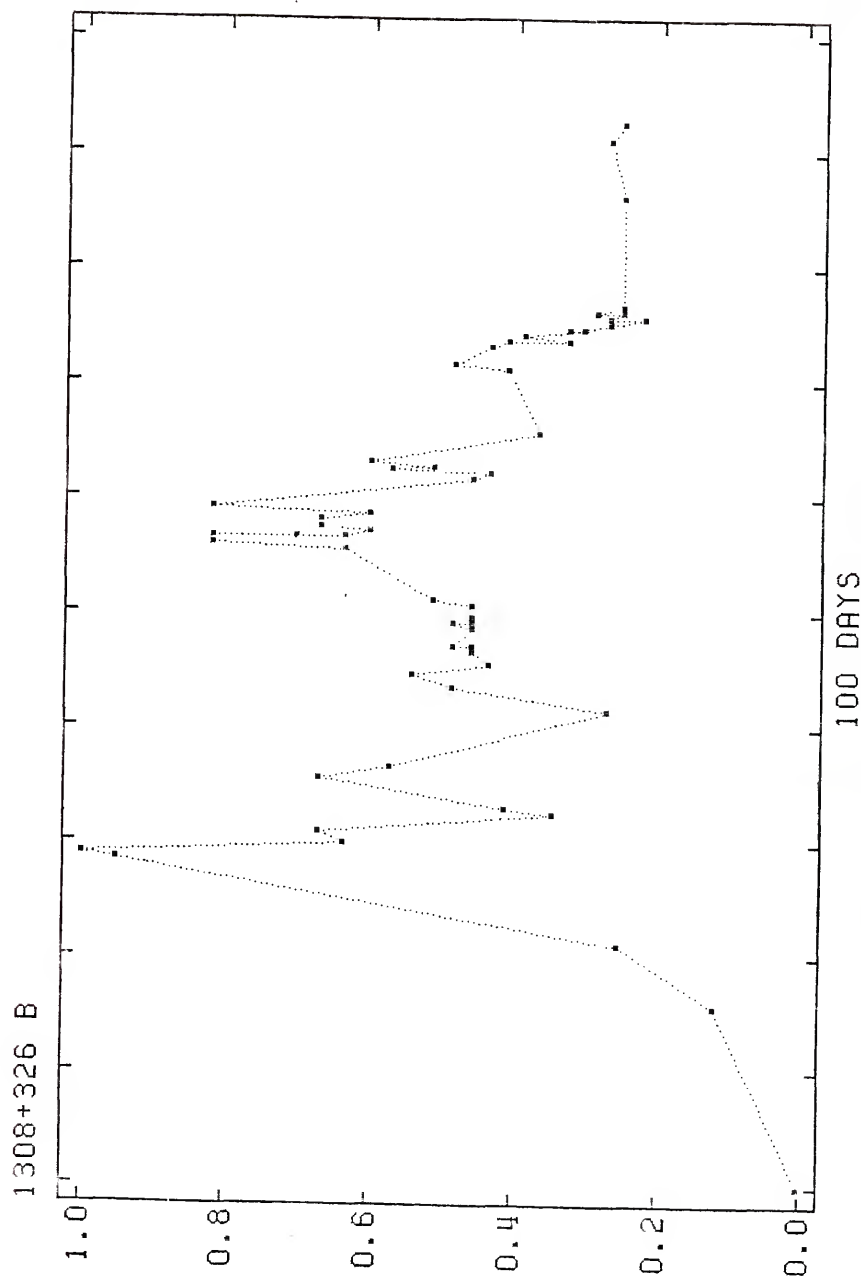


Figure 35. Event 1308+326 B, J.D. 43543 to 43728.

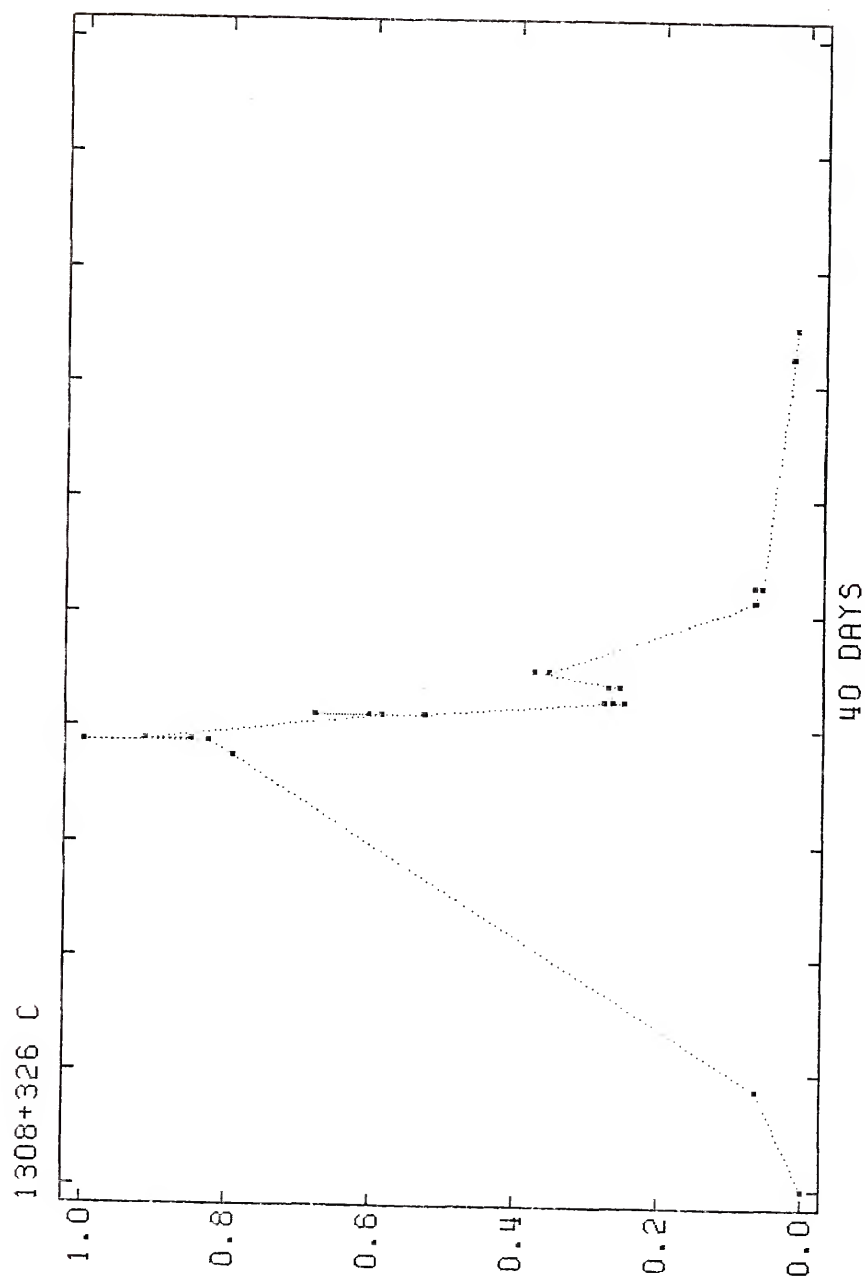


Figure 36. Event 1308+326 C, J.D. 44395 to 44455.

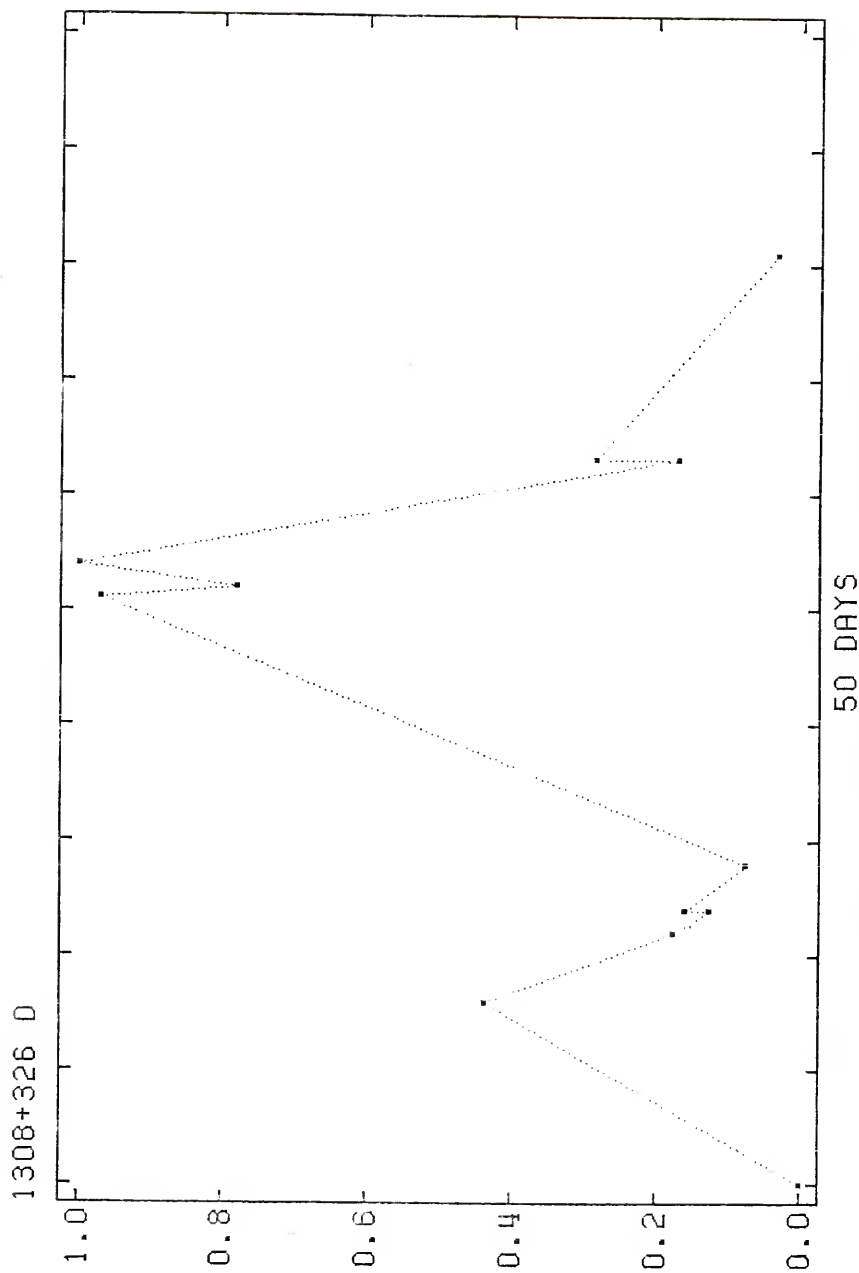


Figure 37. Event 1308+326 D, J.D. 44673 to 44754.

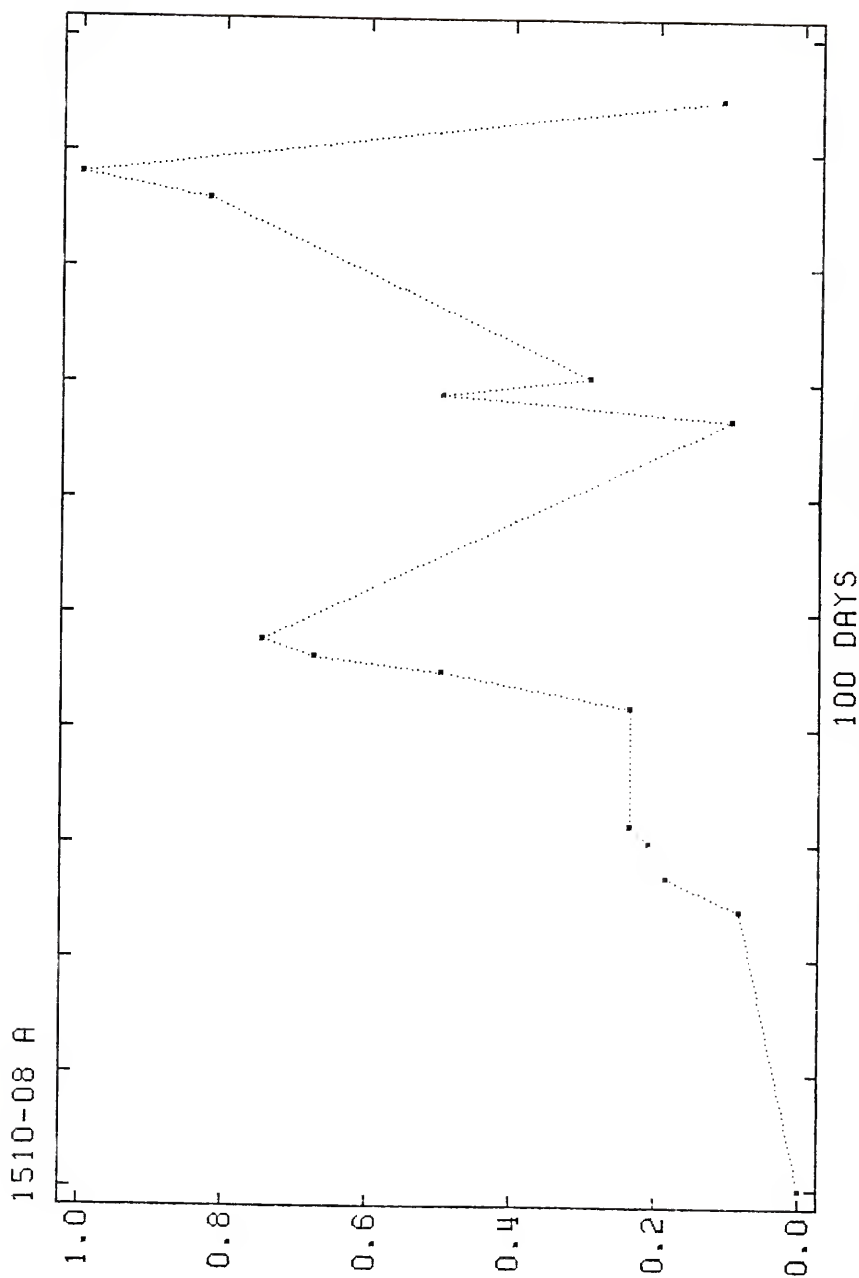


Figure 38. Event 1510-08 A, J.D. 32671 to 32800.

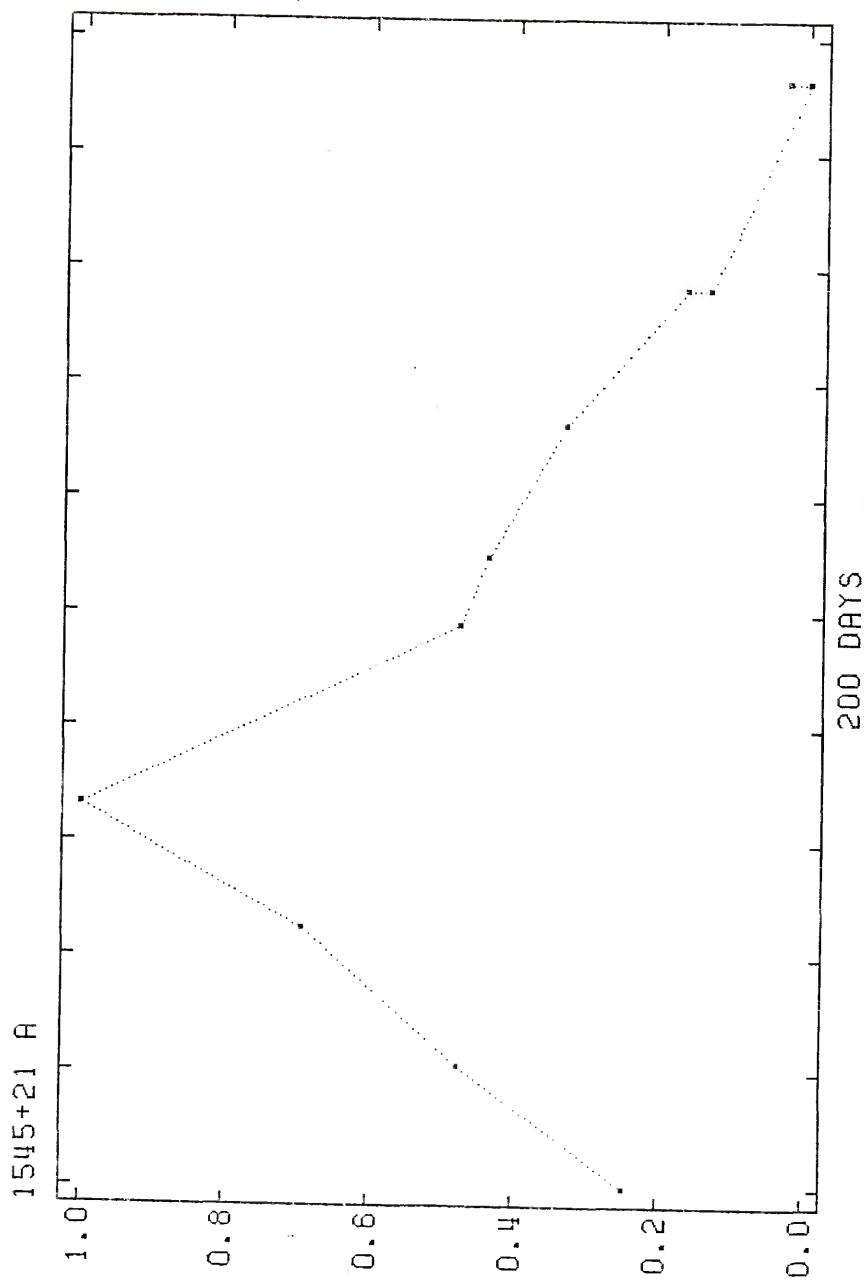


Figure 39. Event 1545+21 A, J.D. 40596 to 40840.

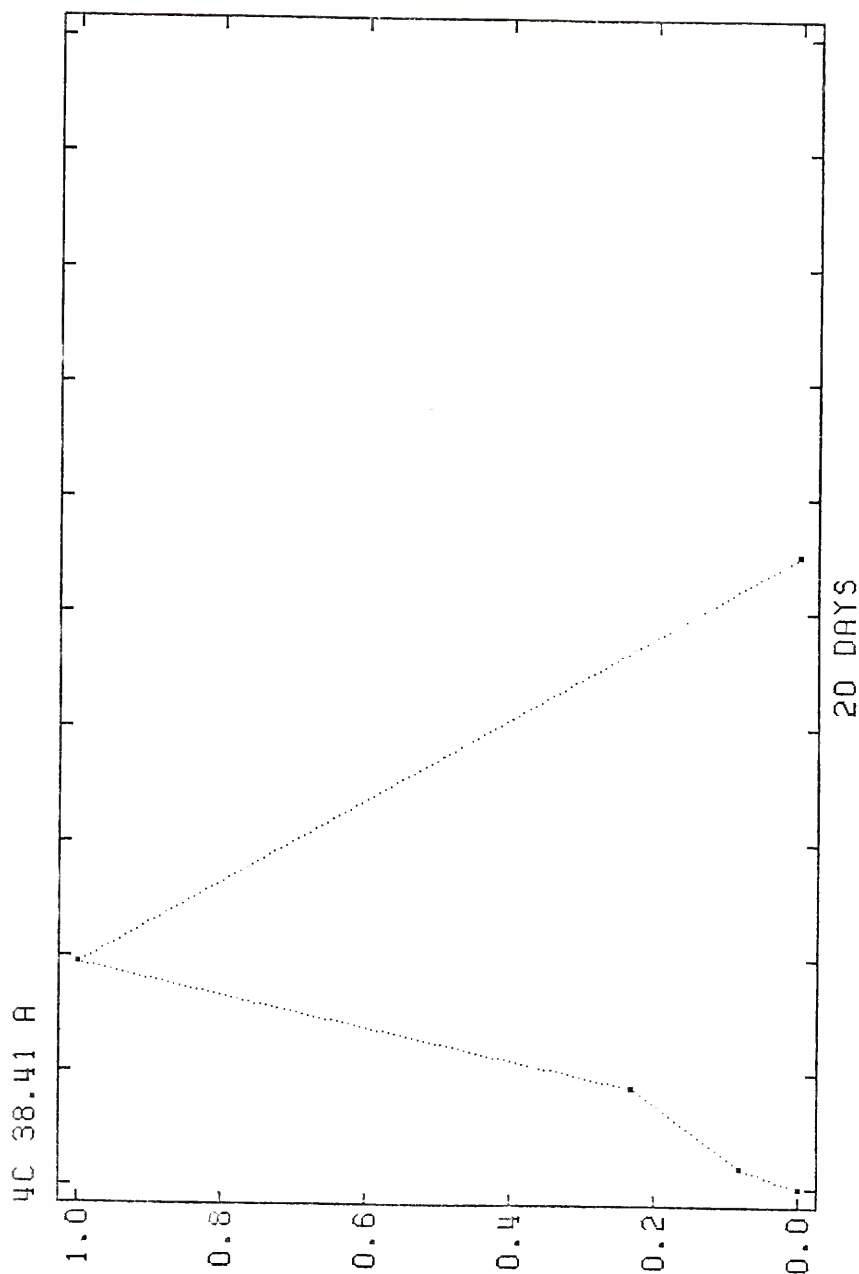


Figure 40. Event 4C 38.41 A, J.D. 41087 to 41119.

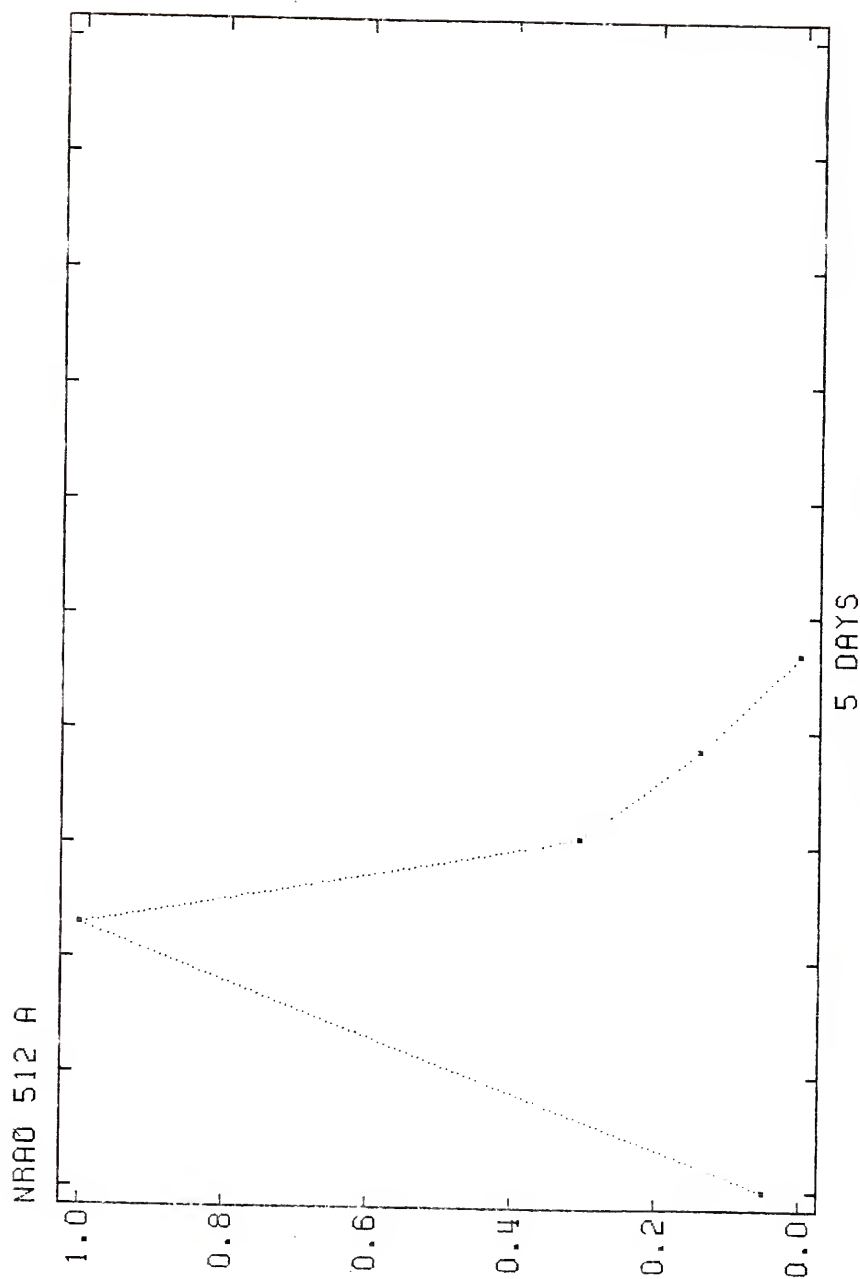


Figure 41. Event NRAO 512 A, J.D. 40703 to 40709.

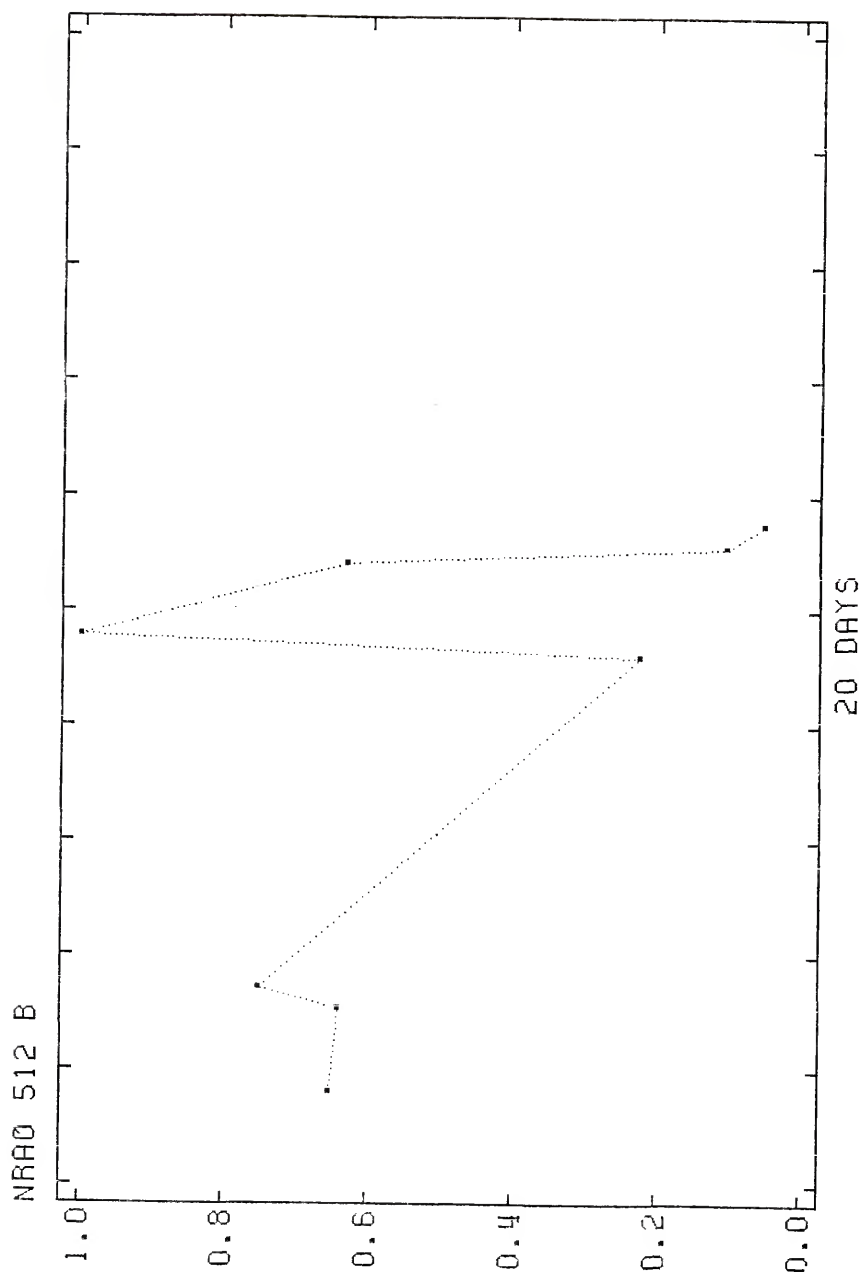


Figure 42. Event NRAO 512 B, J.D. 40709 to 40739.

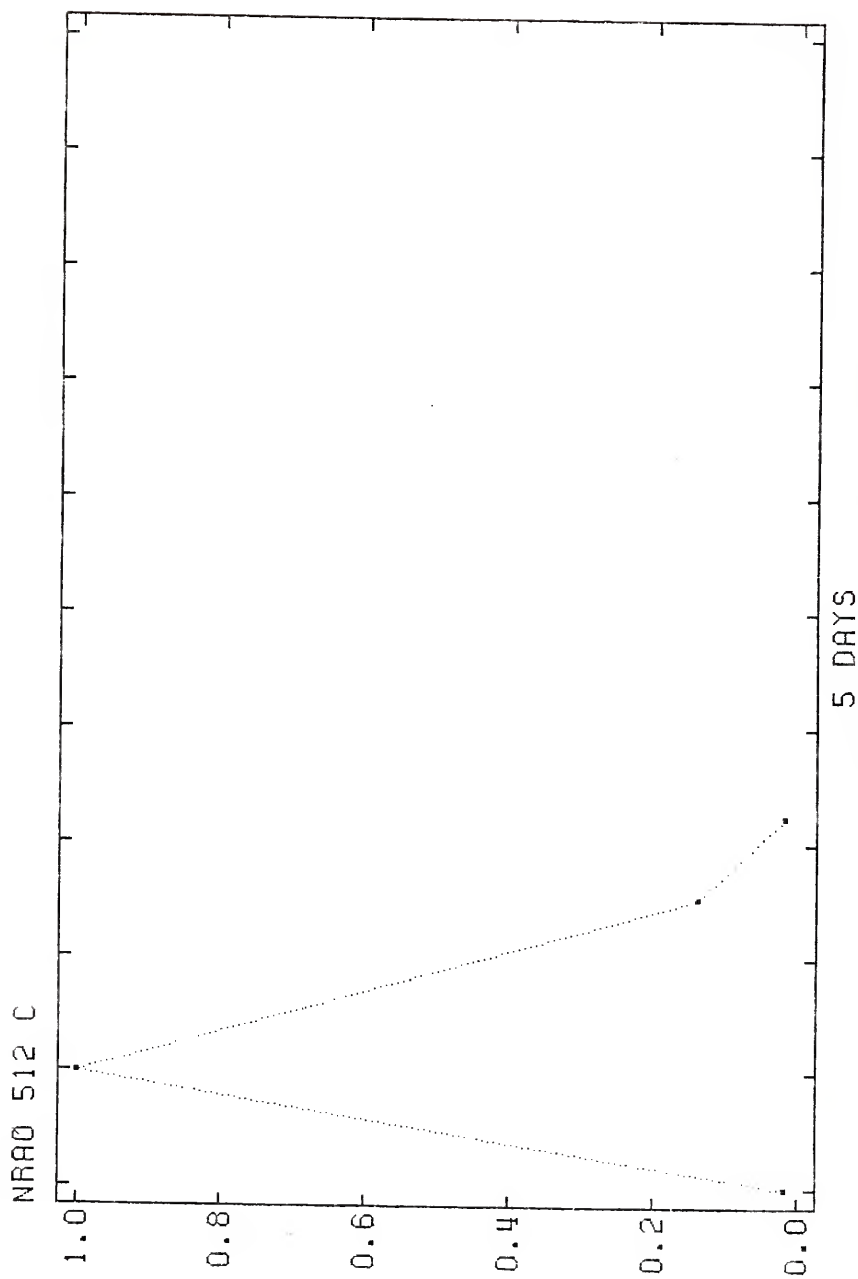


Figure 43. Event NRAO 512 C, J.D. 40739 to 40743.

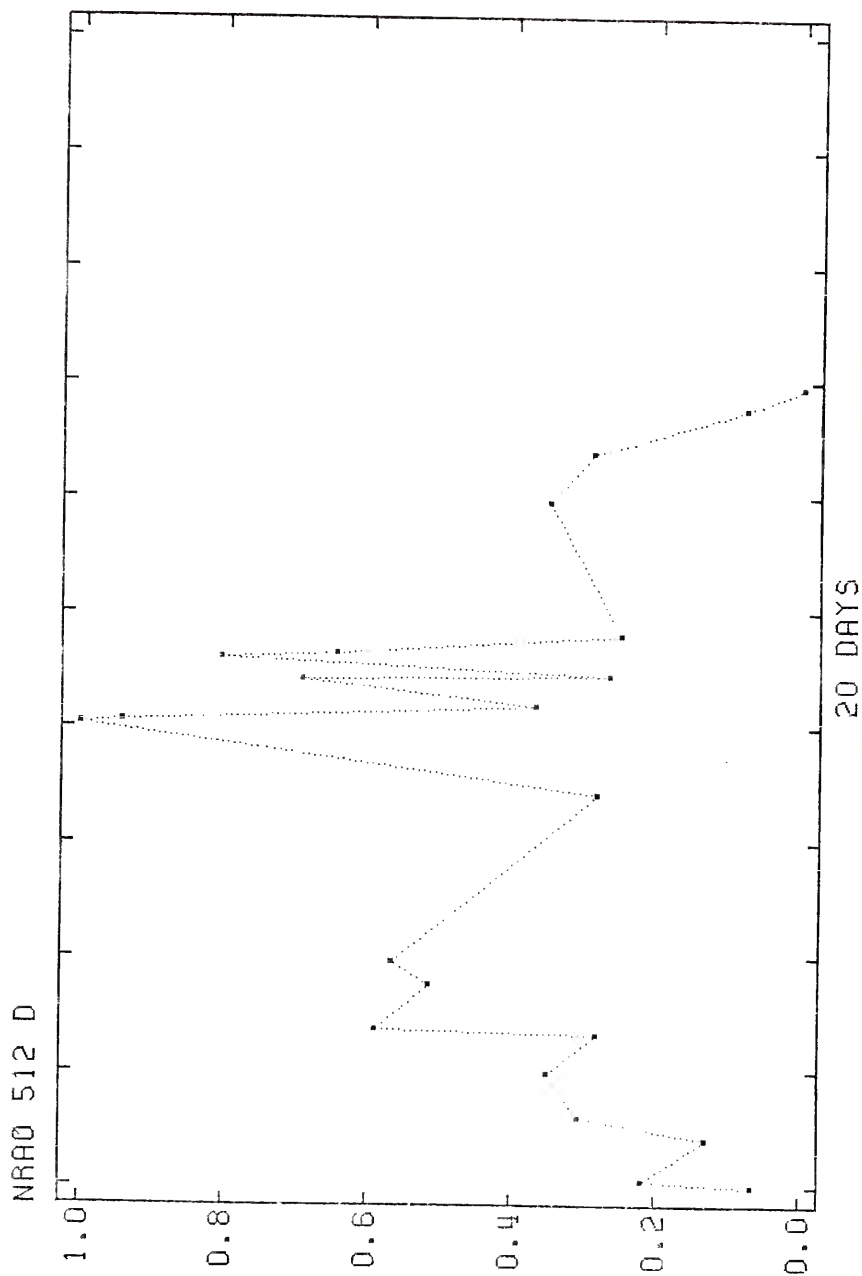


Figure 44. Event NRAO 512 D, J.D. 40743 to 40779.

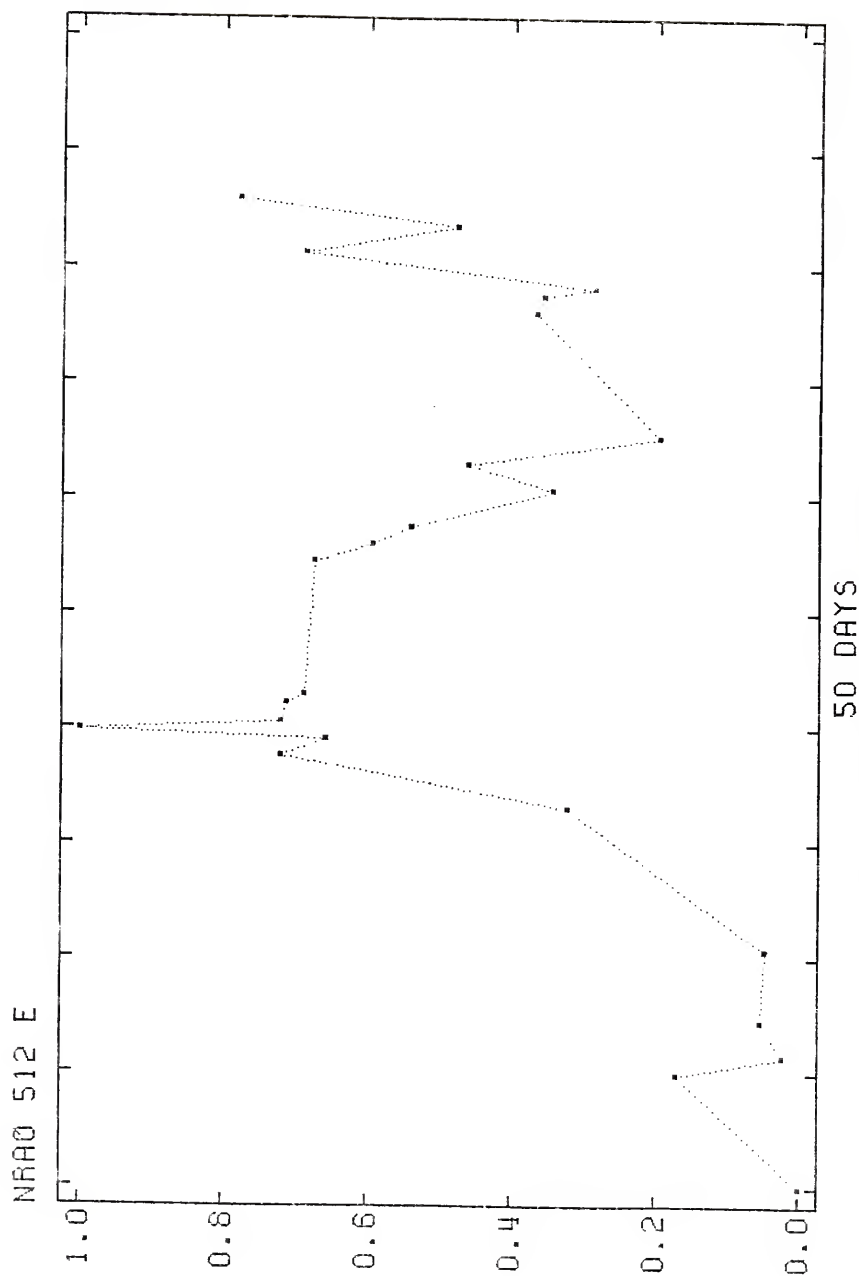


Figure 45. Event NRAO 512 E, J.D. 41134 to 41246.

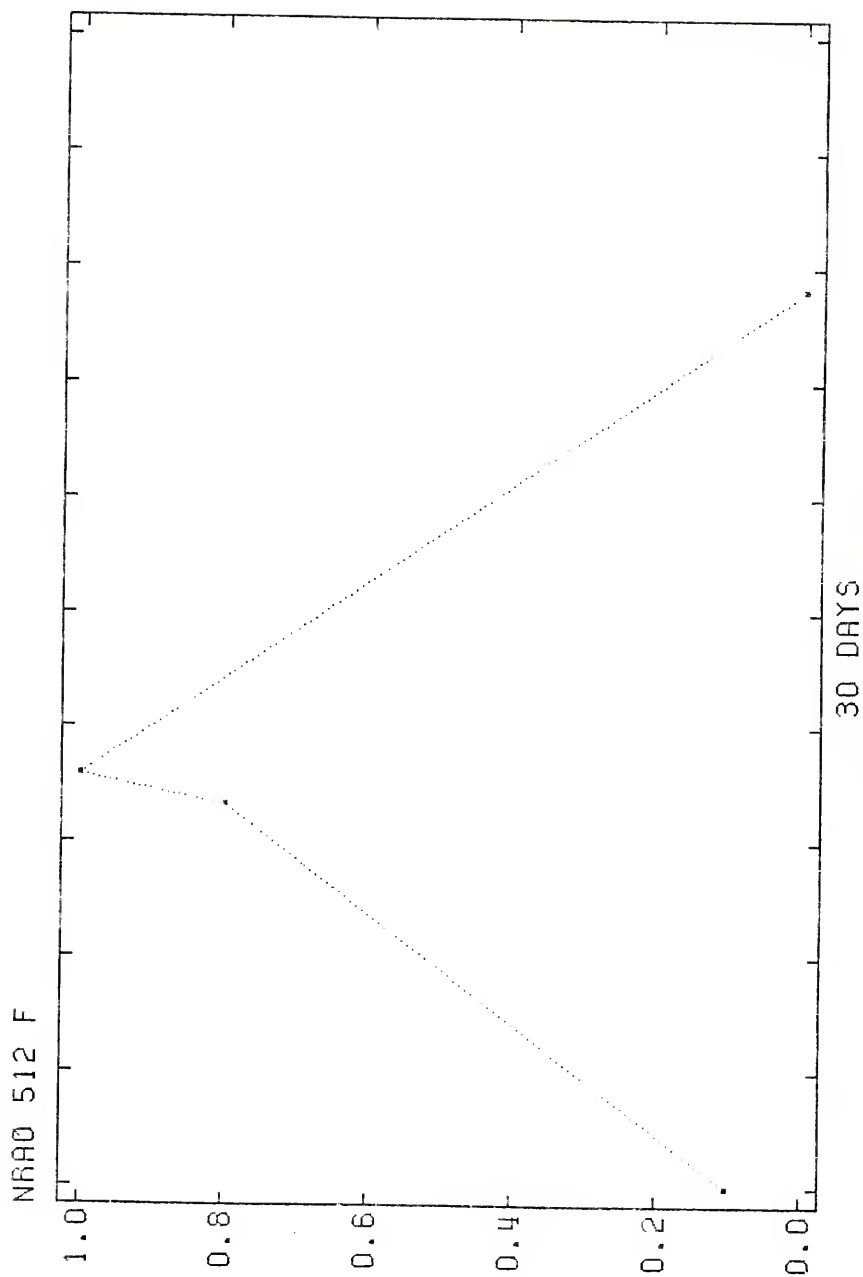


Figure 46. Event NRAO 512 F, J.D. 41397 to 41458.

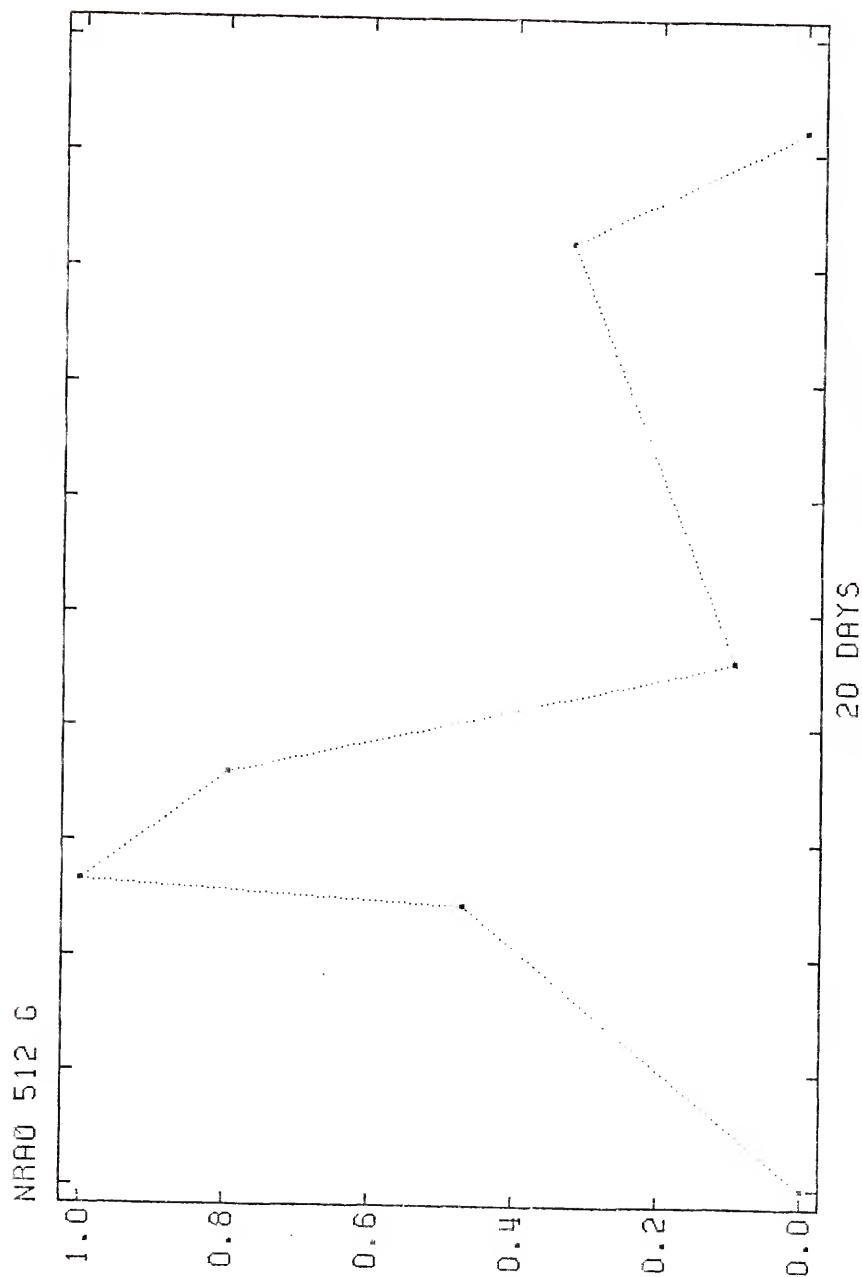


Figure 47. Event NRAO 512 G, J.D. 41458 to 41506.

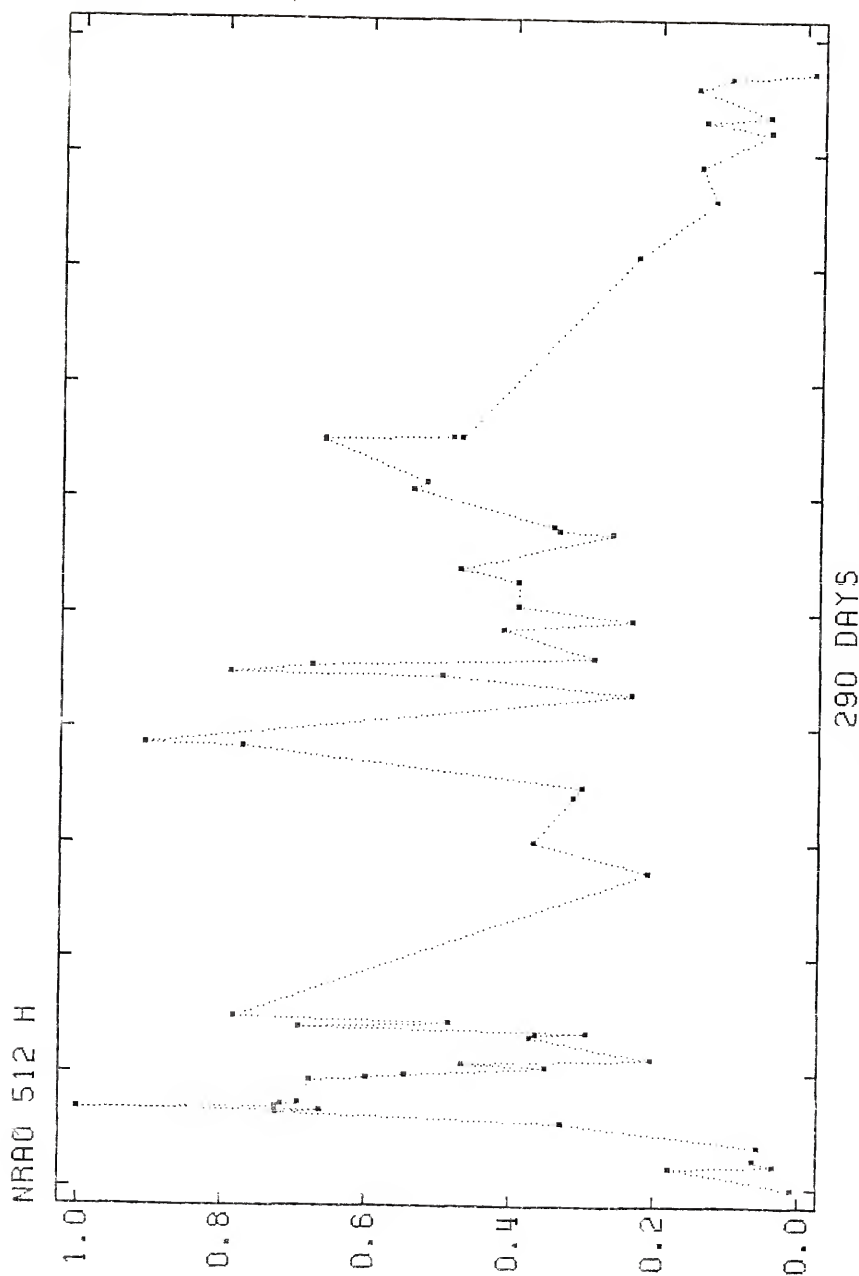


Figure 48. Event NRAO 512 H, J.D. 41134 to 41866.

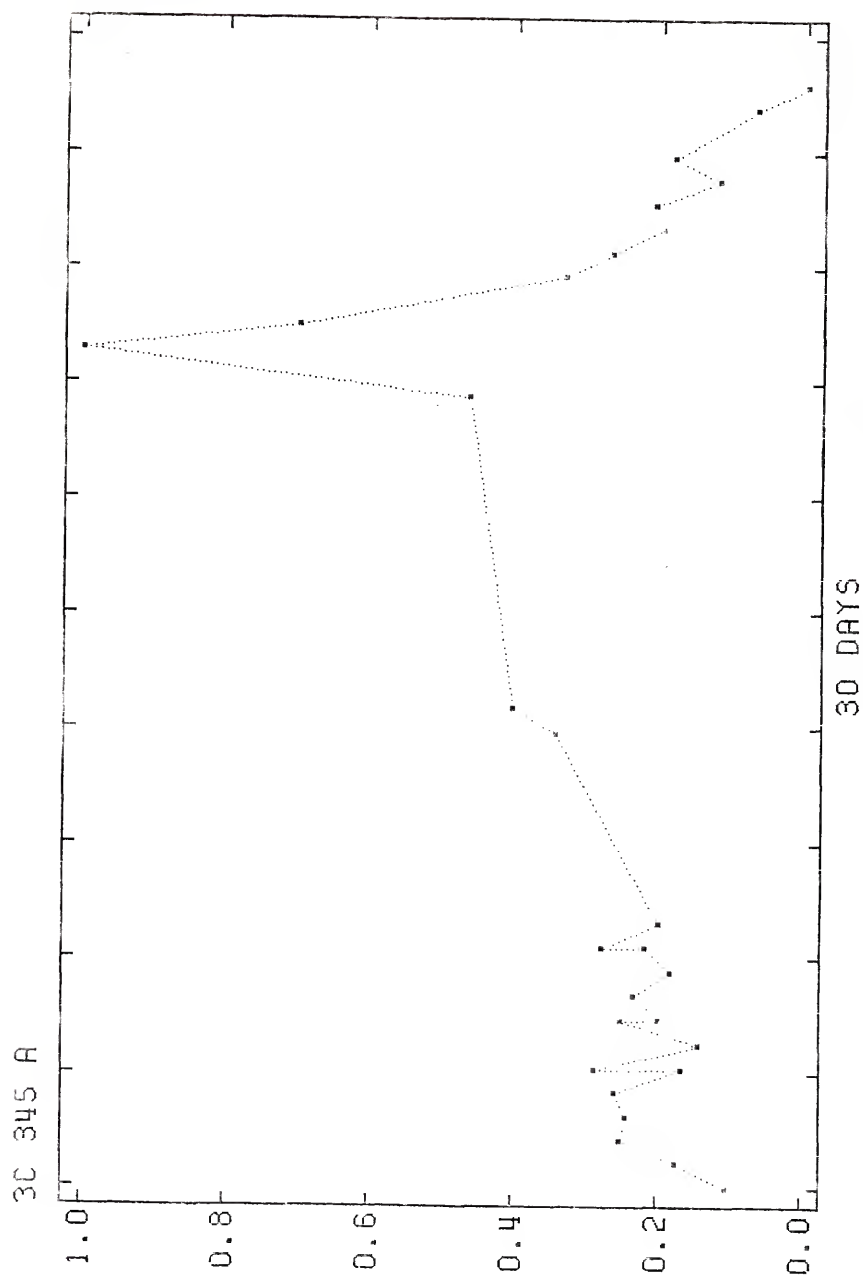


Figure 49. Event 3C 345 A, J.D. 39017 to 39063.

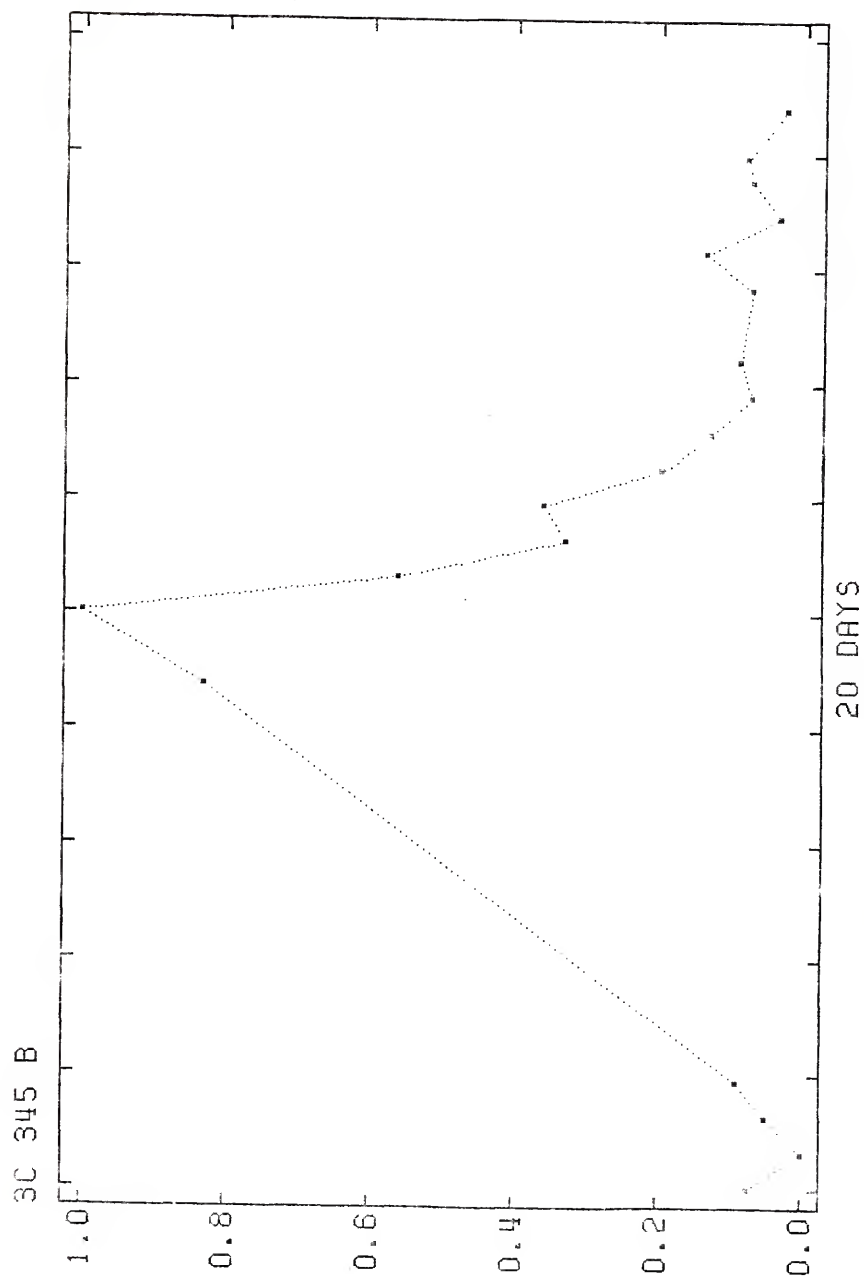


Figure 50. Event 3C 345 B, J.D. 39358 to 39387.

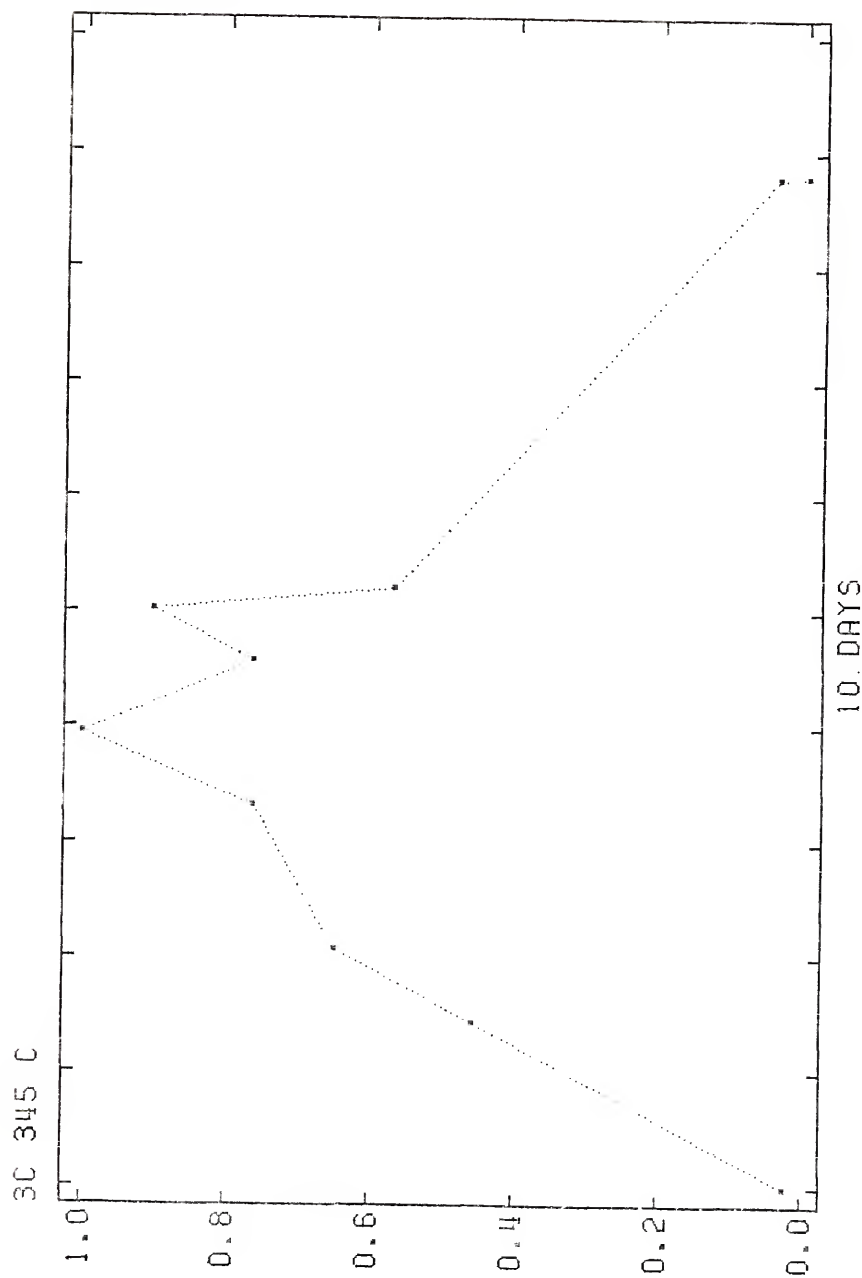


Figure 51. Event 3C 345 C, J.D. 39534 to 39548.

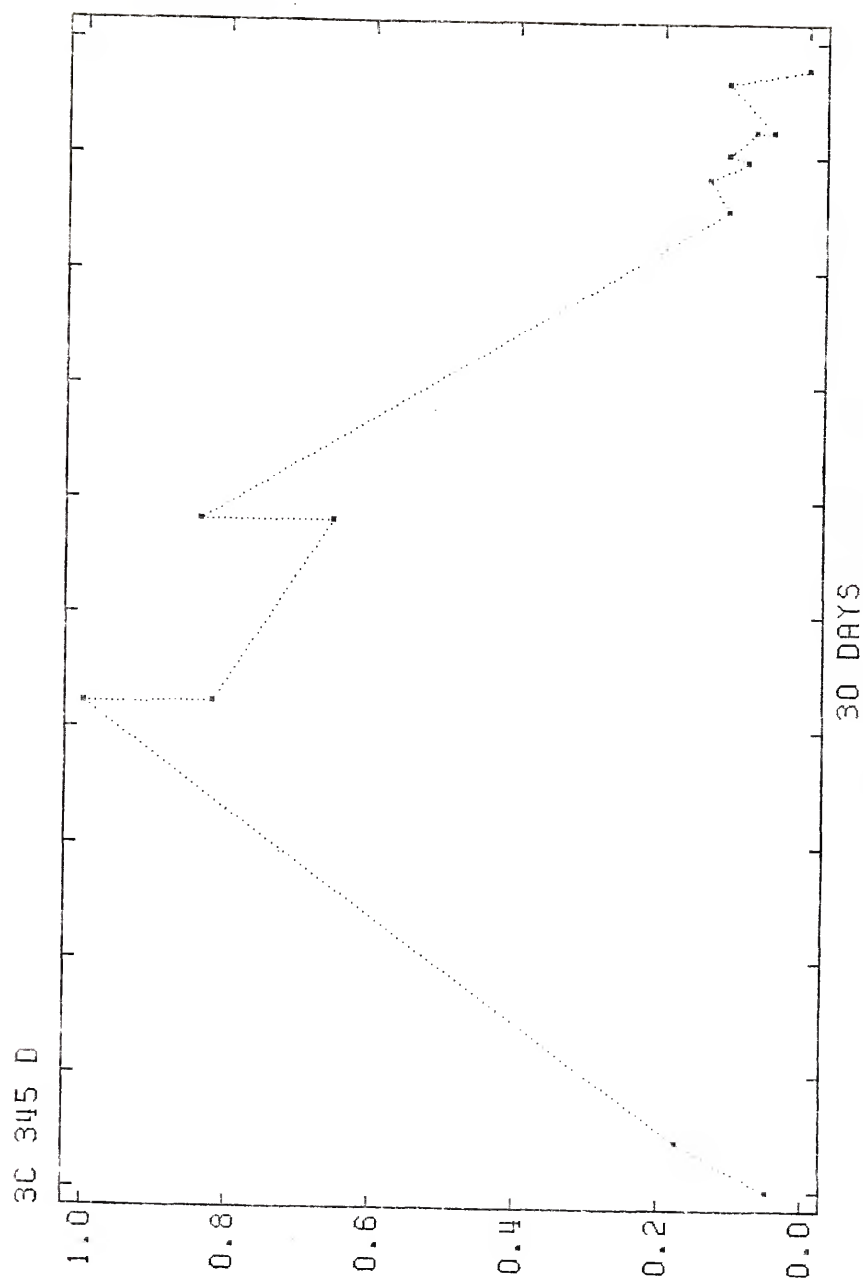


Figure 52. Event 3C 345 D, J.D. 39569 to 39616.

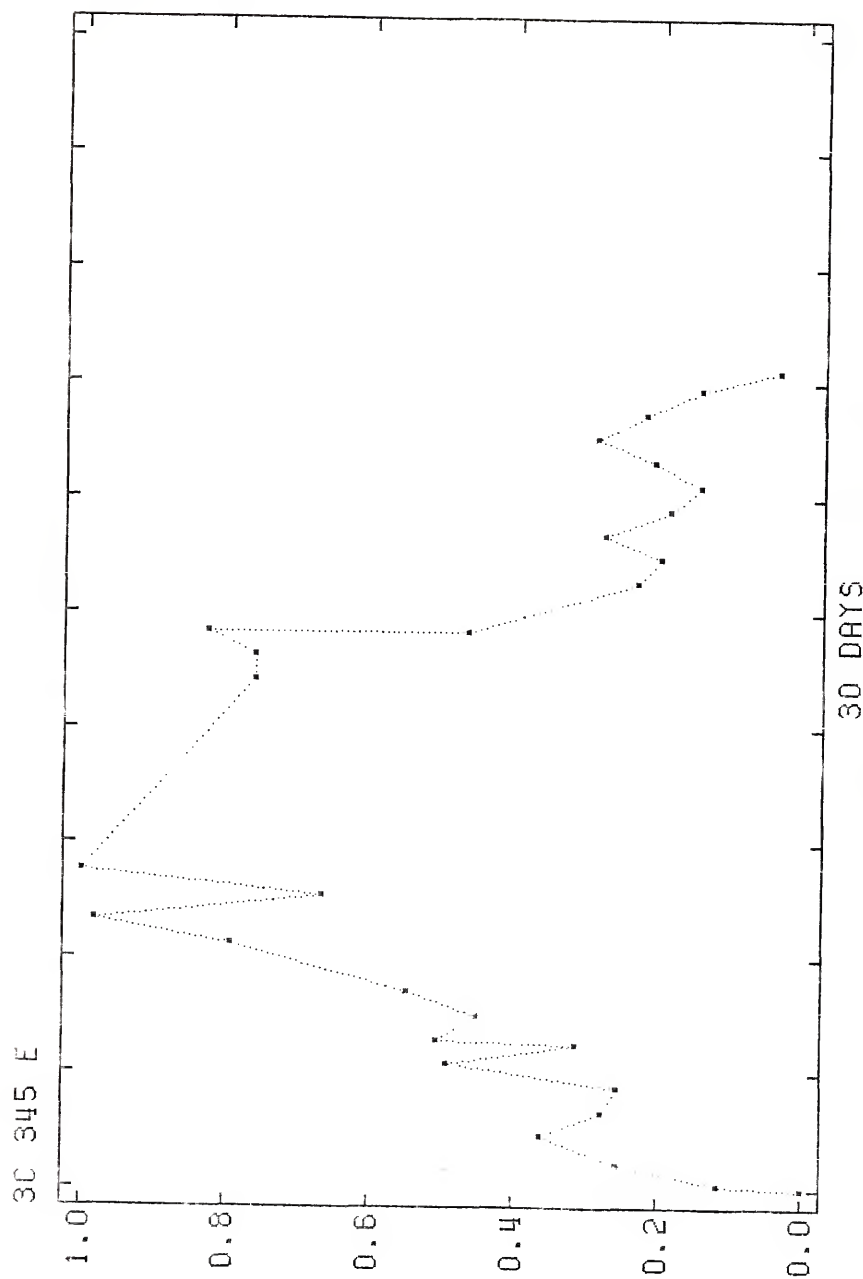


Figure 53. Event 3C 345 E, J.D. 39675 to 39709.

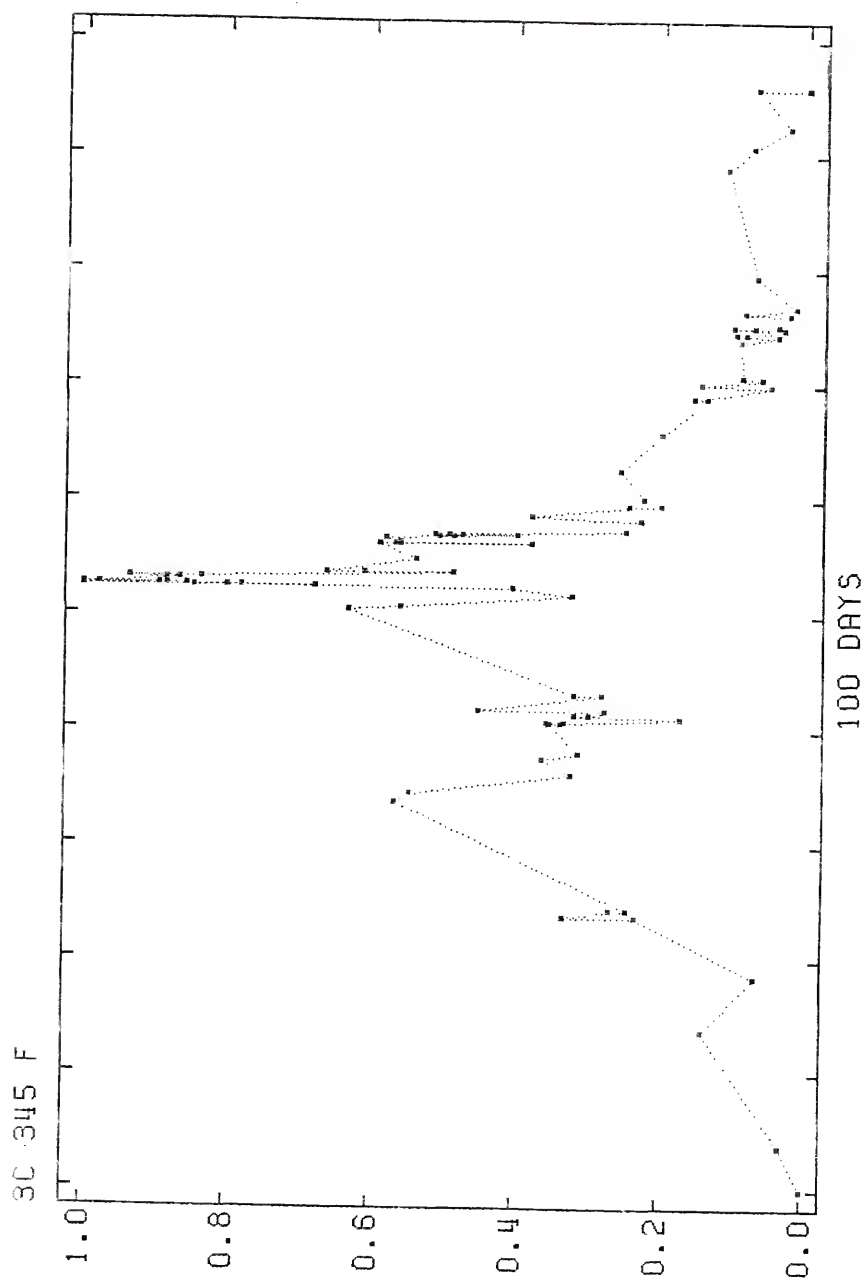


Figure 54. Event 3C 345 F, J.D. 40298 to 40451.

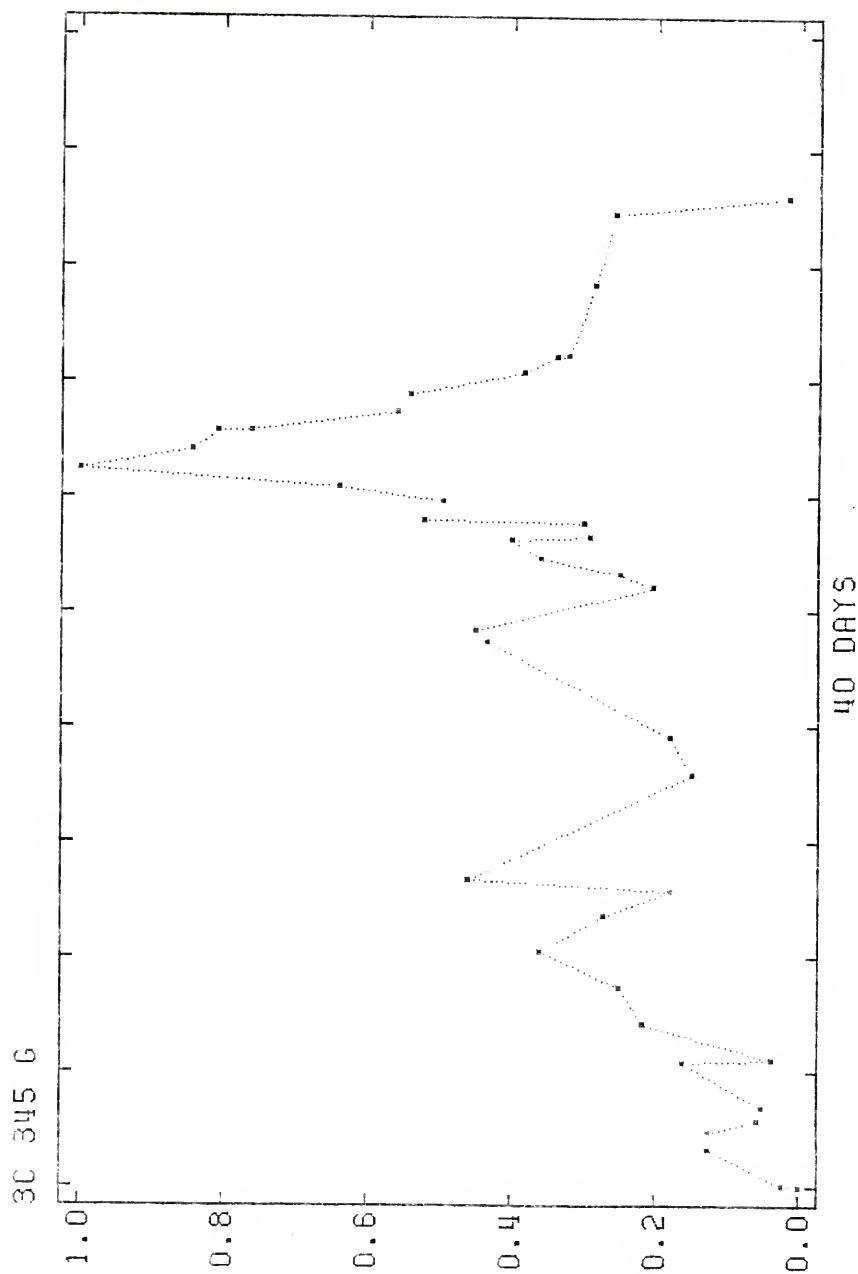


Figure 55. Event 3C 345 G, J.D. 41120 to 41175.

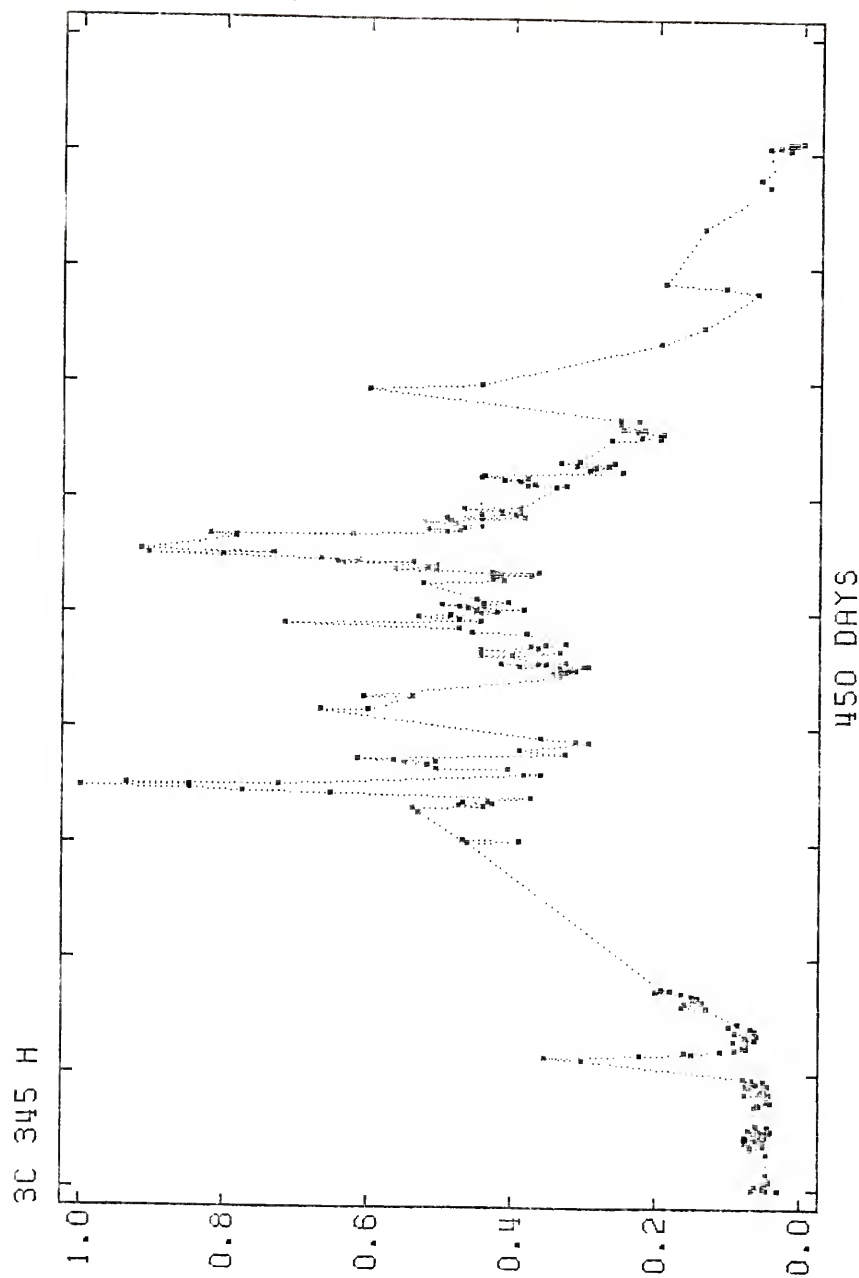


Figure 56. Event 3C 345 H, J.D. 39290 to 39943.

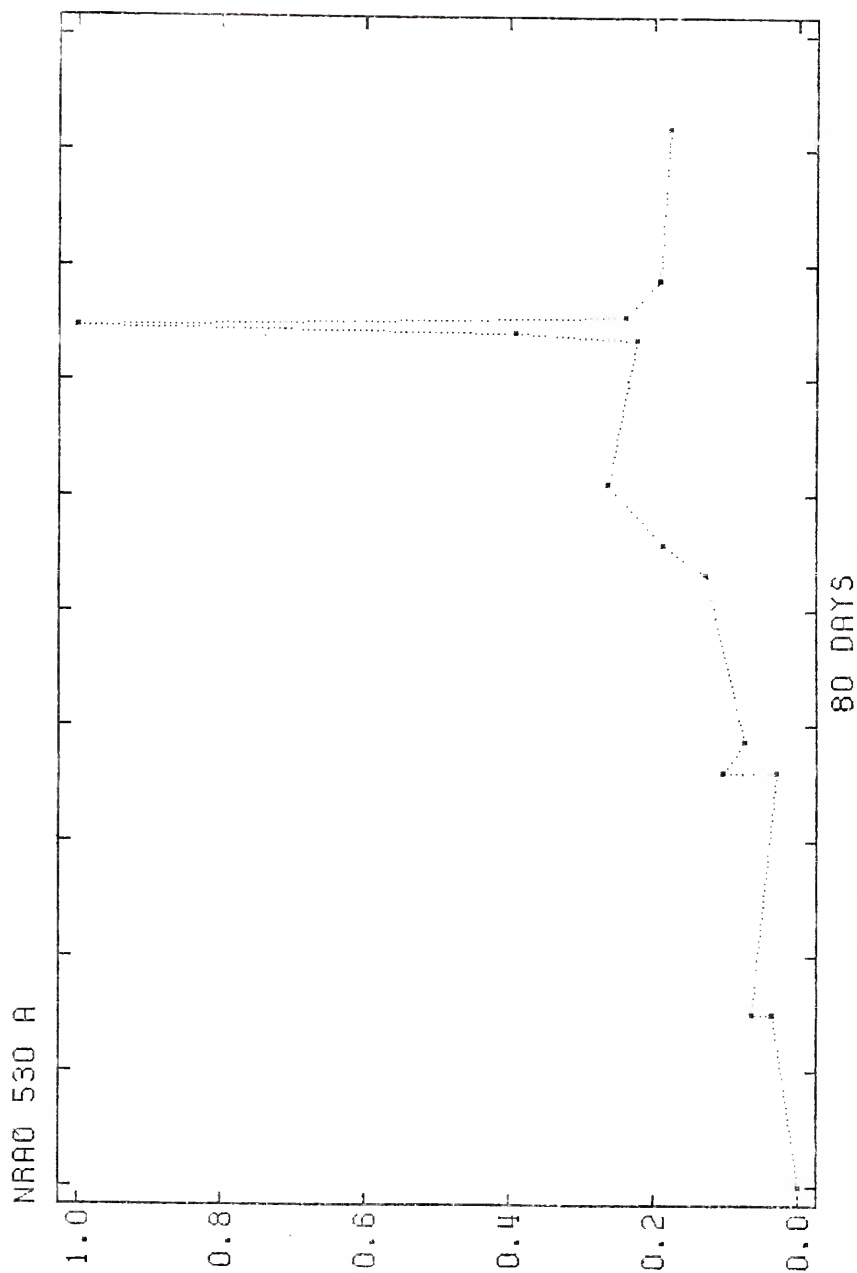


Figure 57. Event NRAO 530 A, J.D. 43280 to 43420.

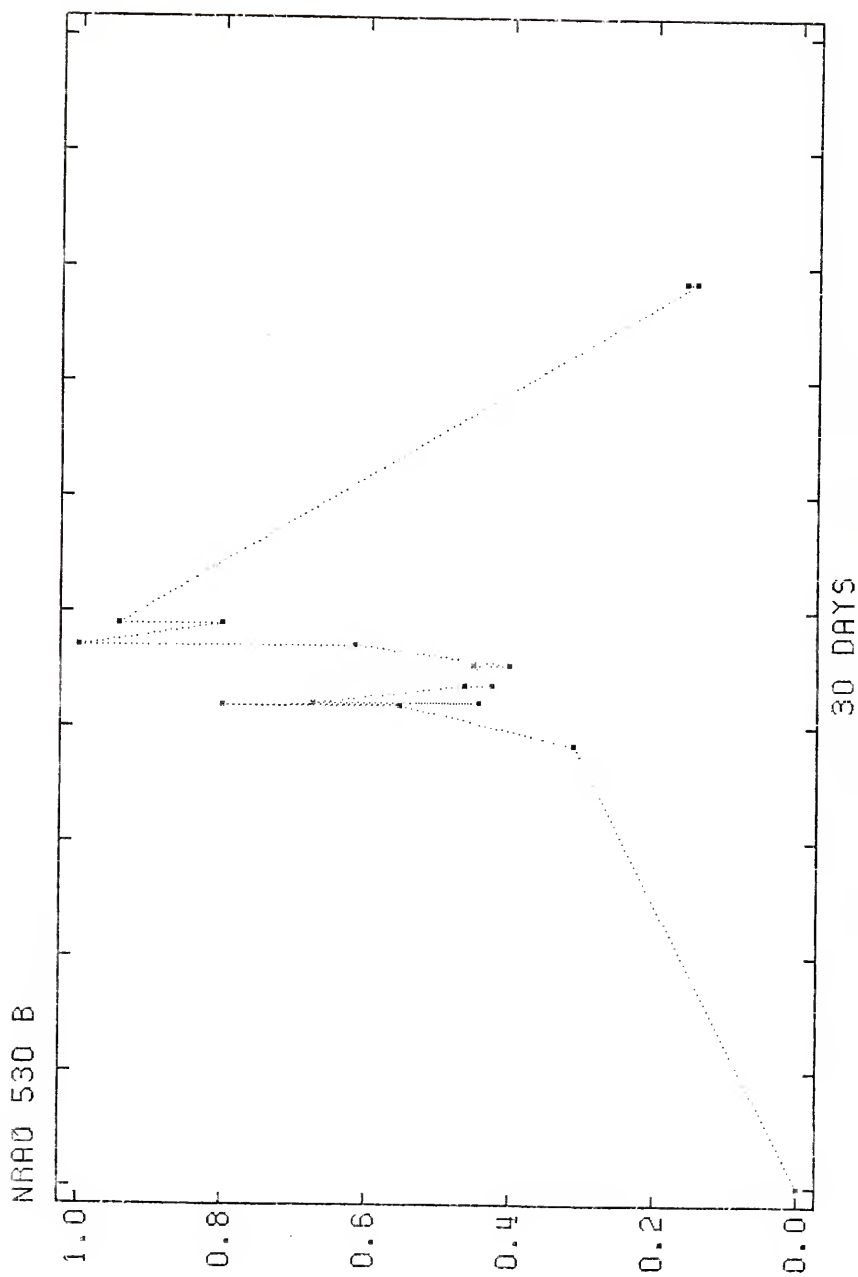


Figure 58. Event NRAO 530 B, J.D. 44764 to 44792.

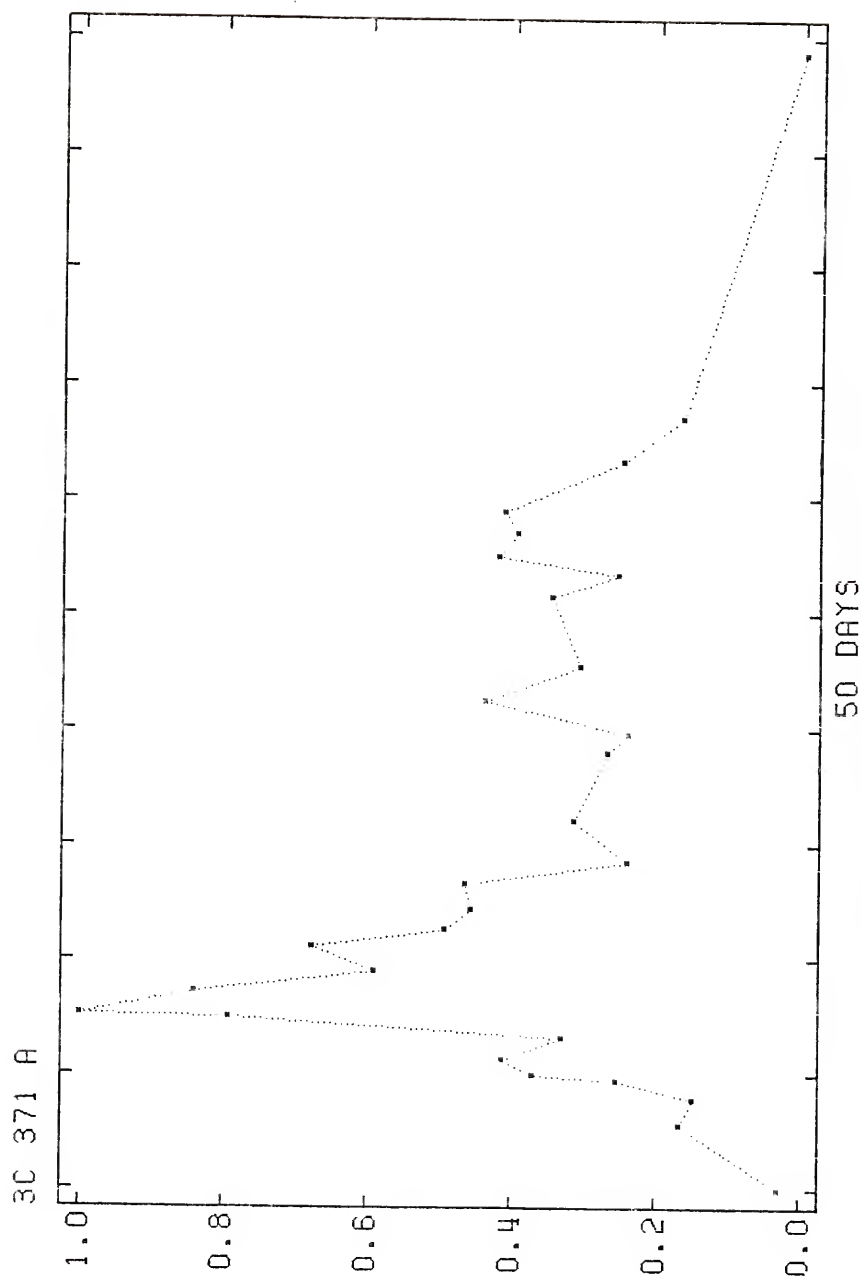


Figure 59. Event 3C 371 A, J.D. 40827 to 40879.

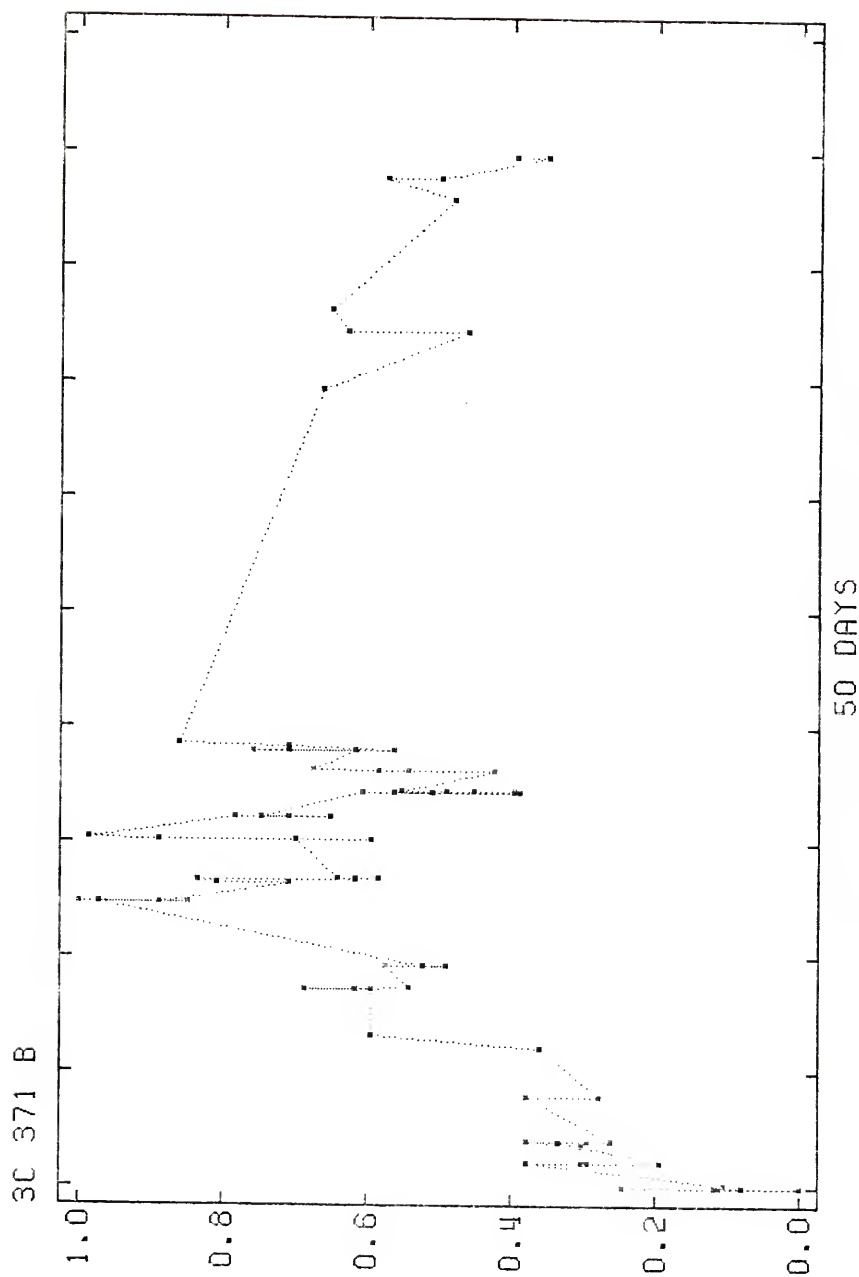


Figure 60. Event 3C 371 B, J.D. 41471 to 41518.

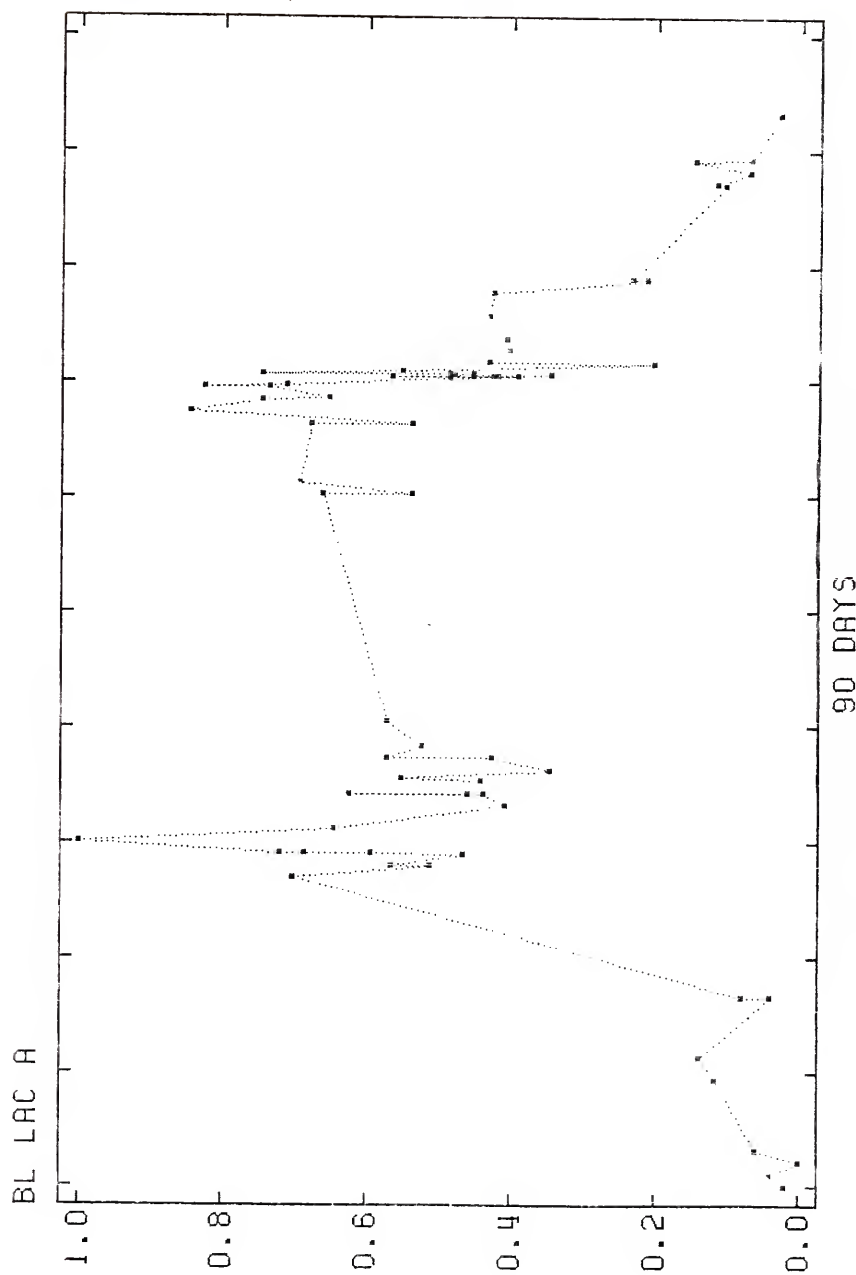


Figure 61. Event BL LAC A, J.D. 40384 to 40747.

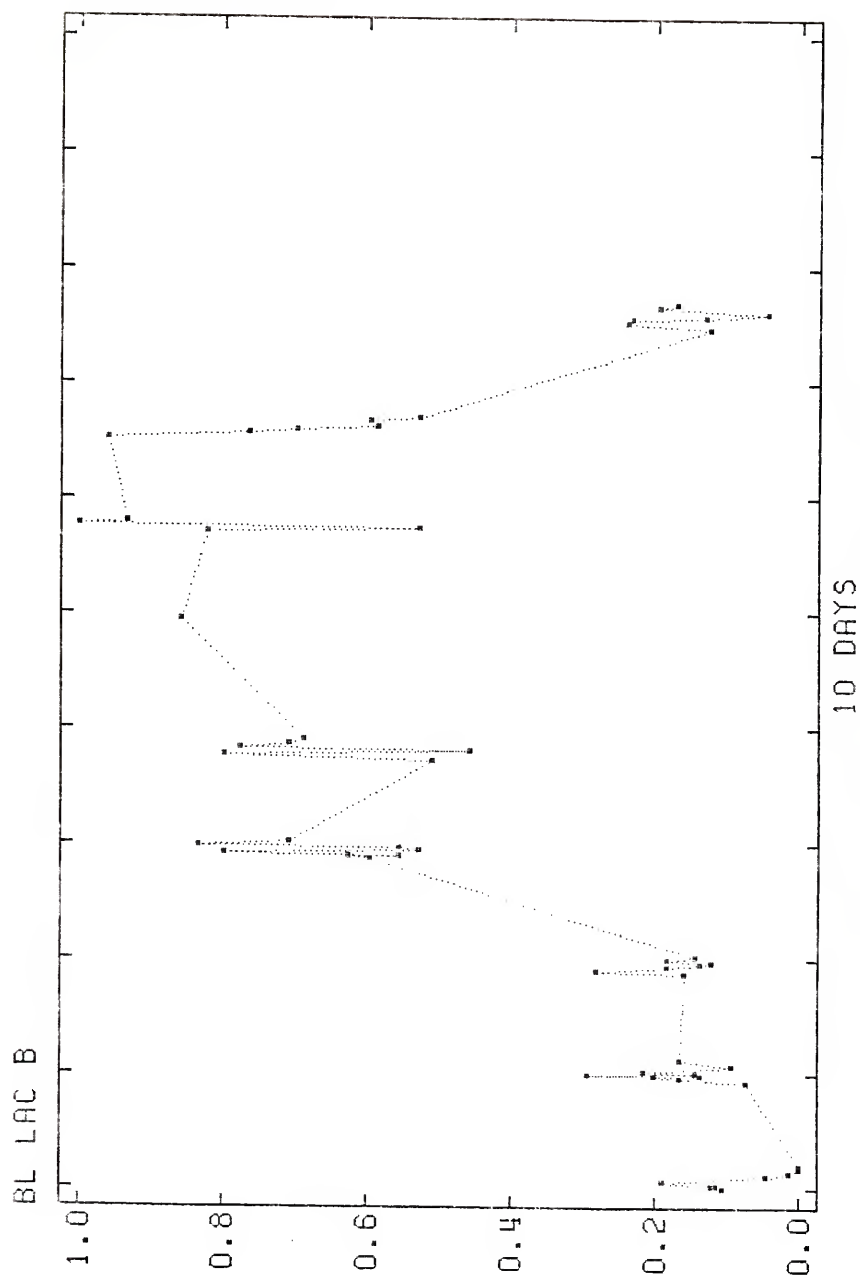


Figure 62. Event BL LAC B, J.D. 41891 to 41899.

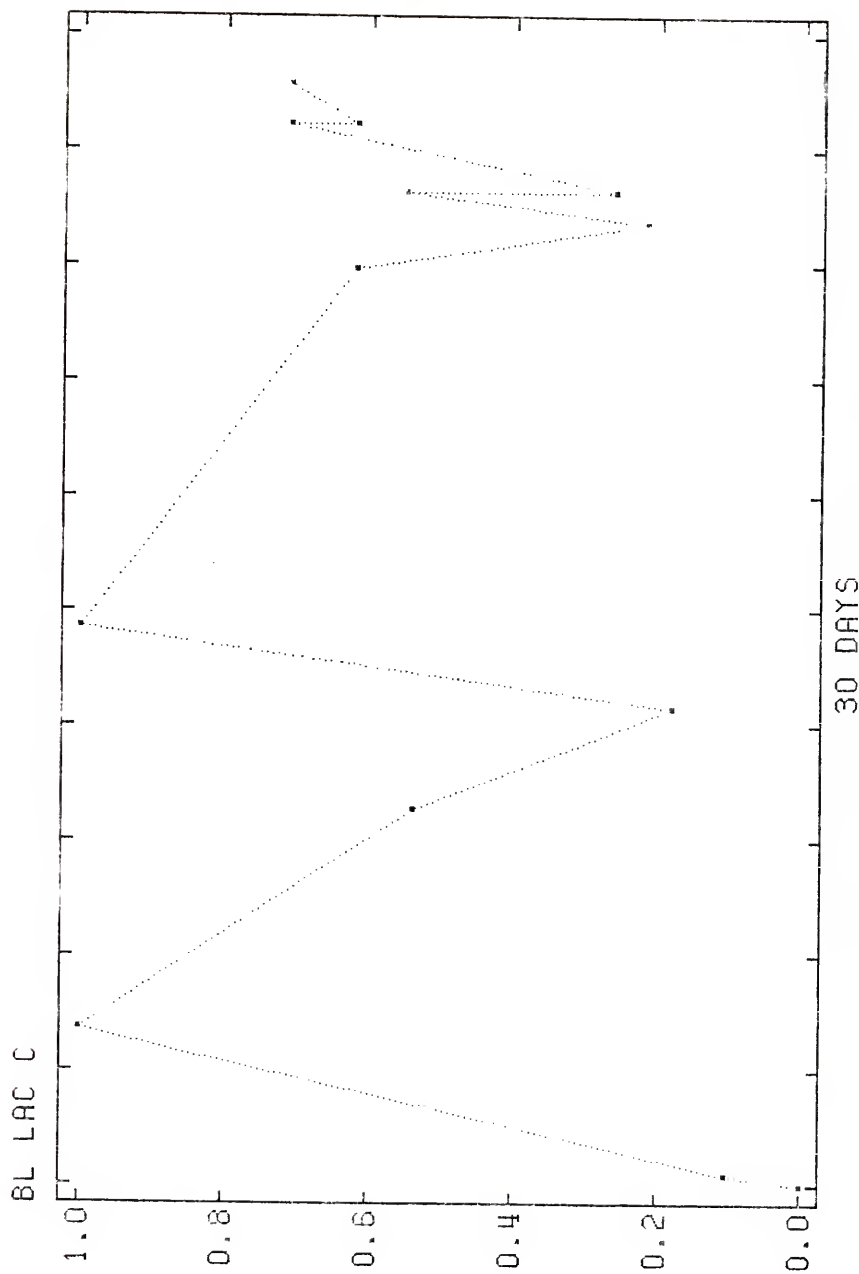


Figure 63. Event BL LAC C, J.D. 32043 to 32073.

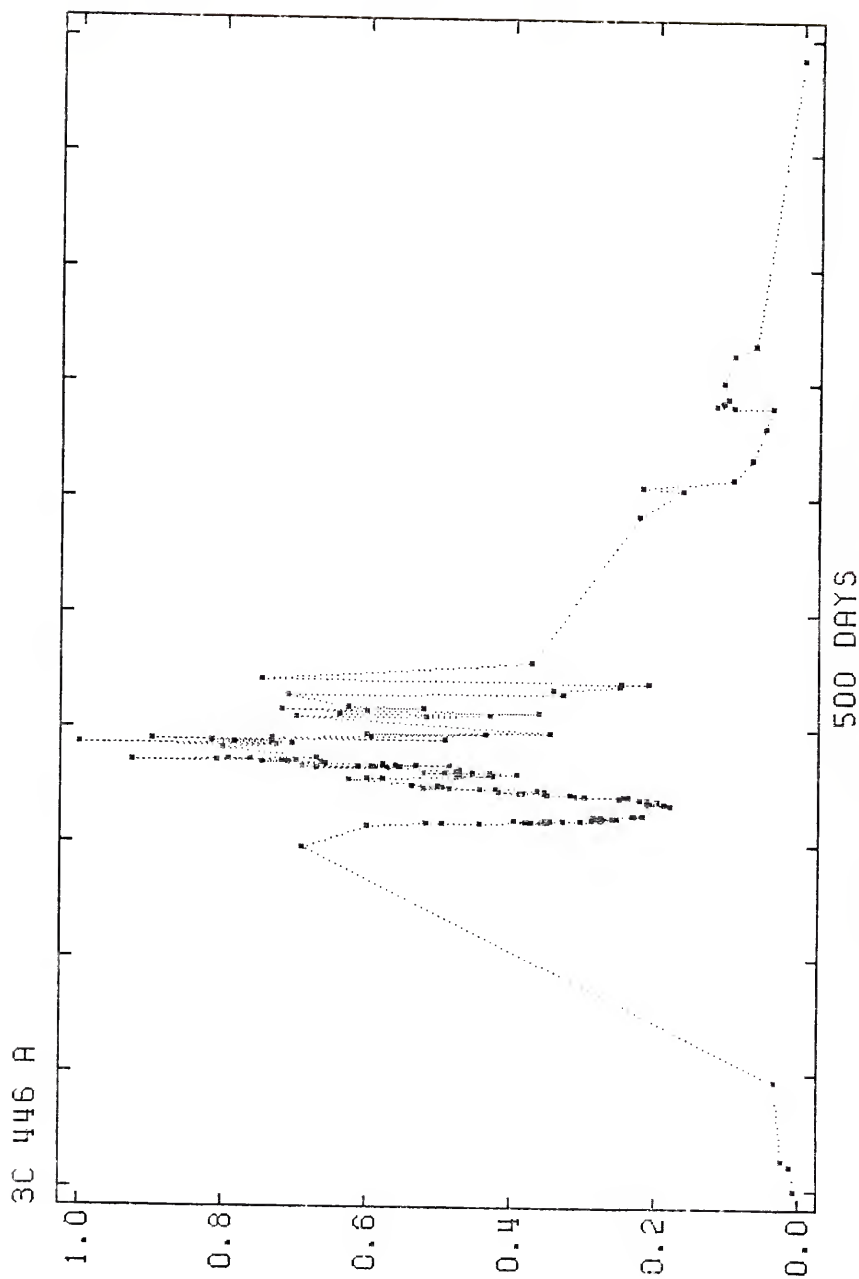


Figure 64. Event 3C 446 A, J.D. 38944 to 40127.

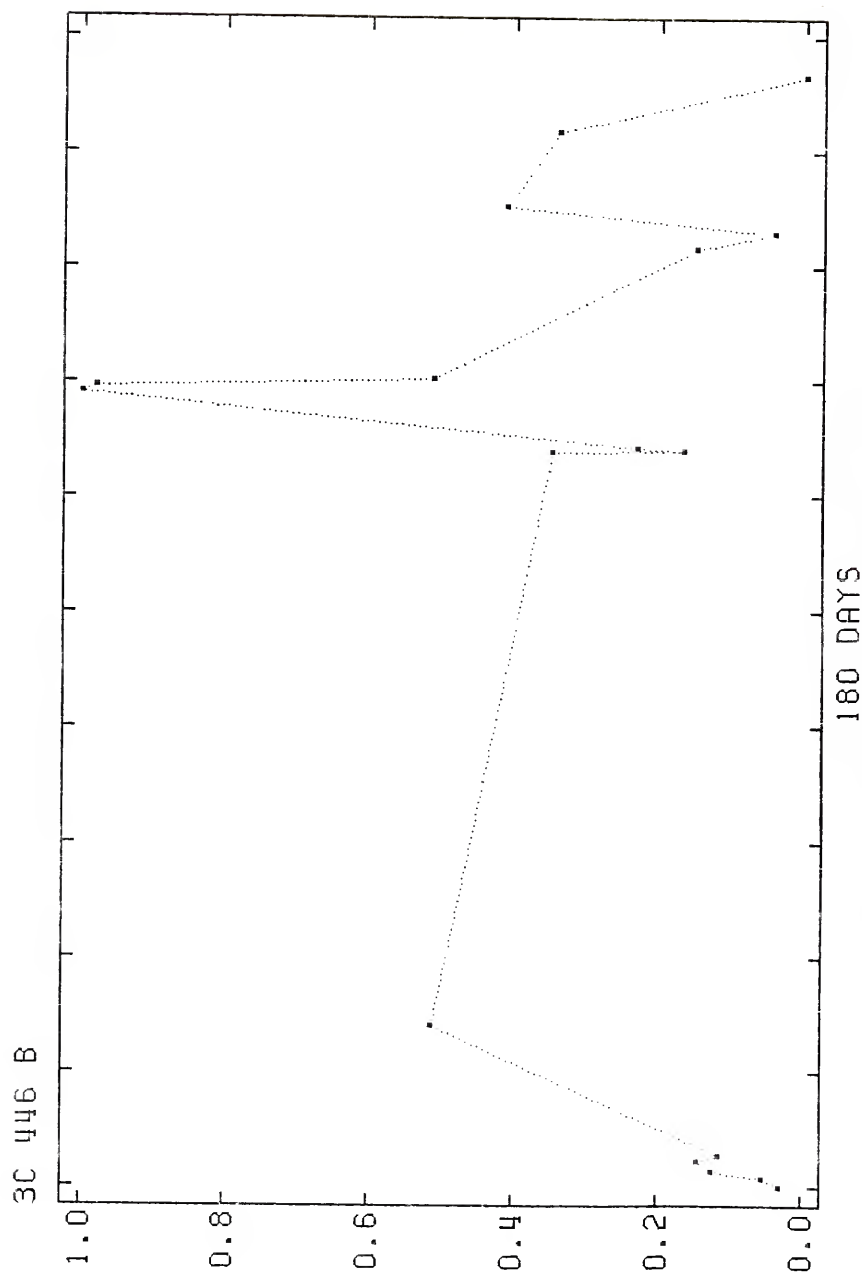


Figure 65. Event 3C 446 B, J.D. 40500 to 40918.

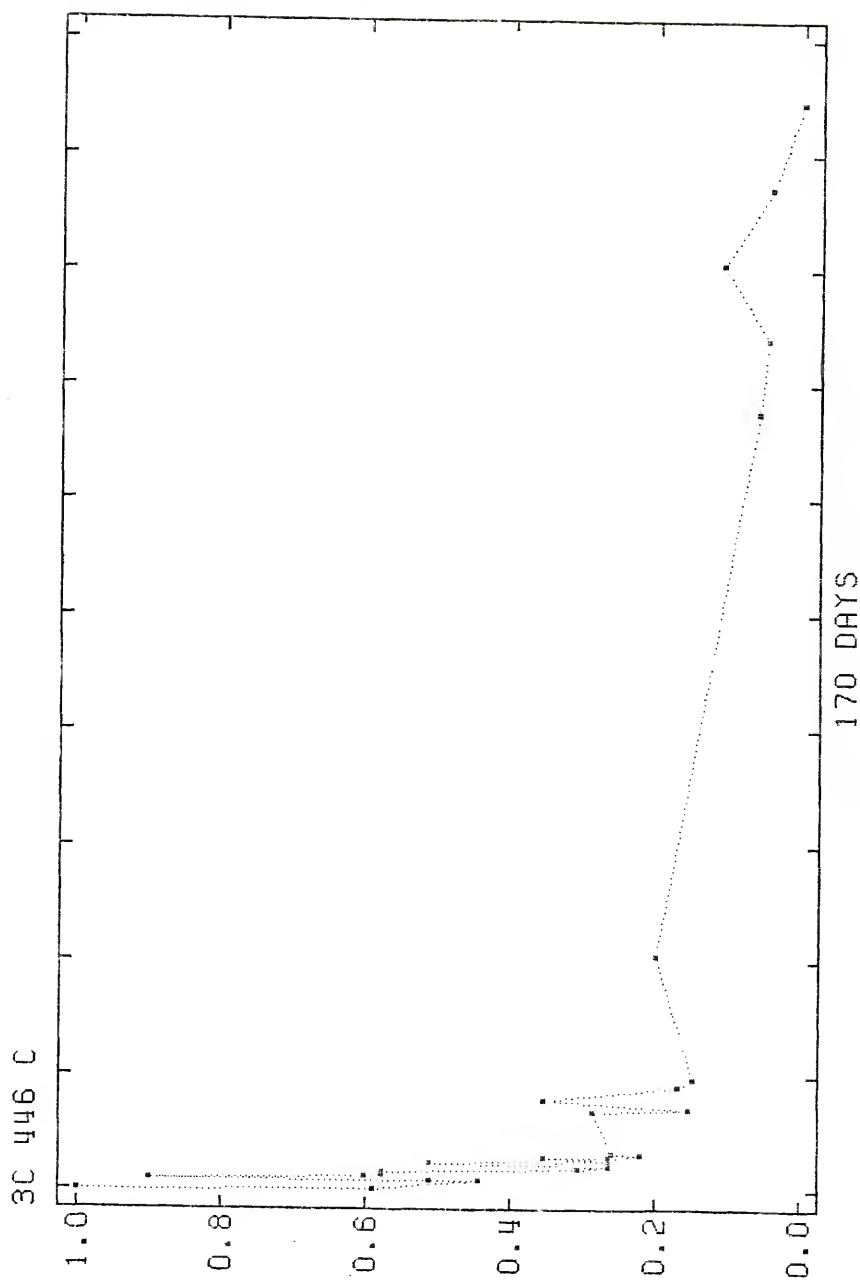


Figure 66. Event 3C 446 C, J.D. 42301 to 42687.

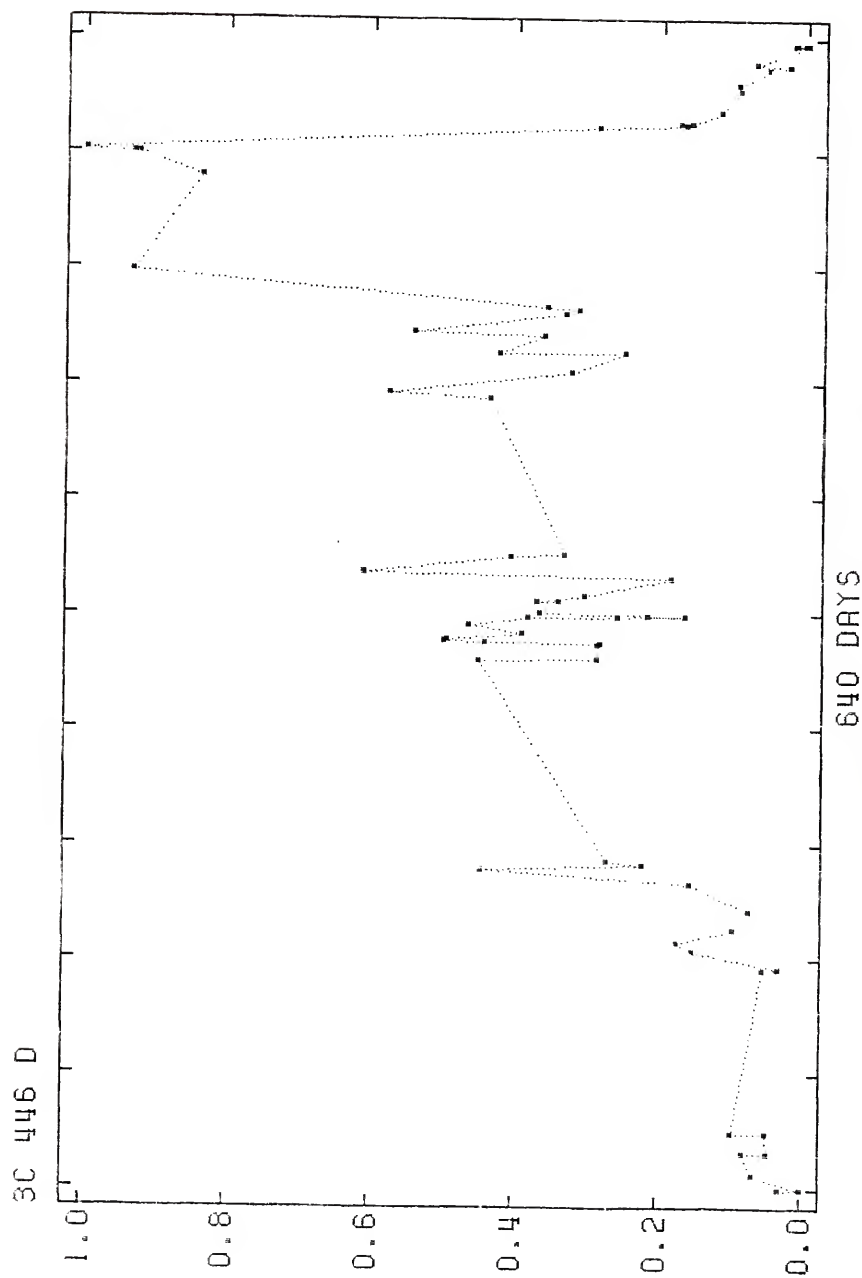


Figure 67. Event 3C 446 D, J.D. 43018 to 44550.

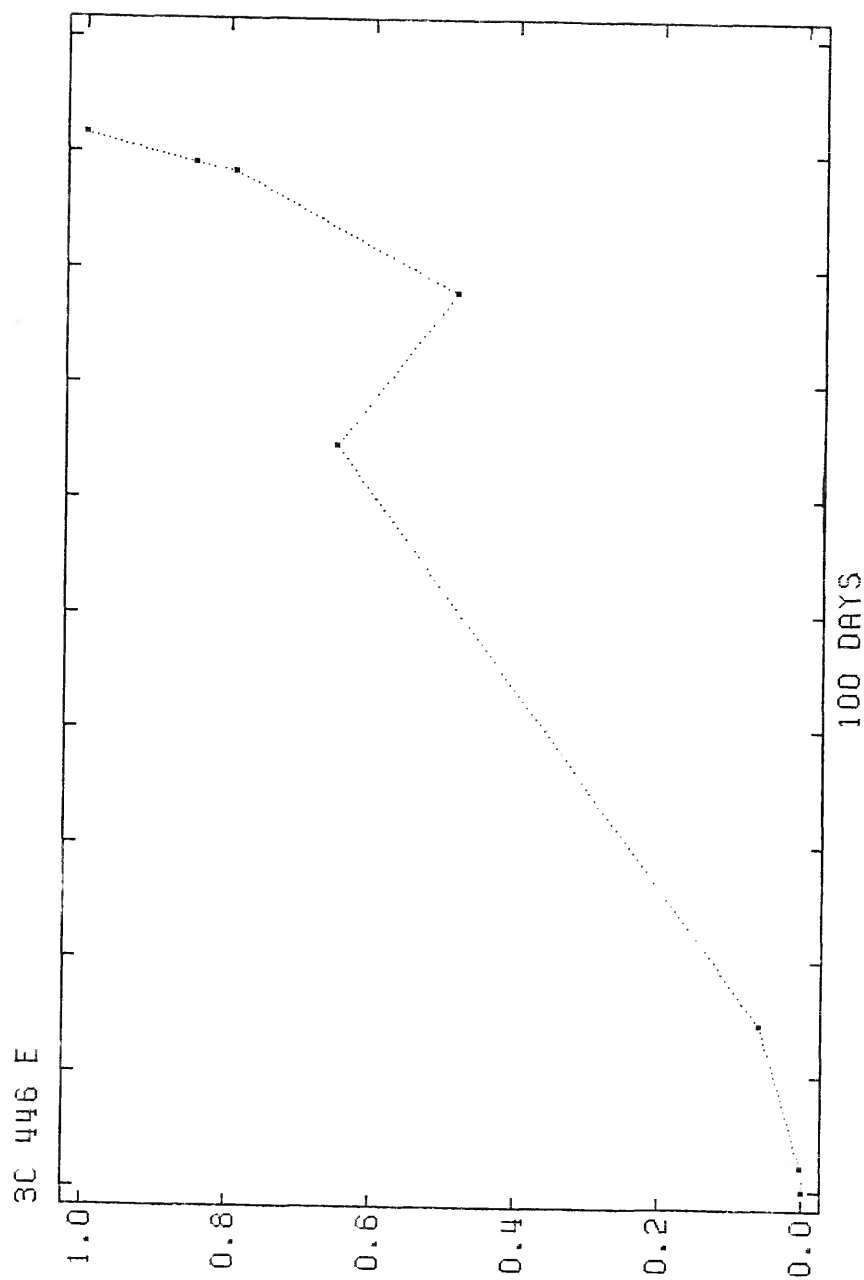


Figure 68. Event 3C 446 E, J.D. 44572 to 44792.

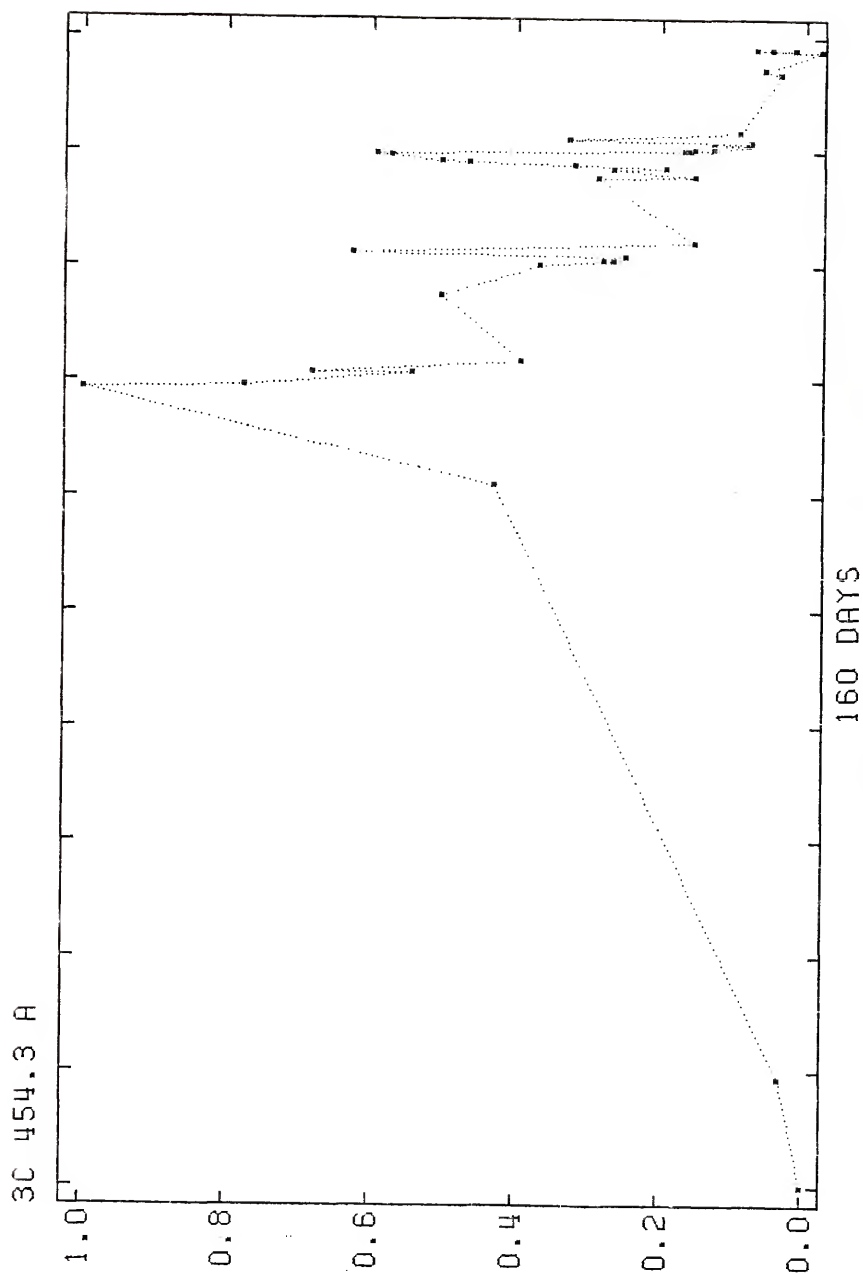


Figure 69. Event 3C 454.3 A, J.D. 39856 to 40150.

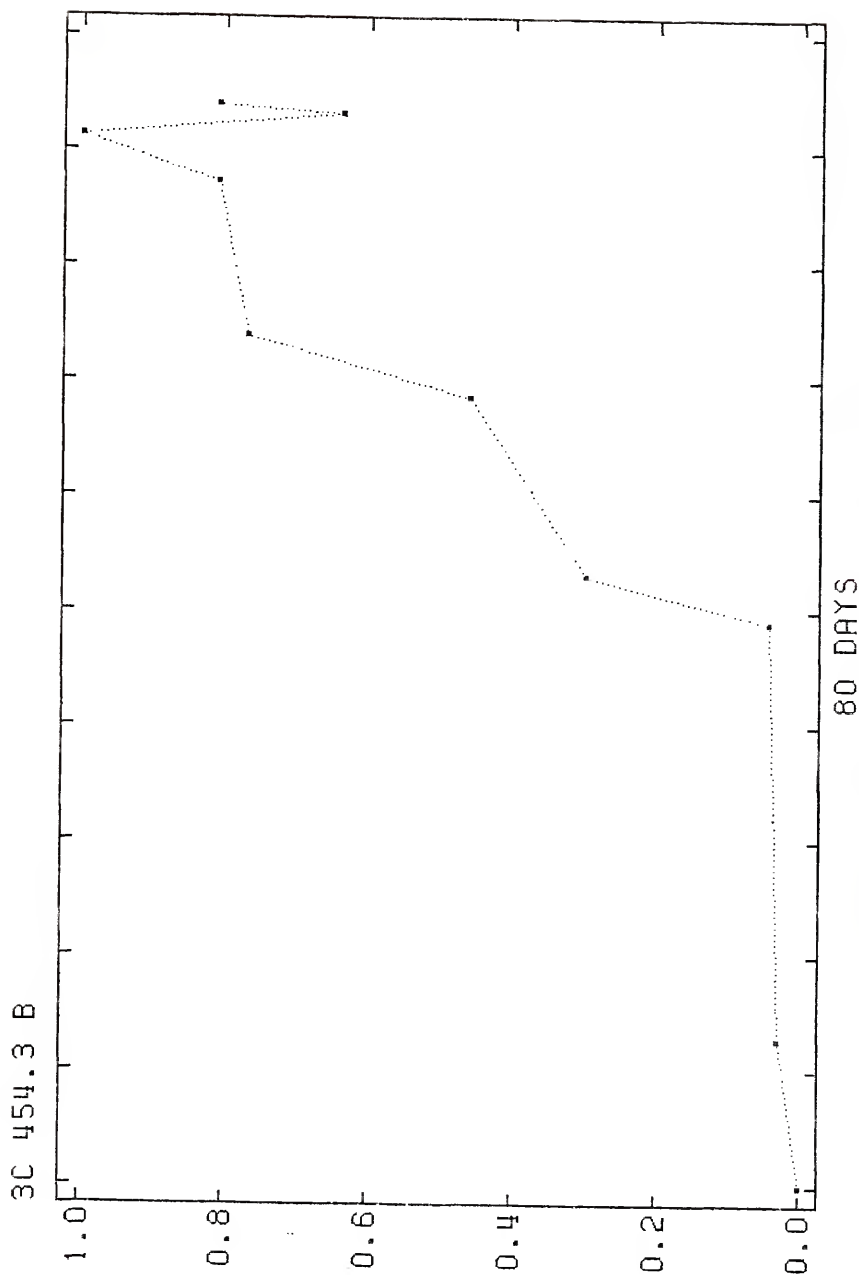


Figure 70. Event 3C 454.3 B, J.D. 44057 to 44246.

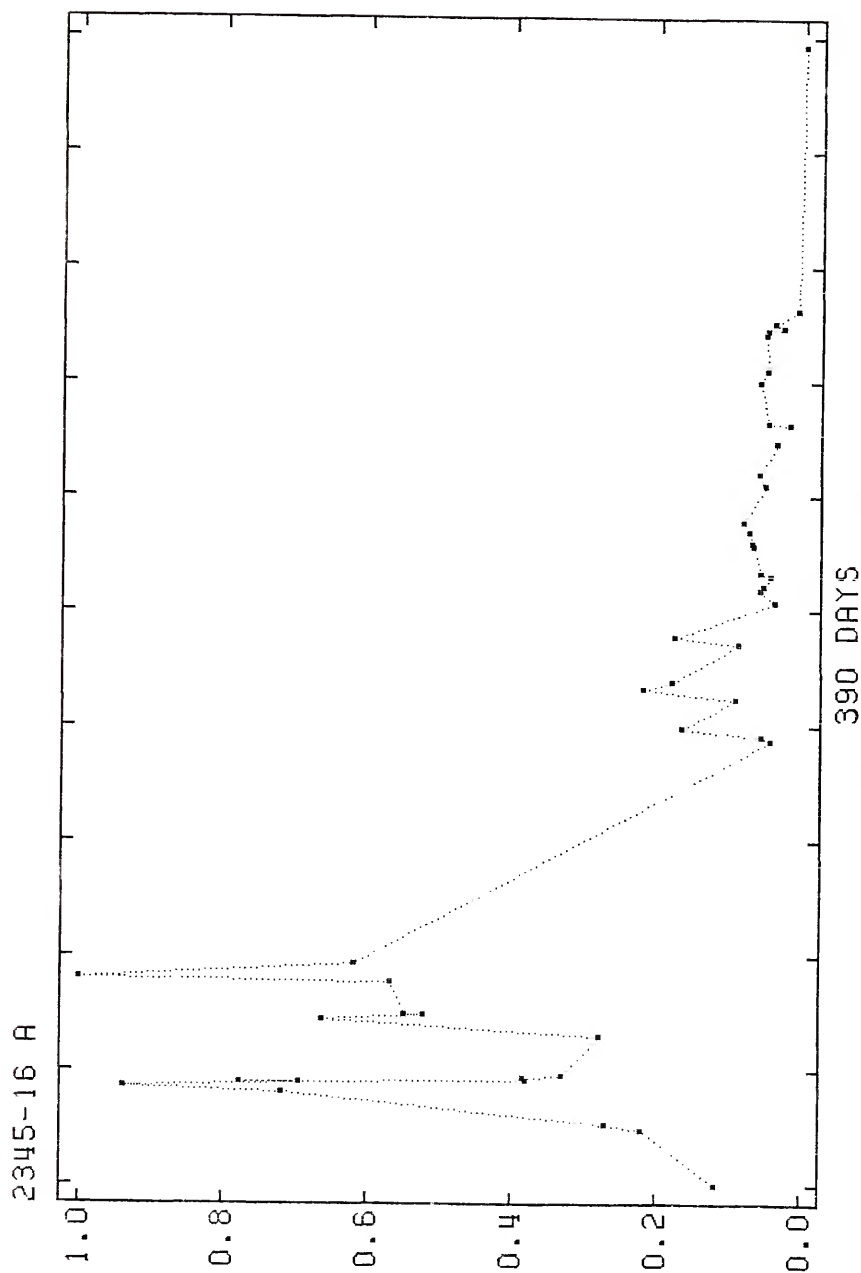


Figure 71. Event 2345-16 A, J.D. 40504 to 41123.

BIOGRAPHICAL SKETCH

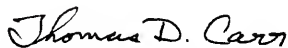
Joseph Thomas Pollock was born in Ridgewood, New Jersey, on December 16, 1950, to Joseph and Cecelia Pollock. His family moved to West Chester, Pennsylvania, in June of 1955 and he graduated from Henderson Senior High School in June of 1968. He earned a B.S. in Astronomy from the Pennsylvania State University in June of 1972 and an M.S. in Astronomy from the same institution in August of 1975. He then enrolled at the University of Florida in Gainesville, and will receive his Ph.D. in Astronomy from there in May of 1982. He is presently a half-time faculty member in the Department of Physics and Astronomy at the Appalachian State University in Boone, North Carolina.

I certify that I have read this study and that in my opinion it conforms to acceptable standards of scholarly presentation and is fully adequate, in scope and quality, as a dissertation for the degree of Doctor of Philosophy.



Alex G. Smith, Chairman
Professor of Astronomy

I certify that I have read this study and that in my opinion it conforms to acceptable standards of scholarly presentation and is fully adequate, in scope and quality, as a dissertation for the degree of Doctor of Philosophy.



Thomas D. Carr
Professor of Astronomy

I certify that I have read this study and that in my opinion it conforms to acceptable standards of scholarly presentation and is fully adequate, in scope and quality, as a dissertation for the degree of Doctor of Philosophy.



John P. Oliver
Associate Professor of Astronomy

I certify that I have read this study and that in my opinion it conforms to acceptable standards of scholarly presentation and is fully adequate, in scope and quality, as a dissertation for the degree of Doctor of Philosophy.



Haywood C. Smith
Associate Professor of Astronomy

I certify that I have read this study and that in my opinion it conforms to acceptable standards of scholarly presentation and is fully adequate, in scope and quality, as a dissertation for the degree of Doctor of Philosophy.

Pradeep Kumar

Pradeep Kumar

Associate Professor of Physics

This dissertation was submitted to the graduate faculty of the Department of Astronomy in the College of Liberal Arts and Sciences and to the Graduate Council, and was accepted as partial fulfillment of the requirements for the degree of Doctor of Philosophy.

May, 1982

Dean for Graduate Studies and Research

UNIVERSITY OF FLORIDA



3 1262 08666 319 1